

Intuitive Impedance Modulation in Haptic Control using Electromyography

K.J. (Kees) van Teeffelen

MSc Report

Committee:

Dr.ir. J.F. Broenink
Dr.ir. D. Dresscher
Dr. A.H. Mader
Dr.ir. W. Van Dijk

January 2018

001RAM2018
Robotics and Mechatronics
EE-Math-CS
University of Twente
P.O. Box 217
7500 AE Enschede
The Netherlands

UNIVERSITY OF TWENTE.

MIRA **CTIT**
BIOMEDICAL TECHNOLOGY
AND TECHNICAL MEDICINE

Preface

This thesis was written to conclude the graduation period of the Master of Science programme in Systems and Control at the University of Twente in Enschede, the Netherlands. The presented work was executed within the joint innovation centre i-Botics, a collaboration between TNO and the University of Twente.

During the execution of the presented research I had the pleasure of combining work within the Robotics and Mechatronics group (RaM) of the University of Twente with a part time internship at TNO in Leiden, the Netherlands. This combination offered me additional learning opportunities and great chances for my future career as a robotics engineer.

I would like to thank my daily supervisors, Dr. ir. Douwe Dresscher of the University of Twente and Dr. ir. Wietse van Dijk of TNO for guiding me through the process of my graduation project and for presenting me with all the help and feedback I needed to successfully complete this thesis. Furthermore, I would like to thank all others involved with RaM, TNO and i-Botics in particular that expressed interest in my research and offered to help me in any way, shape or form. Finally, I would like to thank all of the volunteers that participated in the experiments. Thanks to them I was able to collect insightful data that supports the claims of my research.

I hope you enjoy reading this thesis.

Kees van Teeffelen

Enschede, 2018

Summary

The research presented in this thesis focusses on the haptic control of a robotic teleoperation system. In this system, a KUKA LWR4+ robotic arm (slave device) is remotely controlled by a human operator through a Force Dimension omega.7 haptic device (master device). Besides encoding its position, this haptic device is able to apply force feedback to the operator.

To connect the robotic master and slave devices, an impedance controller is used. This impedance controller can be interpreted as a virtual spring of which the ends are attached to the end effectors of the master and slave devices. The effectiveness of motion tracking and the successfulness of creating the desired interaction with a remote environment is summarised as the level of transparency of the system. The stiffness setting of the impedance controller is closely related to both the transparency and stability levels of the system. Although a stiff connection could in theory create a very transparent interaction between the two devices, stability can become an issue especially when communication delays are present between the two devices. By guaranteeing that all energy that is used by the controller is either added by the operator or the remote environment, stability can be guaranteed through the passivity theorem.

Keeping the transparency and stability properties of the system in mind, there does not seem to be an ideal stiffness setting for the impedance controller. Stability problems can harm the transparency level of the system which can for instance lead to high control efforts or a shaking behaviour of the robotic devices. For this reason, this research focusses on modulating the impedance controller through muscle activation information of the human operator. These activation levels are captured using a Myo Gesture Control Armband, which creates an estimate of the muscle activation levels using electromyography. The goal is to create a teleoperation system that uses impedance modulation in an intuitive way, which should increase the effectiveness of the task execution by the human operator.

The impedance controller is designed using a PF architecture, meaning that the master controller sends information on the master's position to the slave controller, while the slave controller sends back the forces computed by the impedance controller based on the relative position of both devices. This position and force information is sent over the communication channel, in which a delay can be added to simulate communication over a distance.

From the muscle activation data, an estimate of the co-contraction level in the human arm is created. This is the level of simultaneous activation of flexor and extensor muscle pairs, in which the position and the force application by the human arm do not change but the stiffness of the elbow joint is increased. These levels are calibrated to indicate a normalised co-contraction level between zero and one, after which the signal is low-pass filtered to extract the frequencies of interest. This normalised co-contraction level is then used as a scaling factor to scale the settings of the impedance controller.

The master and slave controllers both contain a transparency layer and a stability layer. In the transparency layer, variables are exchanged with the communication channel and the master and slave devices to which they are directly connected. On the slave side, the position information of both devices is used to compute forces that will be applied by the impedance controller. This is the force that is sent back to the master device to be applied here as well. The stability layers use an energy-based monitoring approach to make sure no energy is added by the controller, known as energy leaking. This is the effects that can cause destabilisation of the devices which increases for increasing time delays in the communication channel.

A model of the KUKA robotic arm is simulated in Gazebo to test the functionality of the controller. Friction turned out to be a real limiting factor in the actual hardware, so in this simulation a more ideal robot is created with decreased friction properties. The combination of controllers,

communication channel, co-contraction estimation and Gazebo simulation are all implemented on one PC using ROS.

Hypotheses are included that focus on the expected behaviour of the system and the human operators. Co-contraction behaviour is expected to increase when carrying out a positioning accuracy task with respect to a task in which careful interaction with the remote environment is the main goal. Furthermore, during time delayed communication a decrease in stability is expected to result in a decrease in transparency, which can show as the mentioned shaking behaviour of the devices and the increase of controller efforts, harming the safety level of the system and its environment. Finally, it is expected that the designed impedance modulation approach will enable the operator to create a variable stiffness level of the controller which will correspond to the requirements of the conducted tasks.

Experiments were designed to validate the functional design of the system and to get an indication of static friction levels in the KUKA hardware. Furthermore, experiments were done in which ten inexperienced test subjects volunteered to execute tasks using the simulated KUKA model. These tasks included a task of positioning accuracy, while moving in between and pausing on setpoints, and a task of careful interaction in which control efforts were to be minimised during an impact situation. During these experiments, relatively low and high constant impedance settings were tested versus the designed variable impedance setting that scaled between these low and high impedance levels. The test subjects were never aware of their ability to change the impedance level of the controller through their muscle activation to test the intuitiveness of the design.

The functionality experiments confirmed the expectations, showing a fully functional controller when implemented on the simulated model but a large decrease in functionality when the KUKA hardware was used. This indeed seems to be the result of quite significant friction present in the joints of the hardware. From the data that was gathered during the experiments with test subjects, it was seen that the co-contraction behaviour showed the expected results, creating a stiffer connection between the master and slave devices during the accuracy experiment than during the impact experiment. This resulted in a combination of good results in both the accuracy and impact experiments, creating relatively low positioning errors and low controller efforts. The constant low and high impedance settings performed relatively good during some of the experiments but never during both the accuracy and the impact experiment.

Although the first results seem promising for the designed impedance modulation approach, this research is concluded by presenting recommendations for future work. As indicated, the implementation on the actual KUKA hardware was troublesome, so either an alternative robotic slave device or an adjustment of the slave controller is suggested. The slave controller could for instance be extended with a form of dynamics (e.g. friction) compensation. Furthermore, only two tasks were tested during the conduction of this research. The addition of more tasks, including other requirement and a combination of requirement in one task are suggested. More information on the execution of telemanipulation tasks could also be gathered by using a larger variety of experience of the operators, investigating what the role of awareness of the impedance modulation through muscle activation for the operator will be and to add subjective measures to the collection of data to get a better understanding of the operator experience and intuition.

Contents

1 Introduction	1
1.1 Context	1
1.2 Problem statement	1
1.3 Related work	2
1.4 Research goal	3
1.5 Overview	3
2 Background	5
2.1 Teleoperation control	5
2.2 Available hardware and software	6
3 Analysis	11
3.1 Teleoperation system outline	11
3.2 Transparency	11
3.3 Stability	16
3.4 Variable impedance control based on human motor behaviour	20
3.5 Estimation of human impedance levels	21
3.6 Hypotheses	24
4 Design	27
4.1 Estimation of co-contraction levels	27
4.2 Outline of master and slave controllers	30
4.3 Transparency layer	31
4.4 Stability layer	33
4.5 Kinematic and dynamic KUKA models	40
4.6 Quantifying parameter settings	42
4.7 Implementation	44
5 Experiments	47
5.1 Validating the functional design	47
5.2 Indication of static friction levels in the KUKA hardware	48
5.3 Experiments using test subjects	48
5.4 Data collection and analysis	53
6 Results	55
6.1 Validating the functional design	55
6.2 Indication of static friction levels in the KUKA hardware	59
6.3 Calibration of the co-contraction level estimation	61

6.4 Task execution in simulation	62
7 Conclusions	69
8 Recommendations	73
Appendices	75
A Indication of static friction in KUKA joints	75
B Results of the calibration procedures using test subjects	75
C Results of the accuracy experiments using test subjects	76
D Results of the impact experiments using test subjects	77
E Plots of example results of the accuracy experiments	78
F Plots of example results of the impact experiments	82
G Implementation and use of software packages	86
Bibliography	89

List of Figures

1.1 Pictures of the used hardware components	3
2.1 Overview of joint configurations and names in the KUKA LWR 4+ robotic arm	7
3.1 Simple schematic overview that illustrates the basic interactions between components found in a 1-DOF haptic teleoperation system	11
3.2 Simplified schematic representation of a 1-DOF haptic teleoperation system using an impedance controller as virtual connection	12
3.3 Simple schematic overview that illustrates the basic energetic interactions and communicated variables in an impedance controlled haptic teleoperation system	14
3.4 Simplified schematic representation of a 1-DOF haptic teleoperation system using an impedance controller and a PP communication architecture	15
3.5 Simplified schematic representation of a 1-DOF haptic teleoperation system using an impedance controller and a PF communication architecture	15
3.6 Force application of a linear spring when compressed and extended around its centre position in continuous-time and discrete-time	16
3.7 Visual interpretation of the energy levels and active behaviour of two virtual springs with relatively low and high stiffness values	17
3.8 Schematic example of flexion and extension motions of the human fingers and forearm	21
3.9 Schematic cross-sectional view of the human forearm, just below the elbow	22
4.1 Schematic cross-sectional view of the human forearm, just below the elbow including possible placement of Myo electrodes	27
4.2 Test results of second-order Butterworth low-pass filtered activation level signals versus the original signal received from the Myo Armband	29
4.3 Outline of the omega.7 master controller and the KUKA slave controller	30
4.4 Simple schematic representation of the designed haptic teleoperation system	31
4.5 Energy tank levels in time for switching virtual stiffness levels at time instant k without using energy compensation for impedance modulation	36
4.6 Energy levels of two impedance controllers with different stiffness levels for a constant positional error resulting in different controller efforts	37
4.7 Expected energy tank levels in time for switching virtual stiffness levels at time instant k while using the designed compensation algorithm	37
4.8 Energy levels and difference in clipped energy for two impedance controllers with different stiffness levels for a constant positional error and constant force limitation	38
4.9 Screenshots of the KUKA LWR4+ model simulated in Gazebo in a wall mounted configuration	40
4.10 Schematic overview of the implementation of the discussed design in the teleoperation system as a whole	45

5.1	Set-up configurations during the functional design validation experiments	47
5.2	Photo of the experiment set-up used during the experiments with test subjects .	48
5.3	Screenshot of the camera angle during the accuracy experiments	51
5.4	Screenshot of the camera angle during the impact experiments	52
6.1	Results of the functionality experiment in 3-DOF without any added communication delay while using the simulated KUKA robot	55
6.2	Results of the functionality experiment in 3-DOF with an added communication delay while using the simulated KUKA robot	56
6.3	Results of the functionality experiment in 3-DOF while using the real KUKA robot	57
6.4	Results of the experiment that validates the energy compensation method for impedance modulation	58
6.5	Commanded torques in every joint of the KUKA slave robot during the 3-DOF functionality experiment	60
6.6	Example results of a calibration procedure for estimating the co-contraction levels of the user	61
6.7	Results of the accuracy experiment versus the results of the impact experiment while no communication delay was added to the system	63
6.8	Results of the accuracy experiment versus the results of the impact experiment while a communication delay was added to the system	63
6.9	Overall mean absolute positioning errors for all tested impedance levels and communication delay settings	65
6.10	Overall mean absolute peak controller forces for all tested impedance levels and communication delay settings	67
E.1	Example result of the accuracy experiment for the low impedance setting without added communication delay	78
E.2	Example result of the accuracy experiment for the high impedance setting without added communication delay	78
E.3	Example result of the accuracy experiment for the variable impedance setting without added communication delay	79
E.4	Example result of the accuracy experiment for the low impedance setting with the added communication delay	80
E.5	Example result of the accuracy experiment for the high impedance setting with the added communication delay	80
E.6	Example result of the accuracy experiment for the variable impedance setting with the added communication delay	81
F.1	Example results of the impact experiment for the low impedance setting without the added communication delay	82
F.2	Example results of the impact experiment for the high impedance setting without the added communication delay	82
F.3	Example results of the impact experiment for the variable impedance setting without the added communication delay	83

F.4	Example results of the impact experiment for the low impedance setting with the added communication delay	84
F.5	Example results of the impact experiment for the high impedance setting with the added communication delay	84
F.6	Example results of the impact experiment for the variable impedance setting with the added communication delay	85

List of Tables

2.1	Overview of relevant specifications of the Force Dimension omega.7 haptic device	6
2.2	Overview of relevant specifications of the KUKA LWR 4+ robotic arm	7
3.1	Muscles found in the human forearm related to flexion and extension of the forearm and fingers	22
3.2	Relative advantages and disadvantages of relatively low and high impedance settings of a haptic teleoperation controller	24
4.1	Relevant functions of the forearm and fingers with corresponding muscles and Myo electrode numbers	28
4.2	Recommended parameter settings	42
5.1	Overview of all parameters that were recorded during the experiments	53
6.1	Computed static friction torques in the KUKA joints for clockwise and counter-clockwise rotations	59
6.2	Maximum values of the absolute joint torques that were commanded during the 3-DOF functionality experiment for every direction of end effector motion	60
6.3	Overall mean values and standard deviations of the absolute positioning errors recorded during the accuracy experiments	62
6.4	Overall mean values and standard deviations of the absolute peak controller forces recorded during the impact experiments	62
6.5	Overall mean co-contraction levels during the accuracy experiments for periods of pausing, moving and these periods combined	64
6.6	Percentage of change in overall mean absolute positioning error and the corresponding <i>p</i> -values when comparing the low impedance setting to the high and variable impedance settings	65
6.7	Percentage of change in overall mean absolute positioning error and the corresponding <i>p</i> -values which resulted from the addition of the communication delay	65
6.8	Overall mean co-contraction levels during the impact experiments	66
6.9	Percentage of change in overall mean absolute peak controller forces and the corresponding <i>p</i> -values when comparing the high impedance setting to the low and variable impedance settings	67
6.10	Percentage of change in overall mean absolute peak controller forces and the corresponding <i>p</i> -values which resulted from the addition of the communication delay	67
A.1	Computed static friction torques in the KUKA joints for clockwise and counter-clockwise rotations	75
B.1	Maximum extensor and flexor muscle activation levels established during the calibration procedures	75
C.1	Overview of the results of the accuracy experiments without the added communication delay	76

C.2 Overview of the results of the accuracy experiments with the added communication delay	76
D.1 Overview of the results of the impact experiments without the added communication delay	77
D.2 Overview of the results of the impact experiments with the added communication delay	77

Abbreviations and symbols

Abbreviations

Abbreviation	Definition
DOF	Degree Of Freedom
EMG	Electromyography
ETP	Energy Transfer Protocol
FRI	Fast Research Interface
ROS	Robot Operating System
PC	Passivity Controller or Personal Computer
PD	Proportional-Derivative (controller)
PF	Position-Force (architecture)
PO	Passivity Observer
PP	Position-Position (architecture)
SETP	Simple Energy Transfer Protocol
TLC	Tank Level Controller

Symbols - Latin

Symbol	Unit	Definition (for $i = m$ (master) or s (slave))
d_j	[–]	Joint specific damping ratio setting in the KUKA FRI
D_h	[N·m·s/rad]	Damping characteristic of the human arm
D_v	[N·m·s/rad]	Virtual joint damping
$D_{v,max}$	[N·m·s/rad]	Maximum virtual joint damping
$D_{v,min}$	[N·m·s/rad]	Minimum virtual joint damping
$F_{c,i}$	[N]	Clipped impedance control actions for device i
F_{clip}	[N]	General constant controller action limitation
F_e	[N]	Forces applied by the environment
F_{fr}	[N]	Measured static friction forces
F_h	[N]	Forces applied by the human operator
F_i	[N]	Forces applied to device i
$F_{i,max}$	[N]	Impedance control action upper bound for device i
$F_{K,i}$	[N]	Impedance control actions for device i
$\tilde{F}_{K,i}$	[N]	Delayed impedance control actions for device i
F_{PD}	[N]	PD control actions
F_{TLC}	[N]	Forces commanded by the TLC
H_a^b	[–]	Homogeneous transformation matrix from frame a to frame b
H_{clip}	[J]	Clipped energy as a result of saturation of control actions
ΔH_{clip}	[J]	Energy change due to control action clipping
H_D	[J]	Desired minimum energy tank level
$\Delta H_{e,i}$	[J]	Energy exchanged with the environment by device i
$\Delta \tilde{H}_{e,i}$	[J]	Estimated future energy exchange with the environment
H_i	[J]	Energy tank level of device i
\tilde{H}_i	[J]	Estimated future energy tank level of device i
$H_{i,des}$	[J]	Energy tank level desired by transparency layer of device i
ΔH_{K_v}	[J]	Energy change due to impedance modulation
$H_{+,i}$	[J]	Incoming energy flow for device i
$H_{-,i}$	[J]	Outgoing energy flow for device i
$J(q)$	[–]	Jacobian matrix
k	[–]	Sample instant
k_j	[N·m/rad]	Joint specific stiffness setting in the KUKA FRI

Symbols - Latin (continued)

Symbol	Unit	Definition (for $i = m$ (master) or s (slave))
K_{dis}	[N/m]	Virtual stiffness of disabled DOFs
K_h	[N/m]	Stiffness characteristic of the human arm
K_{rot}	[Nm/rad]	Virtual stiffness of rotational DOFs
K_v	[N/m]	Virtual stiffness level
$K_{v,max}$	[N/m]	Maximum virtual stiffness level
$K_{v,min}$	[N/m]	Minimum virtual stiffness level
o_a^b	[m]	Translation of the origin of frame a with respect to frame b
q	[rad]	Collection of robot joint angles
\dot{q}	[rad/s]	Collection of robot joint velocities
q_{max}	[deg]	Collection of maximum KUKA joint angles
\dot{q}_{max}	[deg/s]	Collection of maximum KUKA joint velocities
q_s	[rad]	Collection of slave robot joint angles
\dot{q}_s	[rad/s]	Collection of slave robot joint velocities
r	[cm]	Radius of force application measured from joint centre
R_a^b	[–]	Rotation matrix from frame a to frame b
$T_a^{c,b}$	[m/s, rad/s]	Twist of frame a with respect to frame b expressed in frame c
$\hat{T}_a^{c,b}$	[–]	Unit twist of a with respect to frame b expressed in frame c
ΔT_s	[sec]	Length of a sample period
$v_a^{c,b}$	[m/s]	Translational velocity of a with respect to b expressed in c
$W^{a,b}$	[N, Nm]	Wrench applied to frame a expressed in frame b
X_c	[m]	Positional error at which control actions get clipped
X_e	[m]	Positional error of an impedance controller
\dot{X}_e	[m/s]	Velocity of the environment
\dot{X}_h	[m/s]	Velocity of (the arm of) the human operator
X_i	[m]	Position of device i
\tilde{X}_i	[m]	Estimated position of device i
\dot{X}_i	[m/s]	Velocity of device i

Symbols - Greek

Symbol	Unit	Definition
α	[–]	Unitless muscle activation level
$\hat{\alpha}$	[–]	Normalised muscle activation level
α_{max}	[–]	Defined maximum muscle activation level
α_{min}	[–]	Defined minimum muscle activation level
α_{flex}	[–]	Flexor muscle activation level
α_{ext}	[–]	Extensor minimum muscle activation level
β	[–]	Transferred fraction of the energy tank level
γ	[N·s/m·J]	Damping parameter of the TLC in the stability layer
η	[–]	Estimated co-contraction level
$\tilde{\eta}$	[–]	Delayed estimated co-contraction level
τ_{Cmd}	[Nm]	KUKA torques commanded by the FRI
$\tau_{D,s}$	[Nm]	Joint damping torques in the slave device
τ_{FRI}	[Nm]	Superposed torque command in the FRI
τ_{max}	[Nm]	Maximum torque application in the KUKA joints
τ_s	[Nm]	Torques applied to the slave device
$\omega_a^{c,b}$	[rad/s]	Angular velocity of a with respect to b expressed in c
$\omega_{c,lp}$	[Hz]	Corner frequency of a low-pass filter
ω_{loop}	[Hz]	Loop frequency of the controllers

1 Introduction

1.1 Context

The well-developed sensory and motor skills that humans possess allow them to effectively interact with a variety of environments. While they perceive their environment through the human senses like sight and touch, they are able to modulate their force application and the compliance of their limbs to dexterously interact with the environment. By modulating these dynamic properties, humans can create the desired manipulation behaviour corresponding to the tasks they are conducting. This task-dependent behaviour allows for a wide range of manipulation tactics, like increasing limb compliance in order to carefully handle delicate objects or decreasing limb compliance to reject disturbing forces (Ajoudani et al., 2012; Brygo et al., 2015; Hill and Niemeyer, 2009; Shin et al., 2015; Walker et al., 2010).

However, humans are not always able to perform tasks safely or efficiently in some environments like space, underwater or when toxic or nuclear materials are involved (Hashttrudi-Zaad and Salcudean, 2001; Hokayem and Spong, 2006; Niemeyer and Slotine, 1991).

Robotic systems on the other hand can be designed such that they can work in these human unfriendly environments, but generally lack the necessary dexterous manipulation skills. Introducing advanced teleoperated robots could bridge the gap between the human dexterous manipulation skills and a robotic system that is designed to work in these environments. Tele-operated robots are remotely controlled by human operators to conduct tasks over a distance while feedback is presented to the operator in many possible forms like vision, audio, forces and vibrations. The research described in this thesis focusses on the haptic control of a robotic arm during which force feedback is provided to the operator. This forms a human-machine interaction which is aimed at projecting human manipulation skills to a remote environment (Chen et al., 2016; Walker et al., 2010).

The design of teleoperated robotic systems involves challenges in creating the feeling of tele-presence for the operator and ensuring stable and safe control of the robotic devices (Hogan, 1989; Hokayem and Spong, 2006). These challenges are faced in the joint innovation centre i-Botics, a collaboration between TNO and the University of Twente. A teleoperation platform is currently being developed within i-Botics, during which research is focussed on establishing effective, intuitive and safe teleoperation control.

1.2 Problem statement

One of the main challenges in the design of teleoperation systems that provide force feedback to the operator is dealing with time delays that occur when communicating with the teleoperated robot over a distance. These delays can especially be problematic in environments characterised by time-varying dynamics, since the human reaction to these changing dynamics will be delayed by the round-trip time of the communication channel (Hashttrudi-Zaad and Salcudean, 2001; Kim et al., 2005; Lawrence, 1993).

As a consequence, the safety levels of the teleoperation system and its environment can be negatively affected as this delayed reaction can lead to increased interaction forces between the robot and the remote environment (Ajoudani et al., 2012; Brygo et al., 2015; Walker et al., 2010).

It can be stated that the dexterity of responses to varying dynamics which humans can create through their compliant body dynamics is (partly) lost when the system is subjected to communication delays. Since communication delays will always be present while exchanging information over a distance, the aim is to find another way of projecting the dynamic properties

of the human limbs such that the negative effects on the execution of telemanipulation tasks can be decreased. On top of that, it might be possible to create a more intuitive experience for the operator. Therefore, the main problem that will be studied in the proposed research is stated as the following:

"Can the dexterous compliant dynamic properties of the human limbs be captured and projected to a haptic controlled teleoperation system and will this allow for more effective and intuitive execution of telemanipulation tasks?"

In order to capture the dynamic characteristics of the human limbs, this research will investigate the potential of using electromyography (EMG). With EMG, myoelectric signals are measured that are sent to the muscles through the human central nervous system in order to activate them. These measured voltage levels can give an indication of the activation levels of muscles, from which an estimation of the dynamic properties can be determined. This estimation can be used at the remote site to respond to sudden changes in environment dynamics in a way that is similar to the human behaviour, without having to rely on information of the actual human reaction that is subjected to round-trip communication delays.

1.3 Related work

Several attempts in solving this problem were found in literature. Focus is placed on teleoperated robots (slave devices) that are controlled by human operators through a haptic device (master device) which presents information on the interaction forces at the remote site through force feedback. Chen et al. (2016) conclude on positive results for the use of EMG, claiming that they were able to control a teleoperated robot more intuitively while increasing the tracking performance as well. The actual effect on safety aspects like interaction forces were not studied in this research. Further indications that EMG can be used to identify human limb dynamics are presented by Ajoudani et al. (2012). Although this research presents the use of EMG as an alternative to force feedback in teleoperation systems, it does show the extent to which EMG can be used in estimating the human limb characteristics. The research shows an identification method for mass, stiffness and damping properties of the human arm in 3D, using EMG data from six relevant muscles.

Besides the use of EMG, other methods for estimating human dynamic characteristics have been applied in combination with force feedback in teleoperated robots. Research presented by Walker et al. (2010) shows the use of a gripper on the master device that is able to measure the grip pressure of the user and relates this data to the desired behaviour of the teleoperated robot. A tighter grip should then result in less compliant behaviour of the robot. This research shows clear benefits of using the variable compliant control on the robotic teleoperation system, mainly in reducing interaction forces in several situations.

Further research on estimating the desired robotic behaviour based on the human characteristics was found in which Hill and Niemeyer (2009) used active vibrations of the master device to measure the response of the human arm. Based on this response the dynamic properties of the arm can be estimated continuously and they suggest that this estimation can be used in a teleoperation system with variable compliance. Brygo et al. (2015) related the robotic behaviour to the load conditions as would be done by humans as well and finally, Shin et al. (2015) related the desired robotic behaviour to the recorded posture of the operator. Although these last publications show similarities in the addressed problem, none of them show clear experimental results on the effects of their control approaches.

1.4 Research goal

From the information on the context and the stated problem the following is stated as the main goal of this research:

"Create a teleoperation system that presents force feedback to the operator in which EMG data from the operator's muscles is implemented in the control architecture to increase the intuitiveness and effectiveness of the execution of telemanipulation tasks while the system is subjected to time delays in its communication channel."

A teleoperation system will be created from available hardware in an attempt to reach this goal. Figure 1.1 shows the devices that will be used in the design of this set-up. The master device that registers the operator's motions and applies force feedback is the omega.7 haptic device by Force Dimension, EMG data will be collected through a Myo Gesture Control Armband by Thalmic Labs and teleoperated slave robot will be a KUKA LWR4+ robotic arm. A computer simulated model of this KUKA robotic arm will be used as well in this research.

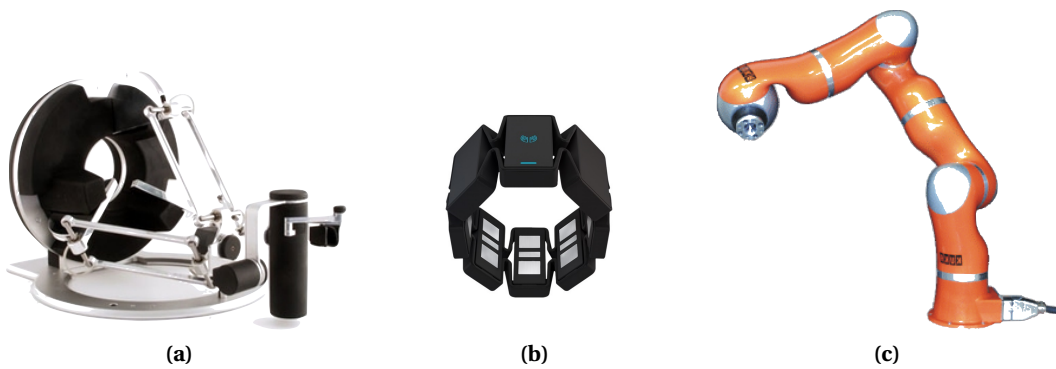


Figure 1.1: Pictures of the used hardware components: (a) Force Dimension omega.7 (master device), (b) Myo Gesture Control Armband (EMG data collector) and (c) KUKA LWR4+ (teleoperated robotic arm). Image credits: Force Dimension website (retrieved June 14th 2017), Myo website (retrieved June 21th 2017) and KUKA Roboter GmbH (2012).

1.5 Overview

After the introduction that is presented here in Chapter 1, Chapter 2 will present some necessary background information on the subjects that are included in this research. It presents the basics of teleoperation control and robotic manipulator control and more details on the available hardware and software. In Chapter 3 the stated problem and possible solutions will be further analysed from which a general approach will be derived to create the desired teleoperation system. At the end of the chapter, the hypotheses of this research are stated based on these analyses. Chapter 4 will then detail the design of the teleoperation set-up, including the estimation method for capturing human limb dynamics, the functioning of the controllers and the implementation of these components on the hardware. In Chapter 5, the design of experiments is detailed which were conducted to collect data on the functioning of the presented design. Chapter 6 presents and interprets the results of these experiments. Finally, Chapter 7 will review and discuss the conclusions of this research, followed by recommendations for future work in Chapter 8.

2 Background

Information in this chapter purely functions as background information on the subjects that are addressed in this research. Readers familiar with one or more of these subjects can skip the corresponding sections. It includes some general information on teleoperation control, robotic manipulator control and specifications of the used hardware and software.

2.1 Teleoperation control

In order to create an effective teleoperation system, the teleoperated robot can be designed such that its sensory and motor systems resemble those of the human operator. By connecting the sensory and motor information of both the robot and the operator, an intuitive experience can be created for the operator. Terms generally found in haptic control, including telepresence, haptic feedback, transparency and stability, will be introduced in this section.

2.1.1 Telepresence

Telepresence describes the extent to which the operator will feel like he or she is conducting a task directly at the remote site (Chen et al., 2016; Lawrence, 1993). Increasing the amount of telepresence can for instance be accomplished through video and audio feeds and haptic feedback. The greater the feeling of telepresence for the operator is, the better he or she will be able to perform tasks in an intuitive way.

2.1.2 Haptic feedback

Over the past decades, the connection between the haptic senses of operators and the tele-operated robots has been studied in order to increase the level of telepresence. The human haptic senses create a tangible perception of the environment by gathering information on aspects like motion, forces, shape, compliance, temperature, texture and vibration. The research that is presented here focusses on haptic feedback in the form of force feedback, which will be applied by a haptic interface (joystick) that can be used to register the operator's motions to control the robot while also being able to apply forces to the operator. This way, information on the dynamic interactions that occur at the remote site can be reflected to the operator. Although haptic feedback creates a great step toward a more intuitive experience for operators, it involves challenges in creating the right feeling of telepresence while guaranteeing stable control of all devices.

2.1.3 Transparency

Closely related to the level of telepresence is the level of transparency. This property is defined as the level in which the teleoperation system is able to accurately control the teleoperated robot and reflect the interaction forces (Hashttrudi-Zaad and Salcudean, 2001; Kim et al., 2005; Lawrence, 1993). This forms the part of the feeling of telepresence related to the robotic devices. A high level of transparency is generally aimed for in the design of teleoperation architectures to increase the effectiveness and intuitiveness of the remote execution of tasks. However, increasing the levels of transparency often increases the risk of instability.

2.1.4 Stability

In controlling any robotic device, stability should always be guaranteed in order to minimise safety risks for the operator, the devices and the environments they are in. Furthermore, unstable behaviour will harm the transparency level of a teleoperation system. Because haptic teleoperation systems have to deal with uncertain dynamics of the environment and a human operator, guaranteeing passivity is often used as a tool with which robust stability can

be guaranteed (Colgate and Schenkel, 1997; Hannaford and Ryu, 2002). A passive component is defined as a component that does not generate energy; the energy input can only be stored or dissipated. Consequently, energy supplied by this component can never exceed the energy stored in the system (Colgate and Schenkel, 1997; Niemeyer and Slotine, 1991). Furthermore, interconnecting passive components results in a system that is stable by definition (Colgate and Schenkel, 1997; Niemeyer and Slotine, 1991; Hogan, 1989).

2.2 Available hardware and software

The hardware components and software packages that are used during this research are discussed in this section. Furthermore, some additional information is provided on the Cartesian and joint space control of a multi-DOF robot like the KUKA arm.

2.2.1 Hardware

Force Dimension omega.7

The Force Dimension omega.7 is a haptic device with 7 degrees of freedom (DOFs). The Cartesian coordinate frame is defined such that the large disc visible in Figure 1.1a is located in the (y, z) -plane with the x -axis perpendicular to the disc. Table 2.1 gives an overview of the relevant specifications of the omega.7. This haptic device allows for encoding translations along and rotations around the three axes, plus encoding the translation of the gripper. Furthermore, force feedback can be implemented along all translation axes, including the gripper. The most obvious limitation is that no torque feedback is possible around the axes of rotation.

DOFs	Workspace	Force application
Translation	x -axis: 110 [mm] (y, z) -plane: \varnothing 160 [mm]	12 [N]
Rotation	q_x : 240 [deg] q_y : 140 [deg] q_z : 180 [deg]	N/A
Grasping	Stroke: 25 [mm]	8 [N]

Table 2.1: Overview of relevant specifications of the Force Dimension omega.7 haptic device.

Source: brochure on Force Dimension website (retrieved June 14th 2017)

Myo Gesture Control Armband

The Myo Gesture Control Armband is a light wearable developed by Thalmic Labs. It can be worn around the forearm, where it uses eight sets of electrodes to receive EMG data from superficial muscles. A software development kit is available which allows for reading levels of muscle activation from the Myo Armband through a Bluetooth connection. It can provide an array of eight integer values corresponding to each electrode at 50 [Hz]. These integers are unitless measures for the muscle activation levels, based on the EMG readings.

KUKA LWR4+

The KUKA LWR4+ is a 7-DOF robotic arm with a working envelope of 1.84 [m^3] and a weight of 16 [kg]. Figure 2.1 presents an overview of the location, orientation and names of the seven joints and Table 2.2 gives an overview of range (q_{max}), maximum speed (\dot{q}_{max}) and maximum torque (τ_{max}) of these joints.

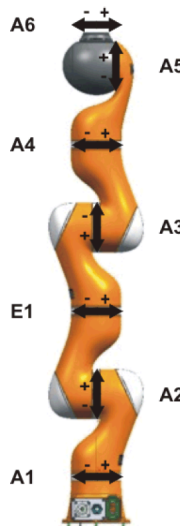


Figure 2.1: Overview of joint configurations and names in the KUKA LWR 4+ robotic arm. Image credit: (KUKA Roboter GmbH, 2012)

Joint name	q_{max} [deg]	\dot{q}_{max} [deg/s]	τ_{max} [Nm]
A1	± 170	110	176
A2	± 120	110	176
E1	± 170	128	100
A3	± 120	128	100
A4	± 170	204	100
A5	± 120	184	38
A6	± 170	184	38

Table 2.2: Overview of relevant specifications of the KUKA LWR 4+ robotic arm. Source: KUKA Roboter GmbH (2012)

The KUKA arm has its own controller named the ‘KRC’, which can be accessed at low-level and at high control rates through the Fast Research Interface (FRI) (Schreiber et al., 2010). This allows for instance for the implementation of the following joint specific impedance control law:

$$\tau_{Cmd} = k_j(q_{FRI} - q_{msr}) + D(d_j) + \tau_{FRI} + f_{dynamics}(q, \dot{q}, \ddot{q}) \quad (2.1)$$

Here, τ_{Cmd} is control actions that is commanded to the joint actuators, k_j includes the joint specific stiffness values representing a virtual torsional spring between q_{FRI} , the desired angular positions of the joints and q_{msr} , the current angular positions of the joints. Furthermore, normalised damping parameters included in the damping ratio d_j can be added to the joints, reaching from no damping ($d_j = 0$) to critical damping ($d_j = 1$). Finally, additional torques can be superposed in τ_{FRI} . The FRI will add a compensation of certain dynamics, $f_{dynamics}(q, \dot{q}, \ddot{q})$. It is known that this contains the options of gravity compensation, other forms of dynamics compensation are unknown. The variables \dot{q} and \ddot{q} might suggest a compensation of (parts of the) friction and inertia of the robot.

So far, all commands and variables are expressed in the robot’s joint space. Because the omega.7 is commanded in Cartesian space and the joint spaces of the two devices do not match, it will be desired to control the KUKA arm in Cartesian space as well. Assuming all

link lengths and joint configurations presented in Figure 2.1 are known, the configuration of the distal end (the end effector) of the robot can be expressed in the frame of its proximal end (its base). Going from joint to joint along the robot, every link will have its own frame which is rotated and translated with respect to the previous one. Such a combined rotation and translation can for instance be represented in a homogeneous matrix:

$$H_a^b = \begin{bmatrix} R_a^b & o_a^b \\ \mathbf{0} & 1 \end{bmatrix} \quad (2.2)$$

This represents the transformation from frame a to frame b , containing the rotation matrix R from a to b and a translation o of the origin from a to b . When multiplied by a vector corresponding to a point in frame a expressed as $[x_a, y_a, z_a, 1]^T$, the expression of this point in frame b results. Once every individual homogeneous matrix along the robot's length is known, the chain rule can be applied to find the configuration of the end effector frame (n) expressed in the base frame of the robot (0):

$$H_n^0 = H_1^0 H_2^1 \dots H_n^{n-1} \quad (2.3)$$

The homogeneous matrix H_n^0 then gives the information on the position and orientation of the robot's end effector with respect to its base.

Another mathematical approach that is often used to relate the joint space and the Cartesian space of the robot is the use of a geometric Jacobian. This matrix, often expressed as $J(q)$, relates the joint velocities of the robot to the velocity of its end effector. In screw theory, these Cartesian velocities are expressed as twists like the following:

$$T_a^{c,b} = \begin{bmatrix} \omega_a^{c,b} \\ v_a^{c,b} \end{bmatrix} \quad (2.4)$$

Here, $T_a^{c,b}$ is the twist of frame a with respect to frame b , expressed in frame c . It consists of an angular velocity ω and a linear velocity v . With a Jacobian matrix, the twist of the end effector with respect to the robots base, expressed in the frame of this base, can be found when the angular velocities of the joints are known:

$$T_n^{0,0} = J(q)\dot{q} \quad (2.5)$$

Twists can also be used to create the contents of the Jacobian matrix. The Jacobian is a collection of unit twists, expressed as \hat{T} . In a unit twist, the length of the vector ω is equal to one or if ω is zero, the length of the vector v should be equal to one. All unit twist express the motion of a link with respect to the previous link in the base frame of the robot:

$$J(q) = [\hat{T}_1^{0,0} \hat{T}_2^{0,1} \dots \hat{T}_n^{0,n-1}] \quad (2.6)$$

This Jacobian can also be used to compute joint torque commands for the robot when a certain combination of end effector force and torque is desired. This combination is called a wrench in screw theory. In the equation below, the transposed Jacobian matrix is used to find joint torques that correspond to a wrench ($W^{0,n}$) applied to the robot's end effector while it is expressed in the robot's base frame:

$$\tau = J^T(q) W^{0,n} \quad (2.7)$$

2.2.2 Software

Robot Operating System (ROS)

In building the proposed teleoperation system, several hardware components will need to be connected to each other through a digital controller. In order to let the different components communicate with this controller, the Robot Operating System (ROS) will be used. ROS offers a framework for writing robotic control software by supplying sets of tools, libraries and conventions which should simplify this communication task. It is aimed at collaborative software development which makes it very useful in connecting the different pieces of hardware through software (ROS website, retrieved July 10th 2017).

All components of the communication structure, like code that controls the hardware or code that includes the general control algorithms, will be written (or already exists) in the form of ROS nodes. These nodes can communicate with each other through topics. Nodes can publish data on these topics and/or subscribe to receive data from the topic. This data is transferred in the form of messages of basic types which allows for independent communication between nodes. Furthermore, nodes can request services from other nodes. Code for the ROS nodes will either be reused from other projects or created for the requirements of the proposed research.

Gazebo

Gazebo is a simulation tool suitable for robotic simulations. It includes a physics engine for realistic simulation of robotic interactions which can be projected through 3D graphics as well. Gazebo offers a connection to ROS which offers a good environment for testing the created controller and its communication (Gazebo website, retrieved July 14th 2017).

3 Analysis

This chapter presents an overview of the analyses conducted during this research to come to a design strategy. It discusses a general teleoperation system outline, after which transparency and stability properties, problems and solutions are discussed. Next, useful literature is discussed in more detail regarding the stated problem and the possibilities of using EMG to solve this problem are discussed. Finally, hypotheses are stated based on the presented analyses.

3.1 Teleoperation system outline

Generally, a haptic controlled teleoperation system that reflects forces to the operator consists of the following components: a human operator that holds a haptic interface (master device), a robotic manipulator (slave device) that interacts with the remote environment and a connection between the two devices that consists of controllers and a communication channel. These components are schematically depicted in Figure 3.1. The components all interact with each other, whether through software or physically. Shaping the interactions is what will be most important when designing the teleoperation system, since the hardware components are known and the system should work for any variety of human operators and environments. As indicated in the figure, focus is therefore placed on designing the controllers and a communication channel, including their interactions with the hardware components.

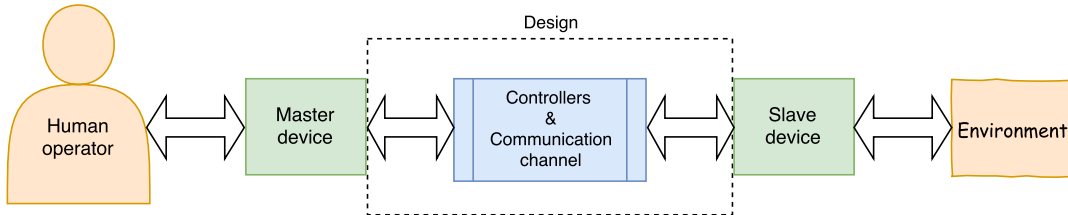


Figure 3.1: Simple schematic overview that illustrates the basic interactions between components found in a 1-DOF haptic teleoperation system.

An energy-based analysis approach is often adopted in designing haptic controlled architectures since stability is often guaranteed through the passivity theorem (Colgate and Schenkel, 1997; Niemeyer and Slotine, 1991; Hannaford and Ryu, 2002; Hogan, 1989). When designing the hardware controllers and the communication channel, the energetic interactions between the components of the system are shaped and passivity can be analysed while striving for the highest level of transparency possible.

3.2 Transparency

The transparency level that results from the energetic interactions between the master and slave devices depends on hardware and design choices. Therefore, the used hardware will be analysed to further specify the inputs and outputs of the controllers. Then, a suitable interaction control strategy between the hardware components is determined. Finally, the methods for transparency control that fit this approach are presented and discussed.

3.2.1 Analysis of the hardware

Within the energy-based analysis approach, hardware devices are often viewed as either being of impedance or admittance type, based on the preferable type of energy exchange (causality) (Hashttrudi-Zaad and Salcudean, 2001; Ott et al., 2010). Impedance type devices preferably receive a force or torque command based on their measured position and are characterised

by dynamic properties like low inertia, low friction and high backdrivability. Admittance type devices preferably receive a position or velocity command as a response to measured forces or torques and are characterised by relatively high inertia and friction properties, for instance caused by heavy gearing.

Based on the description of the characteristics, the omega.7 haptic device can clearly be qualified as being of the impedance type. It has low inertia and friction properties and it is able to execute force commands while data on positions and velocities can be read from the system. The KUKA arm on the other hand is harder to qualify. It possesses more inertia and friction than the omega.7, but when considering its size and degrees of freedom it is a relatively light-weight robotic arm in its class. As discussed in Chapter 2, the KUKA arm can be controlled through its FRI which will command actuator torques. This makes this robotic arm an impedance controlled device as well. However, its inertial and frictional properties might harm the transparency level of the system, especially during free-space motions (Ott et al., 2010).

When viewing both devices as preferably impedance controlled, a controller should be designed that creates the interaction between both the devices which suits their causality.

3.2.2 Interaction control

In order to create both an effective and safe robotic teleoperation system, both motion tracking and interaction force control are of importance (Brygo et al., 2015; Hill and Niemeyer, 2009; Walker et al., 2010). Generally speaking, admittance type devices provide high levels of motion tracking accuracy but suffer from problems like instability when force commanding is desired, for instance when in contact with rigid objects. Impedance type devices can more easily be force controlled in a stable manner, but dynamic properties of the devices can harm the motion tracking capabilities (Ott et al., 2010).

Both devices used in this research will be impedance controlled, creating a fixed causality of the controller. The inputs will be based on the position and/or velocity information of the devices, while the outputs will be forces or torques. An impedance connection between two devices can be seen as a virtual spring, in which the level of transparency of the interaction is limited by the stiffness of this connection. Furthermore, virtual damping is generally added to reduce oscillatory behaviour of the virtual connection. During this research, this virtual damping will be added in every single joint of the KUKA arm. This way, damping is not subjected to the delays in communication between the master and slave devices. Furthermore, adding damping in every joint is preferred over Cartesian damping of the end effector because this will damp out kinetic energy in the robot's null space as well. Since the KUKA is a 7-DOF robot, it will be able to move its links without moving its end effector, which is generally referred to as motion in its null space. Figure 3.2 presents a simple schematic interpretation of such a virtual connection in a haptic teleoperation set-up while only representing 1-DOF for simplification.

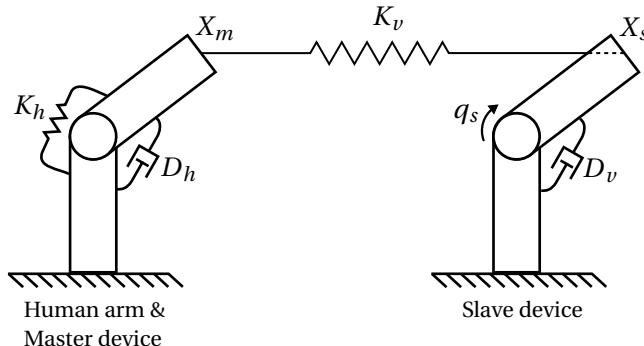


Figure 3.2: Simplified schematic representation of a 1-DOF haptic teleoperation system using an impedance controller as virtual connection.

Here, the arm of the human operator and the master device are seen as one, while possessing the stiffness and damping characteristics of the human arm (K_h and D_h respectively) and while the Cartesian end effector position is referred to as X_m . At this end effector position, one end of the virtual spring with stiffness K_v is attached while the other end is connected to the slave's end effector position X_s . Furthermore, virtual damping D_v is present in its joint which has a rotational displacement of q_s . The stiffness and damping properties present in the hardware are assumed to be negligible here. When the communication channel is disregarded, the implementation of the virtual stiffness will apply Cartesian forces $F_{K,m}$ and $F_{K,s}$ to the master and slave devices respectively:

$$\begin{aligned} F_{K,m} &= K_v \cdot (X_s - X_m) \\ F_{K,s} &= -K_v \cdot (X_s - X_m) \end{aligned} \quad (3.1)$$

Damping is added in the joints of the slave robot by commanding torques $\tau_{D,s}$ to the joints, depending on the angular velocity of the joints (\dot{q}_s):

$$\tau_{D,s} = -D_v \cdot \dot{q}_s \quad (3.2)$$

When aiming for the highest transparency level possible, K_v is generally maximised to represent the stiffest connection possible. This allows for the most accurate reflection of motion and forces. However, high values for K_v can also be the cause of the reported high interaction forces when the system is subjected to communication delays. When no delays are present, the remote environment will experience the slave device as having compliant properties similar to the human arm if $K_v \gg K_h$. When the human reaction is delayed through the communication channel, the behaviour that will be felt will be determined by the stiff connection made by K_v , leading to the high interaction forces. Lowering K_v permanently will however result in poor transparency, since the operator will feel a weak spring in between everything he or she touches and the motion tracking will be less accurate as well. Making K_v (and corresponding D_v) variable is a solution that was found in literature before (Chen et al., 2016; Hill and Niemeyer, 2009; Walker et al., 2010). This method is often referred to as impedance modulation, or the resulting variable impedance control. However, these attempts have been quite exploratory and do not focus on the design of a complete and stable system that includes time delayed communication. The research that is presented here will further investigate an impedance modulation strategy in haptic control by using EMG data from the operator's muscle activation.

3.2.3 Transparency control

Realising an impedance controlled teleoperation system can be accomplished with multiple control architectures. Many strategies have been discussed in literature, Hokayem and Spong (2006) present a basic overview of the most commonly used strategies. Although in theory full transparency can sometimes be achieved when no communication delay is present in the system (Hashtrudi-Zaad and Salcudean, 2001; Kim et al., 2005), it requires many information channels (like the four-channel architecture in which position and force information is exchanged for both master and slave device) and it requires accurate knowledge of the dynamics of the devices and its environments. Since the latter is almost never possible, extensive adaptive control schemes can be used to create accurate estimations of these dynamics. Because of the need of many sensors and complex control architectures, these methods are not further investigated in this research. It is expected that the functioning of the proposed variable impedance control strategy can be indicated with more simple, two-channel control approaches.

Figure 3.3 shows the architecture that can be used in creating the desired impedance interaction control. This scheme extends the analysis of Figure 3.1 and Equations 3.1 and 3.2 to include a communication channel.

In this scheme, the slave controller block contains the impedance controller that is used as the interaction controller on the slave side. This controller relies on an estimation of the master's end effector position (\tilde{X}_m). This is called an estimation because information on X_m can be subjected to communication delays. Because the slave device is located and controlled at a remote site, it is important that a local impedance controller is running here. In case of communication loss, the behaviour of the slave device will be stabilised by its local impedance controller.

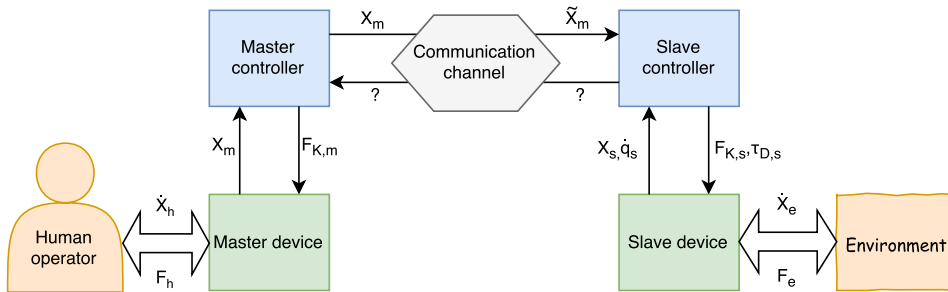


Figure 3.3: Simple schematic overview that illustrates the basic energetic interactions and communicated variables in an impedance controlled haptic teleoperation system.

On the master side, several types of master controllers can be implemented which rely on different types of information received through the communication channel, hence the question marks in the figure. Two approaches found in literature suit the scheme of Figure 3.3, generally referred to as the position-position (PP) architecture and the position-force (PF) architecture (Hashtroodi-Zaad and Salcudean, 2001; Lawrence, 1993). These names indicate the two parameters that are sent through the communication channel: both rely on the master controller sending position information to the slave controller, while the slave controller can either send position information (PP) or force information (PF). The difference between these approaches will be analysed here.

Position-position (PP) architecture

Figure 3.4 shows a simplified sketch of a teleoperation system subjected to time delays in its communication channel while using the PP architecture. It can be interpreted as having two impedance controllers, one on the master and one of the slave side. This configuration has a few benefits. As long as \tilde{X}_s and \tilde{X}_m are stable and the impedance controllers show stable behaviour, both devices will be stable because of their individual controllers. Furthermore, the impedance of the controller will always be felt at both sides, even if time delays or communication losses occur. However, the general drawback of this configuration is that it can be overly conservative. The amount of energy that is injected by the user into this system is determined by the impedance controller on the master side, which does not always match the amount of energy that is used by the robotic slave by definition. Energy can get lost in the communication channel and the amount of energy that is communicated is not immediately recognisable like it is in the PF architecture. These issues are discussed in more detail by Franken et al. (2012).

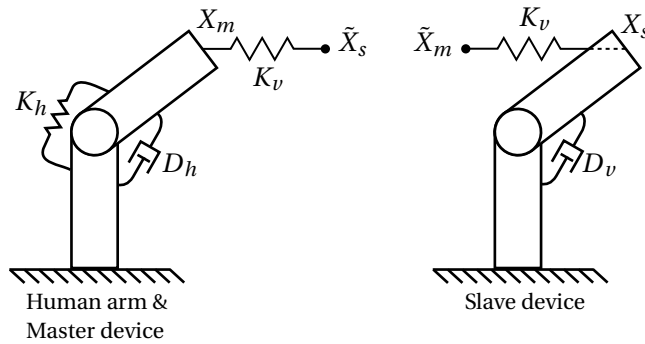


Figure 3.4: Simplified schematic representation of a 1-DOF haptic teleoperation system using an impedance controller and a position-position (PP) communication architecture.

Position-Force (PF) architecture

Figure 3.4 shows the simplified sketch while the PF architecture is applied. The energy transferred over the communication channel is clear, since it is the energy that is stored in and consumed from the same impedance controller. This allows for relatively easy energy monitoring and energy shaping to create a stable system. Furthermore, where the PP architecture tends to receive an overly conservative amount of energy from the operator, the PF architecture generally receives too little energy. In order to provide a stable interaction, this energy should then be compensated for by an additional control facility. These options will be discussed in the next section. By compensating for the correct amount of energy, PF architecture creates the less conservative option. For these reasons, this architecture will be used in the design of the teleoperation system during this research.

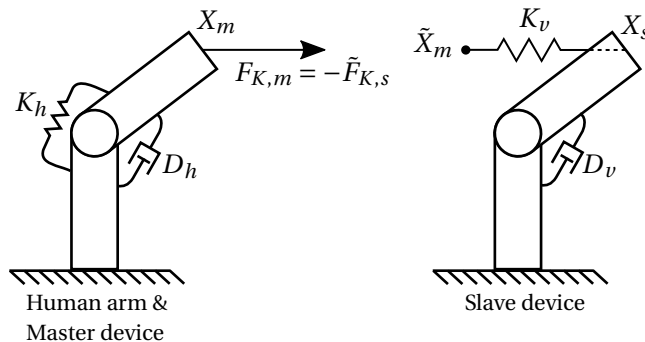


Figure 3.5: Simplified schematic representation of a 1-DOF haptic teleoperation system using an impedance controller and a position-force (PF) communication architecture.

3.3 Stability

In order for the teleoperation system to function both safely and effectively, stability of the system should be guaranteed. Unstable behaviour of the system contains undesired divergent or oscillatory motions of the master and/or slave device (Hannaford and Ryu, 2002). Guaranteeing stability of the system can be achieved by guaranteeing passivity. Experiments conducted by Hogan (1989) indicated that the impedance of a human arm can be assumed passive. Since a system of interconnected passive components is a passive system by definition, a passive teleoperation control system and communication channel which are used in a passive environment and operated by a human can be assumed to be a passive system. The causes of loss of passivity will be analysed here after which possible solutions are discussed.

3.3.1 Loss of passivity

Loss of passivity can occur in delayed systems: in haptic control, this is mainly seen as delays in the communication channel or as the effect of digital sampling in the control architecture (Colgate and Schenkel, 1997). Seemingly passive control architectures, like the impedance controller proposed in this research (see Equation 3.1), can show active behaviour (i.e. production of energy) as a result.

Weir and Colgate (2008) describe that controlling continuous-time systems in discrete-time can cause loss of passivity. They describe the occurrence of energy leaking which adds virtual energy to the controllers, resulting in active behaviour. When transforming from continuous-time to discrete-time in digital control, sampling of motion information (e.g. position or velocity) is used at sample instants spaced by the length of the sample period (ΔT_s). The resulting discrete control actions, in the form of torques or forces, are generally applied to the continuous-time system for the length of this sampling period using a zero-order hold. This means that during the length of a sampling interval, the control action is not adjusted to the continuously changing motion of the system. Figure 3.6 gives a graphical interpretation of the difference between this theoretical continuous behaviour and the discrete behaviour of a digital impedance controller, which can be viewed as a linear spring.

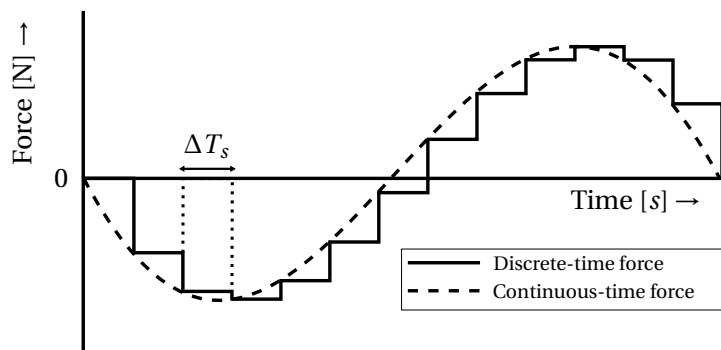


Figure 3.6: Force application of a linear spring when compressed and extended around its centre position (0) in continuous-time (dashed line) and discrete-time (solid line) with sample lengths ΔT_s .

This graph shows that over the course of time, the sampling effects create a stepwise function and that it adds a delay in the form of a phase shift. Although the force application of the impedance controller is present in discrete-time, the compression and decompression of the virtual spring (the position difference between two hardware devices) takes place in continuous time and will be a scaled version of the continuous time plot in Figure 3.6. It can be seen that due to the introduced delay, the discrete time force application is generally too low during compression of the spring while it generally is too high during decompression. This means that during compression, too little energy is stored in the impedance controller and that during

decompression, too much energy is extracted. This creates the active behaviour found in these types of controllers: energy not only stored, but also added by the virtual stiffness. Furthermore, it can be concluded that the general cause of this is time delay, which can be the result of communication delays as well as the result of sampling.

Increased loss of passivity is seen for increased stiffness values of these controllers (Ajoudani et al., 2012; Brygo et al., 2015). This can be understood from Figure 3.6 as well: for higher stiffness values, the slopes in the continuous-time force application will be steeper. This will create a larger mismatch between the desired continuous-time behaviour and the actual discrete-time active behaviour. This mismatch in energetic interaction is depicted in a schematic way in Figure 3.7. Here, the energy levels of two ideal springs with different stiffness levels are indicated by the solid lines, while the springs start at their relaxed states, containing zero energy. Then, the springs are sequentially compressed and decompressed after which they reach their relaxed states again. The discrete-time behaviour of a impedance controller that represents these springs is indicated by the dashed lines. With respect to the ideal spring, which is represented by the solid line, too little energy is added during compression while too much energy is extracted during decompression. This mismatch is indicated by the energy level of the dashed lines, reaching below zero. Since reaching an energy state smaller than zero is not possible, it indicates that energy was generated in the virtual stiffness that caused this behaviour. As mentioned, this mismatch will increase when the stiffness is increased, as is also indicated in Figure 3.7.

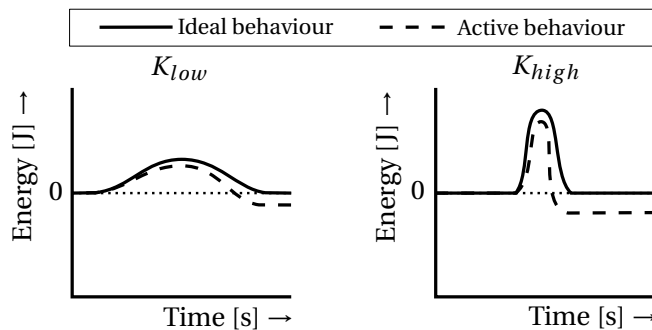


Figure 3.7: Visual interpretation of the energy levels of two virtual springs with relatively low and high stiffness values (solid lines) and the active discrete-time behaviour found in impedance controllers (dashed line). The virtual springs begin at a relaxed state after which they are sequentially compressed and decompressed until the relaxed state is reached again.

Besides the impedance controller, virtual damping is added in every joint of the KUKA slave robot. This makes any active behaviour of the virtual damping of interest as well. However, virtual damping is created to dissipate energy instead of store it, with dissipation being capable of dissipating any leaked energy as well. Furthermore, since it will only be present at the slave side, delays are left out of the consideration and only the effects of sampling are studied for damping. While the danger of the impedance controller is that it almost constantly will leak energy, virtual damping will only fail to dissipate energy during a switch of velocity direction. Due to sampling and zero-order hold, the force might be directed in the direction of the velocity after the switch, instead of opposing the direction of velocity. Instead of dissipating energy, the damper will then add energy for a moment. However, for high control frequencies and relatively low frequent motions this is assumed to be negligible. The added amount of energy by the damper is estimated to be very small compared to the amount of energy that it dissipates. It will never be a continuously leaking component like the impedance controller.

3.3.2 Guaranteeing passivity

Since this active behaviour cannot always be prevented, the system has to be designed such that the produced energy is always dissipated in order to remain passive. However, being too conservative by dissipating too much energy will decrease the transparency of the system (Colgate and Schenkel, 1997; Hannaford and Ryu, 2002; Lawrence, 1993). Here, solutions found in literature will be discussed to guarantee passivity of the system.

Scattering theory and wave variables

Successful attempts of creating passive, delayed communication are seen in the application of scattering theory and wave variables. Within the communication channel, both constant and variable time delays can occur or even loss of data. It was introduced by Niemeyer and Slotine (1991) and many extensions have been introduced for this application to work in all kinds of circumstances and while striving for the best transparency level possible (Hokayem and Spong, 2006). However, it does only concern the creation of a passive communication channel while sampling effects in discrete-time controllers are neglected. Furthermore, creating a system based on this method which can deal with different kinds of communication problems like variable delays and package loss requires complex extensions. Eventually, the method also has to provide stability while the stiffness of the virtual connection is changed through impedance modulation. Extending the current knowledge on scattering theory and wave variables to cope with impedance modulation effects will not be trivial, there are other methods available that use more simplistic energy-based approaches which allow for easier extension. For these reasons, this method is not investigated further. Other methods are able to give better and less complex insights into the energetic interactions of teleoperation systems and allow for more simple extensions.

Numerical integration of conjugate variables

Hannaford and Ryu (2002) describe the use of a "passivity observer" (PO) and a "passivity controller" (PC). The passivity observer monitors the energy flows in systems with high sampling rates by simple numerical integration of the multiplication of power conjugate variables, e.g. velocity and force. These are variables that, when multiplied, indicate the power of the system. Both the operator and the environment can add energy to the system by creating a motion of the devices in the opposite direction of the control forces. Imagine for instance a simple impedance controller, of which the stored energy can be increased by increasing a position error while the controller applies control actions in the opposite direction in an attempt to decrease the position error. In the opposite situation, when the devices move in the direction of the applied control action, energy will be extracted from the system. Whenever the observer notices that more energy is extracted by the control actions than was added by the operator or environment because of the discrete time sampling effects described earlier, the same amount of energy will be dissipated by the passivity controller (e.g. a virtual damper). This means energy is only dissipated to prevent actual active behaviour, resulting in a system that is not overly conservative. The method does require very high sampling rates for the information on the conjugate variables in order to reliably integrate.

Discrete time energy monitoring

As an alternative to the integration of power conjugate variables, Kim and Ryu (2010) propose a method for monitoring energy in discrete time without needing an estimate of an integral. When a zero-order hold is applied in the conversion from discrete-time to continuous-time,

the energy exchange can easily be estimated from available data, after a sample period has ended. The below equation gives an example of this principle in 1-DOF:

$$\Delta H_e(k) = F(k-1) \cdot (x(k) - x(k-1)) \quad (3.3)$$

Where $\Delta H_e(k)$ represents the energy exchange that happened between sample instants $k-1$ and k , $F(k-1)$ represents the (zero-order hold) force applied during this period and $(x(k) - x(k-1))$ is the resulting difference in position which was established during this period.

Using this method, Kim and Ryu (2010) estimate the active behaviour of their controller. Furthermore, they estimate the amount of dissipated energy in the system. Next, they limit their control actions such that the energy leakage will not exceed the amount of dissipated energy, creating a passive system. A disadvantage of this method is that an accurate estimation of the physical dissipation is required that can never exceed the real amount of dissipation in order to guarantee passivity. Underestimating the amount of physical dissipation will however result in decreased transparency levels found in overly conservative systems.

The energy monitoring technique of Equation 3.3 can also be used in a variable damping technique similar to what was seen in the research of Hannaford and Ryu (2002). An approach described by Franken et al. (2011) referred to as the "passivity layer" can be used to stabilise controllers and communication channels. In this method, a clear distinction is made between a transparency layer, which calculates the desired control forces/torques to reach the desired level of transparency, and a passivity layer, that only saturates the control actions and is able to add virtual damping when needed to guarantee a passive system. It monitors energy flows in the same way as discussed for the energy bounding algorithm by Kim and Ryu (2010) but extends the method for separate master and slave systems, both having to deal with active behaviour. In this approach, virtual energy tanks are located at both the master and slave side which are able to send energy packets to each other through the communication line. An algorithm will constantly try to balance the energy levels of both tanks. Energy can only be added to or extracted from these tanks by the operator at the master side or the environment at the slave side. Control actions at each side will be saturated depending on what the energy level of the corresponding tank allows. With knowledge of the system's state and the length of time samples, it can be estimated what control action will be allowed during the sample period in order to not consume more energy than is available at the start of the sample period. This way, only the energy that is put in by the operator or the environment can be used in controlling the robotic devices which should guarantee stability. If more energy is consumed than what was stored in the energy tanks, energy will be extracted from the user into the energy tank at the master side, for instance through a virtual damper. However, since a control action is needed for the operator to add energy to the control system, a deadlock situation can occur when the tanks are completely drained which will not allow for any control action. This can be prevented by maintaining a minimum energy level in the tank at the master side, so energy is extracted from the user to restore this level. It does however mean that there is more energy available for the system to use during a sample period in which the energy extraction at the master side will not change so there is more room for active behaviour during a sample period. The minimum energy level should be pre-set and will not be trivial since it related to some amount of allowed active behaviour. This decision will mainly be influenced by the sampling rate and energy consumption of the system.

Because this passivity layer can be implemented to stabilise both the controllers and the communication channel while the working principle is relatively simple it is seen as the most likely option to offer a suitable solution. Furthermore, because of the energy based approach used in the passivity layer, the effect of impedance modulation on the stability will become clear in this framework which might be extended relatively easily to cope with this effect.

3.4 Variable impedance control based on human motor behaviour

During the analysis of transparency strategies (Section 3.2) a variable impedance control strategy was proposed as a possible solution to the problem stated in this research. With variable impedance control, constant modulation of the spring and damper characteristics can be used to influence both motion tracking effectiveness and force/torque application, similar to human manipulation behaviour. Several attempts to relate the impedance levels of a haptic teleoperation controller to human motor behaviour were found in literature.

Research conducted by Chen et al. (2016) shows a number of similarities with the research that is presented here. Although the nature is quite exploratory, with a number of features added to a telemanipulation system all at once, some testing has been done using multiple test subjects while a Myo Armband was used. The control architecture however is briefly explained and design choices are not very clear, especially regarding stability.

Both Chen et al. (2016) and Walker et al. (2010) indicate promising, desirable effects on the transparency properties and the intuitiveness of the teleoperation systems they designed. Their approaches in creating transparency differ, with Walker et al. (2010) using one impedance controller to determine the forces applied to both the master and slave device, while Chen et al. (2016) changed the gains of a position controller found on the master device while an impedance algorithm determined the amount of force feedback that was presented to the user. When regarding passivity for instance, the approach of Walker et al. (2010) gives a framework in which energetic interactions are more clear and can be compared, balanced and adapted when necessary. Furthermore, Walker et al. (2010) clearly indicate that, although a controller may be very compliant, the interaction forces resulting from an impact situation occur instantly and will be determined by the mechanical properties of the robot rather than its controller settings. This is something that should be kept in mind. Higher compliance might result in lower contact forces, but impacts happen at frequencies far beyond the bandwidth of a controller. To solve this, Walker et al. (2010) introduce a mechanical clutch which can be varied through impedance estimation as well. Regarding the hardware used during the current research, this unfortunately is not a possibility.

Finally, it should be noted that the effects of time delayed communication were no part of any of the found publications and no research was found that investigates the effect of variable impedance on stability of teleoperation systems. These are large knowledge gaps that will be addressed during this research. Furthermore, it is estimated that more information can be retrieved from a Myo Armband than was done by Chen et al. (2016) and more extensive testing with test subjects is necessary to create better conclusions on the working principles of human based impedance modulation in haptic control.

3.5 Estimation of human impedance levels

As mentioned earlier, humans are capable of modulating their dynamic characteristics in order to execute tasks more effectively. These dynamic properties can be seen as impedance properties just as well. The estimation of these properties will be executed through available EMG data during this research. Humans are able to change the impedance of their limbs in three ways: by changing configuration of the limbs, by applying a force or by the co-contracting muscle pairs (Ajoudani et al., 2012; Hill and Niemeyer, 2009; Walker et al., 2010). During co-contraction of muscle pairs, the impedance level of the limbs can be changed without changing the limb's configuration or force application. An estimation of the muscle activation levels can be created with EMG, which can be related to force application and co-contraction levels of a person.

This section presents an analysis of EMG data processing methods, the possibilities of using the Myo Armband as a data collector and the available options for estimation the human dynamic properties.

3.5.1 Motor functions of the human arm and fingers

This research focusses on the muscles located in the forearm, since this is the only area around which the Myo Armband can be worn due to its limited diameter. In the human forearm, muscles are located which can be used in the flexion and extension of the fingers and the forearm. As illustrated in Figure 3.8, the angle between the bones that are connected to a joint decreases during flexion while the the angle increases during extension. Other functions of the arm and fingers, like the rotation around the longitudinal axis which flips the palm of the hand up or down or the spreading of fingers are not considered. These motions will not be used in the designed haptic control architecture since the used haptic device is only capable of applying forces along the translational axes and in the gripper.

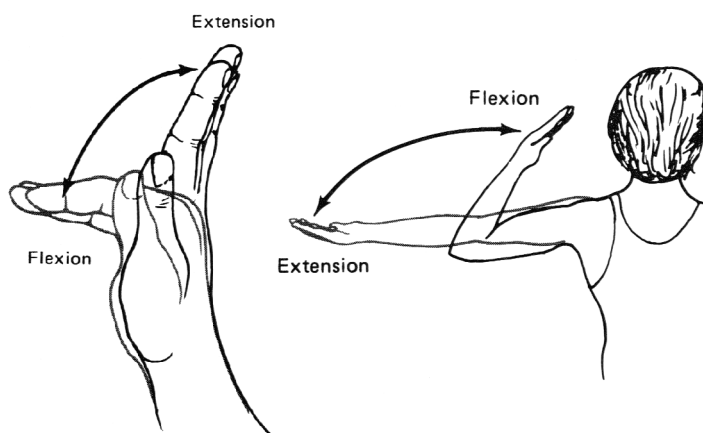


Figure 3.8: Schematic example of flexion and extension motions of the human fingers and forearm. Edited image, original source: Hamilton et al. (2011)

The most important muscles related to forearm flexing and extending are the biceps branchii and the triceps branchii, located in the upper arm (Gilroy et al., 2011). However, supporting muscles are located just below the elbow in the forearm which makes detection of activation with the Myo Armband possible. A cross-sectional view of this location is presented in Figure 3.9. An overview of the highlighted muscles and their function is presented in Table 3.1. As shown in this overview, not only information of forearm flexing and extending can be gathered at this location, flexing and extending information of the fingers can be extracted as well. This can be used to possibly extend the control of the robotic arm with the control of a robotic hand in the future.

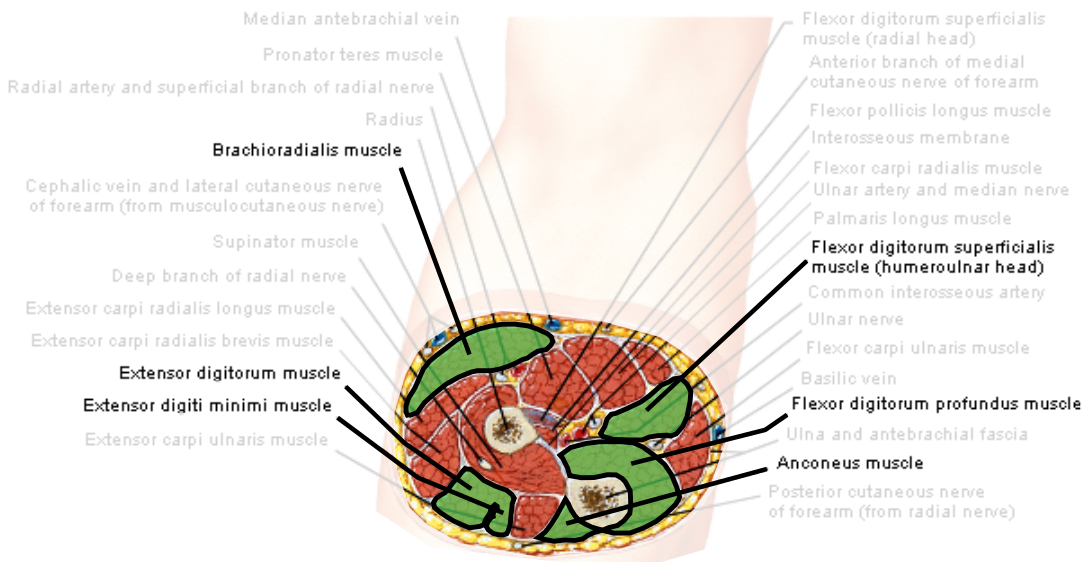


Figure 3.9: Schematic cross-sectional view of the human forearm, just below the elbow. Edited image, original source: Med-Info (retrieved June 28th 2017)

Muscle	Function
Brachioradialis	Supports forearm flexing
Anconeus	Supports forearm extending
Flexor digitorum profundus	Finger flexing
Flexor digitorum superficialis	Finger flexing
Extensor digitorum	Finger extending
Extensor digiti minimi	Little finger extending

Table 3.1: Muscles found in the human forearm related to flexion and extension of the forearm and fingers. Source: Gilroy et al. (2011)

3.5.2 Relating EMG data to human impedance levels

As illustrated by Ajoudani et al. (2012), EMG data can be used to identify the human dynamic properties of the arm through relatively simple filtering techniques. The Myo Armband actually provides unitless activation levels, which are absolute values based on EMG measurements. Unfortunately, exact computation methods of these unitless activation levels are unknown. However, they are expected to give a useful indication of muscle activation levels.

The relationship between the activation levels of muscles and the impedance properties of the human arm strongly depends on the type of muscle and can differ for every person. Furthermore, many variables are involved like muscle length, force application, and velocity of the muscle elongation. In research conducted by Osu and Gomi (1999), similar attempts were done in relating EMG signals to the stiffness of a human elbow joint. This research and a follow-up research (Osu et al., 2002) conclude that non-linearities in this relationship are mainly found in a region of high muscle activation. Based on this research it is estimated that a linear mapping will be sufficient for the goals of this research, assuming that the operator will mostly be working with relatively low muscle activation levels. Even if this is not the case, the linear mapping will most likely not result in problems for the controller.

3.5.3 Mapping human impedance levels to impedance control

The EMG data can be used to create an estimation of both the force application and the level of co-contraction in the human arm. These estimations could then be used to create an estimate of the impedance level of the arm. However, relating force application to the impedance level of the teleoperation controller can create a problematic positive feedback loop. If larger force application by the operator leads to higher impedance levels, the level of force feedback might increase. If the operator reacts to this by increasing the applied force, the impedance will quickly reach its maximum. For this reason, the level of co-contraction will be used as an indicator of the impedance level of the human arm.

Exactly determining the quantity of impedance properties of the human arm will not only be very complex but also unnecessary. The impedance values do not have to be captured and projected to the impedance controller identically since the dynamics of the robotic devices cannot be compared to the dynamics of the human arm on many levels. A scaling value, e.g. a percentage representing the level of co-contraction between set minimum and maximum levels should be sufficient. Based on the hardware properties, suitable minimum and maximum impedance levels can be determined which can then be used to scale the impedance level corresponding to the impedance level estimate of the human arm.

3.6 Hypotheses

This section presents the hypotheses that refer to the goal of the designed teleoperation system. If the research goal stated in Section 1.4 is reached, the system is expected to show the desired behaviour that results in more intuitive and effective teleoperation control. Below, hypotheses are stated covering three categories: the co-contraction behaviour of the user, the influence of communication delays and the overall functioning of the teleoperation system.

3.6.1 Co-contraction behaviour

The user is expected to apply co-contraction behaviour depending on a task and its circumstances. The expected behaviour is included in the following hypothesis:

"During the execution of a positioning task focussed on accuracy, a person will try to reject disturbing forces by increasing the co-contraction level of the arm. During a task in which the focus is placed on careful interaction, a person will try to minimise contact forces by lowering this co-contraction level."

3.6.2 The effects of communication delays

Communication delays are known to create stability problems. Furthermore, this research investigates if communication delays cause additional problems in the form of an increase in (undesired) contact forces caused by increased controller efforts. Regarding the effects of communication delays, the following hypothesis is stated:

"If a time delay is added to the communication channel of the teleoperation system, controller efforts will increase during impact situations. Furthermore, this delay will cause additional unstable behaviour and will require the stability layer to intervene more aggressively, both resulting in decreased transparency."

3.6.3 Overall functioning of the teleoperation system

In the previous chapter, a method was developed that uses EMG data to estimate co-contraction levels of the operator and use these levels to modulate impedance settings of the teleoperation controller. Regarding the research goal and the created design, a main hypothesis is stated:

"Modulating the impedance characteristic of a haptic controlled teleoperated robot through EMG allows an operator to intuitively adapt the behaviour of the robot such that the operator can make use of the advantages of both relatively high and low impedance behaviour."

This hypothesis refers to the relative advantages (+) and disadvantages (-) that are listed in Table 3.2.

Low impedance	High impedance
- Decreased level of transparency	+ Increased level of transparency
+ Decreased control efforts	- Increased control efforts
+ Decreased energy leakage	- Increased energy leakage

Table 3.2: Relative advantages (+) and disadvantages (-) of relatively low and high impedance settings of a haptic teleoperation controller.

High levels of transparency are often desired because of better motions tracking and force application result. Furthermore, the haptic ‘image’ of the remote environment that is presented to the operator will be clearer. However, the increased control efforts can lead to safety risks and the increased energy leakage can cause stability issues, which will harm the transparency level of the system.

By using variable impedance, an operator could modulate the impedance values to make use of advantages that suit the current objective. Especially during time delayed communication it is expected to be beneficial to use a relatively low impedance setting to reduce contact forces between the robot and its environment and to reduce active behaviour of the impedance controller, resulting in less undesired behaviour and less intervention by a stability layer. Relatively high impedance values can then be used when high levels of transparency are desired, for instance during accurate positioning of the robot. As part of this research, experiments will be conducted to test the above hypotheses. The detailed design of the teleoperation system which will be used during these experiments is presented in the next chapter.

4 Design

This chapter further specifies the design of the teleoperation control architecture. First, the estimation of co-contraction levels from EMG data is discussed. Next, the transparency and stability layers of the architecture are presented in more detail and finally, an overview is given of the implementation of the control architecture on the used software and hardware.

4.1 Estimation of co-contraction levels

This section presents the designed method that estimates the human co-contraction levels. Relevant muscles are indicated and a mathematical approach is discussed to find these relative co-contraction levels. Finally, a filter is designed such that the end result is a signal that can be used properly in impedance modulation.

4.1.1 Relevant muscles

As mentioned in Section 3.5, relevant information on flexor and extensor muscle activation can be collected by placing the Myo Armband around the forearm of the operator, located just below the elbow. Figure 4.1 shows this location and the highlighted muscles together with a possible configuration of the eight sets of electrodes of the Myo Armband. Table 4.1 gives an overview of these relevant muscles, their functions and the electrodes which should be able to extract information on the activation of these muscles. If it is desired to measure muscular activity of the left arm, the same configuration can be achieved by putting the arm through the Myo from the other side which basically mirrors the Myo's electrode configuration.

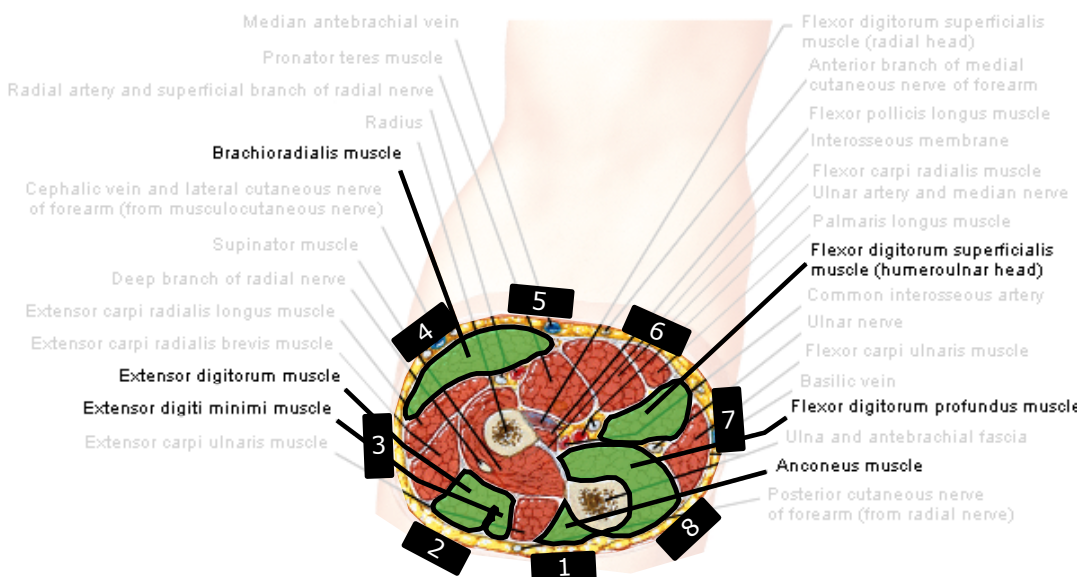


Figure 4.1: Schematic cross-sectional view of the human forearm, just below the elbow, including possible placement of Myo electrodes. Edited image, original source: Med-Info (retrieved June 28th 2017)

Preliminary testing of this configuration showed quite distinctive read-outs for each of these muscles. This indicates that with a single Myo Armband, flexor and extensor activation of both the forearm and fingers can be measured successfully. Although muscular activation of the fingers will not be investigated further in this research, this overview gives an indication of

Function	Muscle	Electrode no.
Forearm flexing	Brachioradialis	4
Forearm extending	Anconeus	1
Finger flexing	Flexor digitorum superficialis	7
	Flexor digitorum profundus	8
Finger extending	Extensor digitorum	2
	Extensor digiti minimi	2

Table 4.1: Relevant functions of the forearm and fingers (index through little finger), the corresponding muscles found in the forearm just below the elbow and corresponding electrode number when using the configuration of Figure 4.1

what information can be gathered with a single Myo Armband. In the future, this could for instance be used in the simultaneous control of a robotic arm and hand.

4.1.2 Co-contraction level estimation

As discussed in Section 3.5, the co-contraction level will be estimated by a linear equation. First, the unitless activation level (α) corresponding to the muscle of interest is collected from the Myo Armband. Next, minimum and maximum activation levels of muscles during co-contraction should be calibrated. The minimum levels (α_{min}) should be recorded when the user's arm and hand are in a relaxed state, the maximum levels (α_{max}) should be recorded when the user is applying co-contraction at a desired maximum level. These levels can now be used in normalising the activation level values from the Myo Armband with a normalisation rule similar to the one utilised by Chen et al. (2016):

$$\hat{\alpha} = \max\left(0, \frac{\alpha - \alpha_{min}}{\alpha_{max} - \alpha_{min}}\right) \quad (4.1)$$

The maximum of zero and the normalised value is taken to ensure the normalised value never reaches below zero, though this should be prevented as much as possible by selecting an appropriate value for α_{min} . If the normalised activation levels for the flexor and extensor muscles are known through the proposed equation, a normalised co-contraction level (η) can be determined:

$$\eta = \min(1, \hat{\alpha}_{flex}, \hat{\alpha}_{ext}) \quad (4.2)$$

Here, $\hat{\alpha}_{flex}$ is the normalised flexor activation level and $\hat{\alpha}_{ext}$ is the normalised extensor activation level. Clipping at 1 is included in the equation to prevent the co-contraction level to exceed 100%, which is possible if the activation levels exceed their declared maximum values.

By taking the minimum of the normalised flexor and extensor activation levels, their overlapping part is selected. For instance, if $\hat{\alpha}_{flex} = 0.5$ and $\hat{\alpha}_{ext} = 0.3$, it can be stated that the co-contraction level is equal to 0.3 because this is the part of the force application by the muscles that gets cancelled out through co-contraction. The remaining flexor activation (0.2) will result in a force application, which is not of interest in this case.

4.1.3 Filtering

Filtering of the the co-contraction levels (η) will take place to reduce the effect of high frequent behaviour of this estimation on the impedance modulation control laws. A disadvantage of this online filtering is that some phase lag (delay) will be introduced in the filtered signal. Considering the effectiveness of the filtering, a second-order Butterworth filter will be used to low-pass

filter the signal with a corner frequency of $\omega_{c,lp}$. In continuous time, this comes down to the following expression, where s is the Laplace complex variable:

$$f_{low-pass} = \frac{\omega_{c,lp}^2}{s^2 + \sqrt{2}\omega_{c,lp}s + \omega_{c,lp}^2} \quad (4.3)$$

Depending on the corner frequency and Nyquist frequency, which will be 25 [Hz] for the EMG data that comes in at 50 [Hz], a discrete time filter can be generated with a comparable effectiveness. In determining a suitable setting for the corner frequency $\omega_{c,lp}$, literature has been reviewed from which can be concluded that human muscular activity within a bandwidth of 15 [Hz] can be of interest (Ajoudani et al., 2012; Osu et al., 2002). However, high frequent impedance modulation is expected to disturb the operator in the form of sensed vibrations. Figure 4.2 shows a quick test of low-pass filters with corner frequencies at 3, 5 and 10 [Hz] compared to the original activation level signal received from the Myo Armband. During this test, co-contraction was varied as quickly as possible in the human arm and the activation level of the extensor muscle was measured. It can be seen that the filters at 10 and 5 [Hz] do a comparable job resulting in a smooth signal without adding too much lag, while at 3 [Hz] the signal is changed drastically and the lag is clearly noticeable. From this analysis it is estimated that a second-order Butterworth filter with a low-pass frequency at 5 [Hz] will be a good balance between filtering high frequent signals and keeping the important information in tact as much as possible.

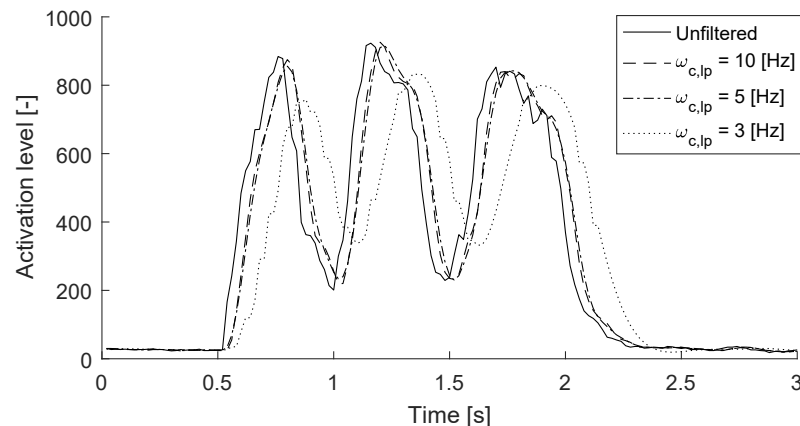


Figure 4.2: Test results of second-order Butterworth low-pass filtered activation level signals versus the original signal received from the Myo Armband. Corner frequencies ($\omega_{c,lp}$) are set at 3, 5 and 10 [Hz]. During this test, co-contraction was varied as quickly as possible in the human arm and the activation level of the extensor muscle was measured.

4.2 Outline of master and slave controllers

This section briefly introduces the outline of the master and slave controllers, used to control the omega.7 haptic device and the KUKA robotic arm respectively. An overview of the functioning of both controllers is presented in Figure 4.3. The definition and functioning of the control laws stated in the figure will be detailed in the next sections of this chapter.

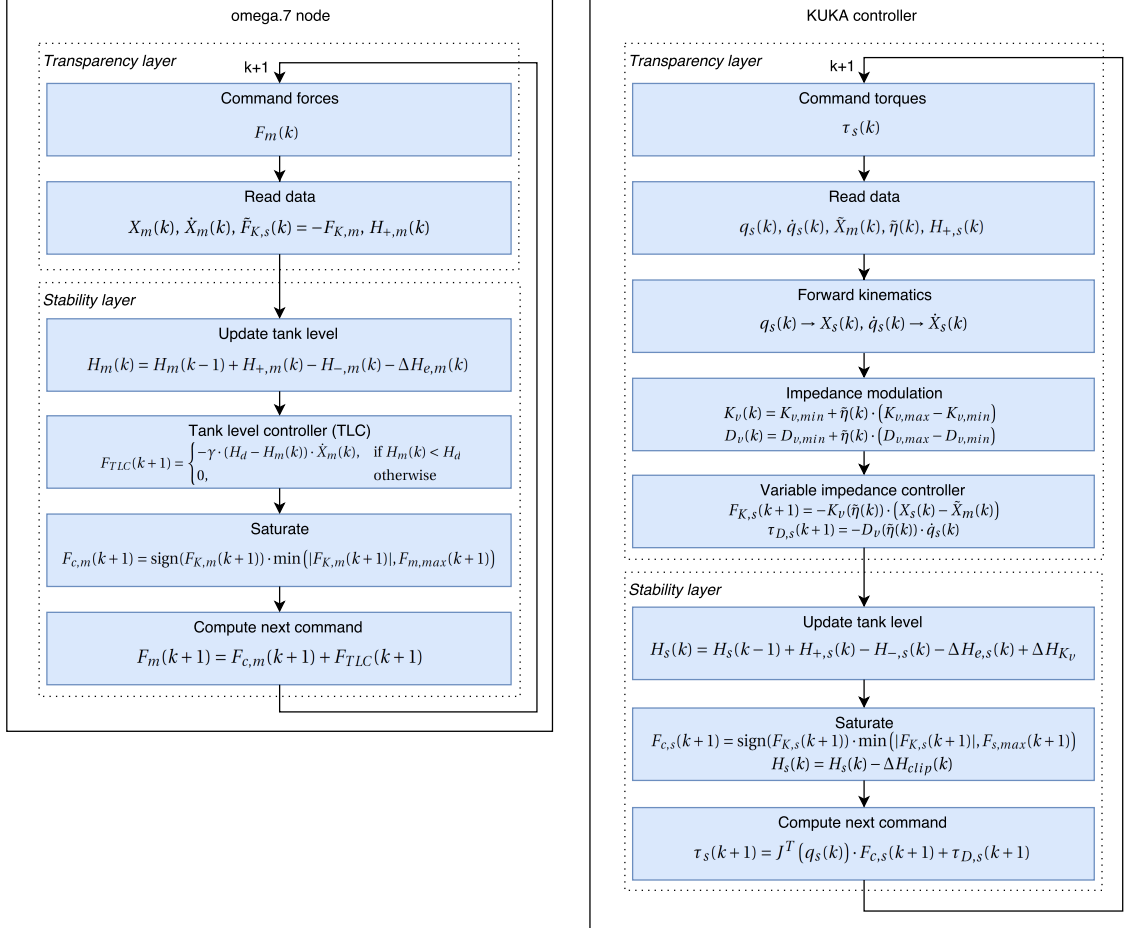


Figure 4.3: Outline of the omega.7 master controller and the KUKA slave controller. The indicated paths through the functional blocks are completed every iteration. The exact contents of the blocks is discussed in the next sections.

The scheme presents the actions that are executed by the controllers during an iteration k . Both controllers are designed such that, at every iteration, they write commands to the corresponding devices, then read data from the attached device and other sources and then start computation of next actions based on the received data. These next actions will then be used in the next iteration ($k + 1$). Because of this structure, the moment of writing the commands to the hardware is independent of the computation time. It will always happen at the beginning of an iteration (provided that the controller succeeds in finishing the computation before the start of the next iteration should take place).

The controllers consist of a transparency layer and a stability layer, the next sections will discuss the exact contents of these layers. These layers will be discussed in a generalised form, while remarks will be placed on the exact location of some of the components or differences between implementation on the master and slave devices. Figure 4.3 can then be used as a reference to check the exact, controller-dependent implementation and its location in the computation process.

4.3 Transparency layer

In this section, the design of the transparency layer is detailed. This includes the impedance modulation approach, the actual impedance control laws and the desired control of degrees of freedom (DOFs) and the workspaces.

4.3.1 Impedance modulation approach

The impedance modulation laws that will be used in the proposed research are similar to the ones utilised by Walker et al. (2010) and Chen et al. (2016) which can be stated independently of the amount of controlled DOFs:

$$\begin{aligned} K_v(\tilde{\eta}) &= K_{v,min} + \tilde{\eta} \cdot (K_{v,max} - K_{v,min}) \\ D_v(\tilde{\eta}) &= D_{v,min} + \tilde{\eta} \cdot (D_{v,max} - D_{v,min}) \end{aligned} \quad (4.4)$$

Here, $\tilde{\eta}$ indicates a delayed estimate of the co-contraction level of the operator's arm. This estimate is delayed because the EMG data is recorded at the master side while the variable impedance controller is located at the slave side. The minimum and maximum damping values are hardware dependent. Since an accurate model of the hardware is not available at this point, these values should be tuned empirically to reach the desired dynamic behaviour.

4.3.2 Variable impedance control laws

The modulated impedance levels presented above are used in the impedance control laws of the teleoperation system. The architecture first includes a forward kinematics computation, finding the slave's end effector position and velocity from joint angle and velocity data. For this computation, ROS's Kinematics and Dynamics Library (KDL) is used. Background information on robot kinematics can be found in Chapter 2, more information on the used kinematic model will be addressed in Section 4.5.

The implementation of the proposed PF control architecture can be interpreted in 1-DOF as shown in Figure 4.4.

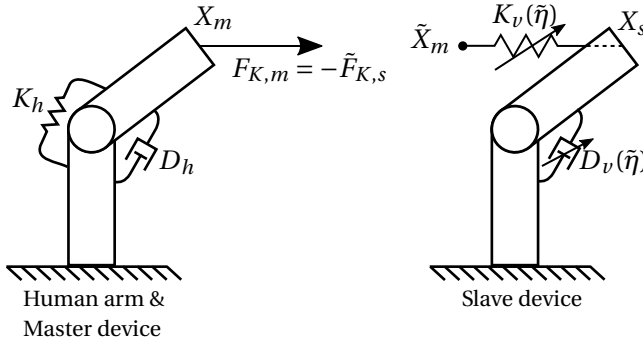


Figure 4.4: Simple schematic representation of the designed haptic teleoperation system, using a PF architecture. It is capable of modulating the dynamic characteristics of its control by the estimated co-contraction level η computed with the relevant EMG data

The variable impedance controller computes the control actions that are desired to be applied to the hardware at the next iteration ($k + 1$) according to the transparency layer:

$$\begin{aligned} F_{K,s}(k+1) &= -K_v(\tilde{\eta}(k)) \cdot (X_s(k) - \tilde{X}_m(k)) \\ F_{K,m}(k+1) &= -\tilde{F}_{K,s}(k+1) \end{aligned} \quad (4.5)$$

The impedance controller is based on delayed information of the master position ($\tilde{X}_m(k)$) and the force feedback is determined by delayed information of the outcome of the impedance

control law $\tilde{F}_{K,s}(k+1)$. Along with the impedance controller, variable virtual damping will be added in the slave's joints during the next iteration:

$$\tau_{D,s}(k+1) = -D_v(\tilde{\eta}(k)) \cdot \dot{q}_s(k) \quad (4.6)$$

4.3.3 Workspaces and degrees of freedom

In order to match the relatively small workspace of the omega.7 to the much larger workspace of the KUKA, the initial Cartesian position of the KUKA slave device will be used as the origin of its coordinate system. As a consequence, the KUKA will be able to move in a workspace identical to the size of the workspace of the omega.7, surrounding its initial position.

The above control laws are all stated independently of the amount of controlled DOFs. Since the omega.7 is only able to apply forces along its translational axes, the controller will be designed to only follow translational commands of the omega.7. Rotations will be controlled to stay equal to their initial configuration by using a impedance controller with constant stiffness K_{rot} . When desired, the control of one or more of the translational DOFs of the KUKA with the omega.7 can be disabled as well. These DOFs will then also be controlled by an impedance controller with constant stiffness K_{dis} . Furthermore, if desired, these DOFs can then be 'blocked' on the omega.7 by adding a simple PD controller that controls the blocked DOFs to the centre position.

4.4 Stability layer

The passivity layer presented by Franken et al. (2011) will be used as the base idea for guaranteeing stable behaviour of the impedance controller that was just proposed in Equation 4.5 for creating transparency. Since the concept of energy is not restricted to a DOF, the stability layer will be expressed independent of the amount of controlled DOFs. Energy can always be computed per DOF and then summed to compute a total amount of energy present in all relevant DOFs.

4.4.1 Energy tanks and flows

Virtual energy tanks will be implemented in the control software of both the master and slave controller which have an energy level of H_m and H_s respectively. In the following equations, tank levels and other variables will sometimes be generalised with subscript i to indicate an identical implementation on both master and slave devices. Both controllers have the following three energy flows in common that occur during a sample period: one flow that adds energy coming from the system on the other side ($H_{+,i}$), one flow that sends energy to the system on the other side ($H_{-,i}$) and one flow of energy exchange with the environment of the system ($\Delta H_{e,i}$). This creates the following general expression of the computation of master and slave tank levels:

$$H_i(k) = H_i(k-1) + H_{+,i}(k) - H_{-,i}(k) - \Delta H_{e,i}(k) \quad (4.7)$$

The flows ($H_{+,i}$) and ($H_{-,i}$) are created by an energy transfer protocol which is an algorithm that tries to balance the levels of both tanks. The implementation of this will be discussed in the next section. The flow that represents the energy exchange with the environment (i.e. the operator on the master side or the remote environment on the slave side) during a sample interval in 1-DOF Cartesian space can be monitored as follows:

$$\Delta H_{e,i}(k) = F_i(k-1) \cdot (X_i(k) - X_i(k-1)) \quad (4.8)$$

This expression gives, at the sample instant k , the energy that was extracted from or added to the tank through the interaction with the environment during the previous sample period in which the control action $F_i(k-1)$ was applied and a motion from $X_i(k-1)$ to $X_i(k)$ was detected. The energy exchange $\Delta H_{e,i}(k)$ will be positive if energy is extracted from the system by the environment and negative when energy is added to the system by the environment.

4.4.2 Energy transfer protocol

As mentioned, a balancing algorithm will be implemented which determines the energy flows $H_{+,i}(k)$ and $H_{-,i}(k)$ between the energy tanks at the master and slave sides. The simple energy transfer protocol (SETP) described by Franken et al. (2011) was tested and proved to be sufficiently effective in the circumstances of this research. At every sample instant, the tank level is updated by addition of the incoming flow $H_{+,i}(k)$ and subtraction of the interaction energy $\Delta H_{e,i}(k)$ from the previous tank level $H_i(k-1)$. Next, $H_{-,i}(k)$ is determined by taking a fixed fraction ($\beta < 1$) of this updated level and sending this to the other side. This creates the current tank level $H_i(k)$ as presented in Equation 4.7. This simple algorithm is asymptotically stable and will converge to a balanced situation for any time delay in the communication channel. For more information on the exact implementation and proof of stability see Franken et al. (2011).

4.4.3 Tank level controller (TLC)

A tank level controller (TLC) will be installed which aims to refill the tank at the master side to a desired minimum energy level by extracting energy from the operator. Energy is only extracted from the operator into the tank when the direction of the control action is opposite to the direction of motion of the master device, as can be understood from Equation 4.8. This means that the following expression will be able to extract energy from the operator when necessary during the next iteration ($k + 1$):

$$F_{TLC}(k+1) = \begin{cases} -\gamma \cdot (H_d - H_m(k)) \cdot \dot{X}_m(k), & \text{if } H_m(k) < H_d \\ 0, & \text{otherwise} \end{cases} \quad (4.9)$$

Here, H_d is the pre-set desired minimum tank level, γ is a tunable parameter and \dot{X}_m is the velocity of the master device. This equation can be interpreted as viscous damping being added while $H_m(k) < H_d$. This damping has a varying coefficient equal to $\gamma(H_d - H_m(k))$, so it linearly scales with the difference in actual tank level and desired tank level. Choosing H_d and γ is not trivial, more details on the used parameter setting during this research will be discussed in Section 4.6.

The commands for the omega.7 should include the control action of the TLC. The computation of the final hardware commands will be discussed in Section 4.4.5.

4.4.4 Control action saturation

The control action determined by the transparency layer (Equation 4.5) should sometimes be saturated in order to limit active behaviour of the system. At time instant k , a control action $F_{K,i}$ is computed that will be saturated if necessary after which it can be applied starting at $k + 1$ until $k + 2$ is reached. The available energy during this period will be the energy tank level at $k + 1$ which is not known yet so it will be estimated:

$$\tilde{H}_i(k+1) = (1 - \beta) \cdot (H_i(k) - \Delta \tilde{H}_{e,i}(k+1)) \quad (4.10)$$

This equation is a worst case scenario estimation of Equation 4.7. $H_i(k)$ is known, $H_{+,i}(k+1)$ is taken equal to zero (worst case) so it is left out of the above equation and $\Delta H_{e,i}(k+1)$ is not known yet so should be estimated as well. $H_{-,i}(k+1)$ is incorporated by taking the portion β of this estimated energy level. Taking the worst case scenario might be overly conservative, however for relatively small portions β this is not expected to have a significant influence. In order to estimate $\Delta H_{e,i}(k+1)$ while the position $X_i(k+1)$ is not known either, the moved distance will be estimated by using the current velocity of the system:

$$\Delta \tilde{H}_{e,i}(k+1) = F_i(k) \cdot \dot{X}_i(k) \Delta T_s \quad (4.11)$$

In which ΔT_s is the length of the sample period. Here it is assumed that the velocity at the end of the force application from $k + 1$ until $k + 2$ is equal to the velocity at k . A better estimate of the velocity would require an accurate dynamic model of the system, however for small time steps this equation should provide the necessary limit in order to functionally limit active behaviour.

Now that the available energy at $k + 1$ is estimated, this value gives an indication of how much energy the system is allowed to use during the application of the control action from $k + 1$ until $k + 2$. The first limit that is applied to the control efforts is that no control action is allowed when there is no energy available in the tank corresponding to the device:

$$F_{i,max1}(k+1) = \begin{cases} 0, & \text{if } \tilde{H}_i(k+1) \leq 0 \\ F_{K,i}(k+1), & \text{otherwise} \end{cases} \quad (4.12)$$

A more advanced control action saturation method is used as well. Instead of allowing all control actions until the tank is completely empty like suggested by Equation 4.12, control actions can be saturated based on the (non-zero) energy level of the system's tank. The amount of energy that the transparency layer would like to consume can be estimated as follows:

$$H_{i,des}(k+1) = F_{K,i}(k+1) \cdot \dot{X}_i(k) \cdot \Delta T_s \quad (4.13)$$

Next, a new control action limitation can be computed by multiplying the desired control actions from the transparency layer by the ratio between the estimated available energy and the estimated desired energy consumption:

$$F_{i,max2}(k+1) = \frac{\tilde{H}_i(k+1)}{H_{i,des}(k+1)} \cdot F_{K,i}(k+1) \quad (4.14)$$

This limit will decrease the chance of an energy tank being drained completely.

Finally, the force application limitations of the omega.7 were taken into account by limiting all x -directional force application to 15 [N] and all y - and z -directional force application to 10 [N]. This creates the third limit, $F_{i,max3}$. This way, chances of large force application mismatches between the two devices are decreased. If forces would be clipped on the master device but not on the slave device, chances are that much more energy is exchanged at the slave device for which the TLC will have to compensate. The values of the forces were empirically determined to minimise the chance of the occurrence of clipped omega.7 forces. Although the device specifications suggest a maximum force application of 12 [N] in all directions, it was discovered that these values are highly dependent of the configuration of the actuators.

In order to determine the most dominant control action limit, the minimum of the absolute values of all computed control action limits is computed:

$$F_{i,max}(k+1) = \min(|F_{i,max1}(k+1)|, |F_{i,max2}(k+1)|, |F_{i,max3}(k+1)|) \quad (4.15)$$

Then, the desired control action $F_{K,i}(k)$ commanded by the impedance controller of the transparency layer is saturated when necessary to find the force commands that will be applied to the hardware at the next iteration. If necessary, part of the force will be 'clipped' in this process, resulting in the force $F_{c,i}(k+1)$:

$$F_{c,i}(k+1) = \text{sign}(F_{K,i}(k+1)) \cdot \min(|F_{K,i}(k+1)|, F_{i,max}(k+1)) \quad (4.16)$$

4.4.5 Final hardware commands

At the end of every iteration, the stability layer computes the force or torque commands that will be applied to the master and slave device respectively. For the master device, this force is a combination of a (possibly clipped) impedance control action $F_{c,m}(k+1)$ and the determined control action of the TLC, $F_{TLC}(k+1)$:

$$F_m(k+1) = F_{c,m}(k+1) + F_{TLC}(k+1) \quad (4.17)$$

For the slave device, it is a combination of the (possibly clipped) impedance control action $F_{c,s}(k+1)$, which is transformed to find the torques in the joint space of the robot by multiplying with the transpose of the Jacobian $J^T(q_s(k))$, and the torques $\tau_{D,s}(k+1)$ that result from the added damping in the robot's joints:

$$\tau_s(k+1) = J^T(q_s(k)) \cdot F_{c,s}(k+1) + \tau_{D,s}(k+1) \quad (4.18)$$

At the start of the next iteration ($k + 1$), these forces and torques will be commanded like seen in the overview of Figure 4.3.

4.4.6 Effects of control stiffness modulation on energy levels

Until now, the effect of impedance modulation on the monitoring of energy levels in the system has not been taken into account. Through impedance modulation, the operator is offered an additional method to change the energetic interaction with the remote environment through the teleoperation system.

Because of the digital (discretised) nature of the controller, a change of stiffness level of the impedance controller will occur instantaneously. While active behaviour occurs because of the continuous application of a force that was determined in discrete-time based on discretised position information, the instantaneous energy ‘jumps’ seen in impedance modulation will not introduce any additional active behaviour. For this reason, active behaviour will be disregarded in the next analysis, assuming that the stability layer will take care of the active behaviour that was already present. It is however important to record the energy exchange properly such that the stability layer will not lose its functionality.

Consider for instance Figure 4.5, in which two examples of expected energy tank behaviour are depicted when the effects of impedance modulation are not taken into account. Based on the algorithms explained until now, the monitored energy is only based on the exchange of force between the devices and their environments.

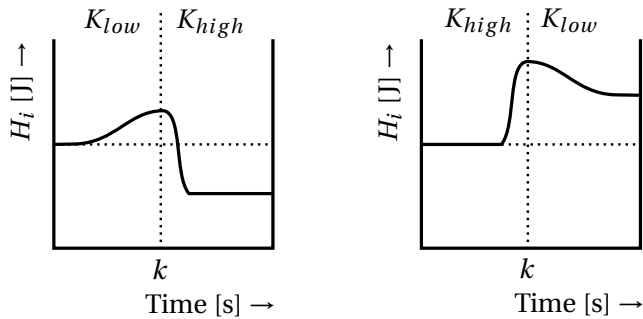


Figure 4.5: Energy tank levels in time for switching virtual stiffness levels at time instant k without using energy compensation for impedance modulation. The virtual spring is compressed until k , after which it returns to its relaxed state.

Here it is assumed that the virtual spring is compressed during the period before k and relaxed during the period after k until it reaches its initial state. It can be seen that when the stiffness level is increased at k , more energy is extracted from the tank level than the amount that was added because of the resulting increase in controller forces. On the other hand, if stiffness is decreased at k , less energy was extracted than then amount that was added. This means that the energy level of the tank will not be restored which might lead to an over- or underestimation of active behaviour by the stability layer. The problem here simply is that the energy tanks are not registering the energy flows in and out of the controller in the right way, since the effects of stiffness modulation are not taken into account.

The graph in Figure 4.6 demonstrates the change of energy when increasing the stiffness of the impedance controller from K_1 to K_2 . The relationships between the positional difference X_e and the applied control actions corresponding to the two stiffness levels, F_{K_1} and F_{K_2} are plotted. When the controller uses K_1 , the energy contained in it is equal to the surface area of the white triangle:

$$H_{K_1} = \frac{1}{2} F_{K_1} X_e = \frac{1}{2} K_1 X_e^2 \quad (4.19)$$

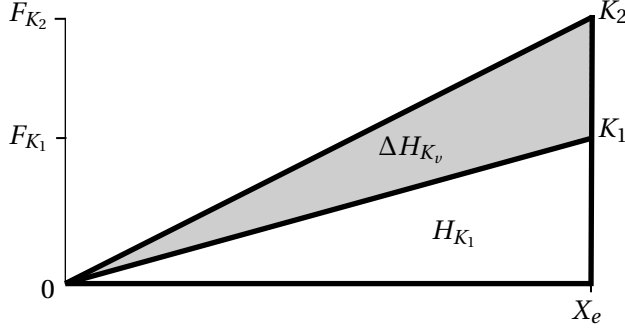


Figure 4.6: Energy levels of two impedance controllers with stiffness levels K_1 and K_2 for a constant positional error X_e resulting in controller efforts F_{K_1} and F_{K_2} respectively.

When increasing the stiffness to K_2 , the grey area (ΔH_{K_v}) will be added to the energy level of the controller. The surface area of the grey triangle is equal to:

$$\Delta H_{K_v} = \frac{1}{2} (K_2 - K_1) X_e^2 \quad (4.20)$$

Now the new energy level of the controller will be equal to the combined white and grey areas:

$$H_{K_2} = H_{K_1} + \Delta H_{K_v} \quad (4.21)$$

The energy tank algorithms can be extended to compensate for this effect. Compensation can be added to the tank level computation at the slave side, where the impedance controller is located:

$$H_s(k) = H_s(k-1) + H_{+,s}(k) - H_{-,s}(k) - \Delta H_{e,s}(k) + \Delta H_{K_v}(k) \quad (4.22)$$

This compensation adds $\Delta H_{K_v}(k)$ to Equation 4.7. With compensation, the behaviour that is expected is shown in Figure 4.7.

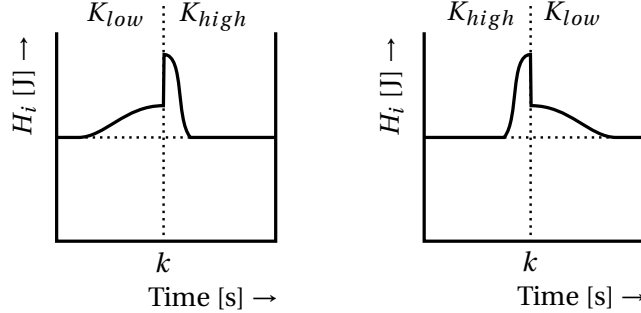


Figure 4.7: Expected energy tank levels in time for switching virtual stiffness levels at time instant k while using the compensation algorithm that adds $\Delta H_{K_v}(k)$. The virtual spring is compressed until k , after which it returns to its relaxed state.

The energy tank level should now restore to its original level, again disregarding active behaviour. The stability layer will now possess the right energy level information to react to any active behaviour that occurred.

Although it can be argued that this energy is not injected by the user directly which violates the passivity condition, the injections will be limited due to the upper boundary of K_v . Furthermore, damping D_v will be modulated correspondingly to dissipate any additional energy

to create the desired dynamic behaviour. This will not result in excessive stability problems like observed when an impedance controller is continuously leaking energy.

4.4.7 Effects of saturating control actions on energy levels

The effects of saturating the control actions by the stability layer on the recorded energy tank levels has not been discussed until now. Just like in the previous section, active behaviour will not be included in this analysis but the energy tank algorithms might have to be changed to deal with the effects caused by control action clipping.

The main reason why the effect of control action saturation has not been mentioned is because it does not result in problems in most cases. Some of the control action limitations are based on the energy level, which makes them adapt automatically if the energy level changes through interaction with the environment or impedance modulation. During this research, constant limitations of applied forces are incorporated as well to cope with the limitations of the master device. These limitations will not cause any problems for constant stiffness values in the impedance controller, since the energy that goes and out of the controller will be limited similarly. However, when the impedance is modulated while constant force clipping is applied, not all energy contained in ΔH_{K_v} can be used by the impedance controller due to this clipping. This will be illustrated by using Figure 4.8.

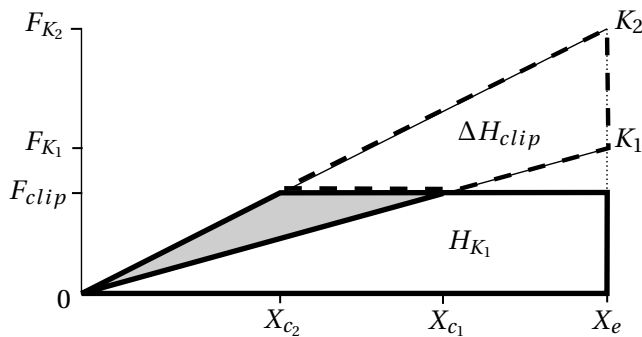


Figure 4.8: Energy levels and difference in clipped energy for two impedance controllers with stiffness levels K_1 and K_2 for a constant positional error X_e and constant force limitation F_{clip} . Hypothetical non-clipped controller efforts F_{K_1} and F_{K_2} are indicated as well together with hypothetical positional errors at which clipping would be initiated: X_{c_1} and X_{c_2} .

When controller actions are clipped at the level of F_{clip} , the energy contained in the controller with stiffness K_1 will be equal the white boxed area indicated with H_{K_1} . When compared to Figure 4.6 it can be seen that a small triangular shaped area was ‘clipped’ of the energy level of the controller. When increasing the stiffness to K_2 , the grey area will be added. The combined white and grey areas will be equal to the new energy level H_{K_2} . Again, it can be seen that this energy level is different from the energy level computed in the previous section, this time a larger triangle of energy is clipped from the controller. The difference between these clipped triangles of energy is indicated with ΔH_{clip} .

It can quickly be seen that the grey area in this figure is smaller than the grey area of Figure 4.6 which represented ΔH_{K_v} . In fact, the difference between the two is the indicated ΔH_{clip} . So, in the case of a constant control action limitation, the energy that is added after impedance modulation is equal to $\Delta H_{K_v} - \Delta H_{clip}$.

As indicated, ΔH_{clip} is the difference in clipped energy between the situation in which K_2 is used versus the situation in which K_1 is used:

$$\Delta H_{clip} = H_{clip}(K_2) - H_{clip}(K_1) \quad (4.23)$$

The amount of clipped energy can be determined for a current positional error X_e , a stiffness level K_v and a force limit F_{clip} in the following way:

$$H_{clip}(K_v) = \frac{1}{2} (F_{K_v} - F_{clip}) (X_e - X_c) \quad (4.24)$$

In which F_{K_v} is the non-clipped force that corresponds to the impedance controller with stiffness K_v and X_c is a hypothetical positional error at which the clipping behaviour will start, indicated in Figure 4.8 as X_{c_1} and X_{c_2} for stiffness levels K_1 and K_2 respectively. The equation can be rewritten to only depend on K_v , F_{clip} and X_e :

$$H_{clip}(K_v) = \frac{1}{2} (K_v X_e - F_{clip}) \left(X_e - \frac{F_{clip}}{K_v} \right) \quad (4.25)$$

Using this equation, the clipped energy can be found for K_1 and K_2 . The difference between the two will result in ΔH_{clip} . In general terms, this expression is implemented in the controller design:

$$\Delta H_{clip}(k) = H_{clip}(K_v(k)) - H_{clip}(K_v(k-1)) \quad (4.26)$$

At the end of every iteration, the tank level of the slave controller is now compensated to include the clipping effects. This step is also included in the controller overview of Figure 4.3:

$$H_s(k) = H_s(k) - \Delta H_{clip}(k) \quad (4.27)$$

4.5 Kinematic and dynamic KUKA models

As explained in the previous section and in the background information of Chapter 2, a kinematic model is needed to transform commands and data between Cartesian space and joint space. During this research, kinematic and dynamic models of the KUKA LWR4+ are used which are based on models created by researchers at Research Center E. Piaggio at the University of Pisa, Italy¹.

Figure 4.9 shows a screenshot of the KUKA model while it is simulated in Gazebo. To correspond with the i-Botics set-up, the model is placed in a wall mounted configuration. This model can be viewed as a kinematic model, consisting of link lengths and joint configurations, combined with a dynamic model, consisting of parameters like link dimensions, inertia and joint friction and damping parameters.

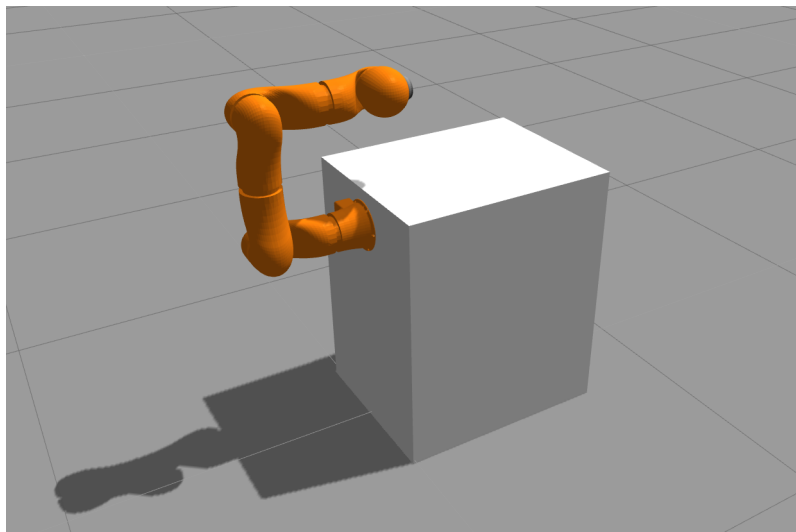


Figure 4.9: Screenshots of the KUKA LWR4+ model simulated in Gazebo in a wall mounted configuration.

The dynamic model of this robot is not assumed to be accurate and is therefore not used in the design of the controller. The accuracy of the mass, friction and damping parameter values are all unknown. The mass properties are assumed to represent the real hardware accurately enough based on the credibility of the mass distribution and the total mass of the links. The static friction and viscous damping parameters however seem to be set very roughly, since they were configured at the same values for all joints at 10 [N·m] and 1 [N·m·s/rad] respectively. Preliminary testing showed a very slow robot in which the operator had to invest a lot of energy to move it the slightest bit. As discussed in Section 3.2, clearly noticeable dynamics of the slave device like its friction levels will harm the transparency of the overall system when using an impedance control approach. With the original settings, successful testing of the transparency properties of the controller was impossible mainly because of the dominant, non-transparent friction and damping properties of the model. For this reason, more ideal settings were adopted by setting the static friction and viscous damping parameters at 0.01 [N·m] and 0.01 [N·m·s/rad] respectively. As a result, the (variable) virtual damping that is added in the joints will be dominant and can be tuned in the controller settings. The dynamics of the variable impedance controller will therefore be more dominant which results in clearer data regarding its behaviour.

¹This model is available on the Centro E. Piaggio GitHub:
<https://github.com/CentroEPiaggio/kuka-lwr>

Literature was researched to see if any, more realistic, models of the KUKA robotic arm could be found or if any reliable identification procedure was ever completed. Because frictional levels of the robot are expected to be a main issue when comparing the real hardware to the simulated model, a study was done to reach conclusions on the friction levels of the actual hardware. Research by Jubien et al. (2014) presents the most complete set of identified parameters found, including viscous and Coulomb friction parameters, not specifying if this involves static or dynamic friction. Although friction is clearly present in the robot according to this research, it remains unclear what the actual differences are with the model that is used in this research. Early hardware tests showed quite distinctive static friction creating stick-slip behaviour in the robot's joints. In an attempt to reach conclusions on the functionality of the proposed controller when it would be implemented on realistic KUKA arm dynamics, hardware tests were conducted to point out any clear differences in behaviour with respect to the simulated, more ideal robot model. These experiments will be discussed in Chapter 5 and the results are presented in Chapter 6.

4.6 Quantifying parameter settings

Over the past sections, a number of tunable parameters were mentioned that will determine the behaviour of the designed controller. This section will detail the design choices that were made regarding the quantification of these parameters. An overview of all parameters that are used throughout this research, unless explicitly indicated otherwise, is presented in Table 4.2.

Parameter	Value	Parameter	Value	Parameter	Value
$K_{v,min}$	100 [N/m]	$D_{v,min}$	0.2 [N·m·s/rad]	H_d	0.1 [J]
$K_{v,max}$	600 [N/m]	$D_{v,max}$	0.5 [N·m·s/rad]	γ	200 [N·s/m·J]
$K_{v,rot}$	100 [N·m/rad]	ω_{loop}	1000 [Hz]	β	0.01 [-]
$K_{v,dis}$	1000 [N/m]	$\omega_{c,lp}$	5 [Hz]		

Table 4.2: Recommended parameter settings. These settings were used throughout this research, unless explicitly indicated otherwise.

Setting the impedance parameters is mostly a matter of tuning. Creating the desired behaviour does not only depend on the dynamic properties of the robotic devices and the human operator but also on their respective configurations. Furthermore, it is hard to quantify the feeling of the operator when determining the quality of the haptic feedback. For these reasons, the minimum stiffness level of the controller ($K_{v,min}$) was empirically determined at a value of 100 [N/m], such that a minimum allowable level of interaction control was achieved. With this setting, low frequent motion tracking and a limited but distinguishable sense of touch were achieved, of course still depending on the circumstances.

As for the maximum stiffness level $K_{v,max}$, the upper boundary is a bit more clear. For motion tracking, only relatively low frequencies (say, up till 5 [Hz]) are of importance, since higher frequencies will never be commanded by a human operator and might only cause a disturbance. However, increasing the stiffness as much as possible might be beneficial for accurate haptic feedback of the robot's interactions. Here, the limiting factor will be a result of active behaviour of the impedance controller. Although the stability layer will make sure the system remains stable, a large amount of energy leakage will still cause some resonance behaviour plus the added damping by the TLC might decrease the transparency level. As a benchmark, an absolute upper bound is determined at 1000 [N/m]. With this setting, the most important motions of the human arm (in a range of 0–3 [Hz]) will quickly be tracked by the slave arm, assuming the equivalent moved mass will be equal to 5–10 [kg] of the total 16 [kg]. Initial testing however showed that, due to the relatively high inertia of the simulated robotic arm and the additional frictional properties found in the real KUKA arm, the arm behaves as quite a slow object causing high controller efforts which quickly results in large amount of energy leakage. Limiting this behaviour can be achieved most effectively by tuning down the stiffness level of the controller and decreasing the time delay of the communication. Throughout this research, a maximum time delay of 10 [msec] will be used, in combination with a maximum stiffness of $K_{v,max} = 600$ [N/m]. This was empirically determined to still give satisfactory transparency properties due to limited necessary intervention by the stability layer, while the effects of time delayed communication still become apparent. In case a more lightweight robot would be used with lower overall frictional properties (a robot with better transparency properties, i.e. dynamics that can more easily be assumed negligible), communication with larger time delays is expected to be less of a problem.

The other stiffness settings, K_{dis} and K_{rot} , are not used while interacting with the master device, so these controllers are not subjected to communication delays. This makes it easy to establish K_{dis} at the benchmark of 1000 [N/m]. K_{rot} is established at 100 [N·m/rad], since the moment of inertia of the KUKA can be assumed to be much lower than its mass properties regarding its dimensions.

The desired amount of joint damping cannot easily be related to these stiffness values because of the conversion between Cartesian and joints space and the dependency on configuration and unknown dynamic characteristics of the devices. Because of this, the joint damping settings were chosen equal for each joint while quick experimenting with impacting objects showed the damped behaviour of the impedance controller's oscillations. The damping values were tuned at 0.2 and 0.5 [$N \cdot m \cdot s / rad$] for $D_{v,min}$ and $D_{v,max}$ respectively.

Quantifying suitable stability layer properties is not trivial either, because of large dependency on the characteristics of the systems, controllers and communication channel. With the impedance settings quantified and the time delay limited to 10 [msec], suitable settings are first estimated and then tuned empirically. The minimum tank level, H_d , should be chosen such that there is a bit of an energy buffer such that the controller also runs smoothly with the added communication delay. The upper bound will be defined by the amount of energy that is allowed to be translated into active behaviour. It was experimentally determined that a value of 0.1 [J] resulted in smooth functioning of the controller for the circumstances tested in this research. This value is assumed to not cause dangerous levels of active behaviour, since this amount of energy can be interpreted as the amount of kinetic energy that the slave robot would posses while travelling at about 0.1 [m/s].

The parameter quantification of the damping parameter γ is hard to determine analytically as well, since it highly depends on system characteristics, the implemented energy transfer protocol and the time delays in the communication channel. Its value should guarantee stability while not disturbing the user too much which would be the case during aggressive damping. As an indication, it was assumed that an allowable damper force should not exceed 2 [N], which would be about one fifth of the maximum force application by the master device. For a tank level of 0.1 [J] and a maximum velocity of the master device of 0.1 [m/s], this would come down to γ being equal to 200 [$N \cdot s / m \cdot J$]. This parameter setting was tested and proved to guarantee stability under the conditions tested in this research while not disturbing the user too much.

The final parameter that is part of the stability layer is β . This value partly determines the successfulness of the energy transfer protocol that balances the tank levels. A value of $\beta = 0.01$ was experimentally determined to show satisfactory results, meaning that at every iteration one percent of the levels of each tank is send through the communication channel.

Finally, the corner frequency $\omega_{c,lp}$ of the low-pass filter used on the muscle activation signals was set at 5 [Hz], which was already discussed in Section 4.1 of this chapter. The loop frequency ω_{loop} was set at 1000 [Hz] which was empirically determined as a maximum rate at which the controller could smoothly function on the used hardware.

4.7 Implementation

On the next page, Figure 4.10 presents a schematic overview of the implementation of the discussed design in the teleoperation system as a whole. A central PC running Ubuntu (version 14.04) is used which is connected to the hardware components through communication ports (USB, Bluetooth and Ethernet). Within this PC, a ROS master is running (Indigo distribution) in which code runs in the form of nodes. Besides the ROS master and all the nodes, a Gazebo simulation can run on this PC as well to simulate the KUKA arm. During this research, Gazebo 7 was used. The communication lines between the components are indicated by arrows, through which the indicated variables are communicated.

On the master side, the omega.7 master device communicates with the omega.7 node through a USB connection. This node contains the transparency and stability layers of the master's side that were discussed before. This means it not only arranges communication with the hardware, but it also computes the commands. Furthermore, muscle activation data is extracted from the Myo Armband through a Bluetooth connection by the Myo node. This node sends relevant information to the co-contraction estimator node which estimates the relevant co-contraction levels following the procedure discussed earlier in this chapter. Both the Myo and co-contraction estimator node run at 50 [Hz], as opposed to the rest of the software which runs at 1 [kHz]. This is a result of restrictions on the Myo hardware and software.

Between the master and slave side of the teleoperation system, a communication node is installed. This node simply forwards information from one side to the other. It is able to hold on to messages for a time period if the addition of a communication delay is desired for testing purposes.

On the slave side of the system, either the real KUKA hardware is controlled through an Ethernet connection with the FRI node, or the Gazebo simulation is controlled through the Gazebo node. Depending on the setting, the block indicated as the Hardware Interface will convert data and commands in the appropriate way such that the main KUKA controller can be written in a generalised way. This KUKA controller contains the transparency and stability layers that were discussed in this chapter.

While this section gives a general overview of the implementation, Appendix G presents a more detailed description on how to use the relevant software packages to recreate the system in the form of a demonstration or the experiment set-up.

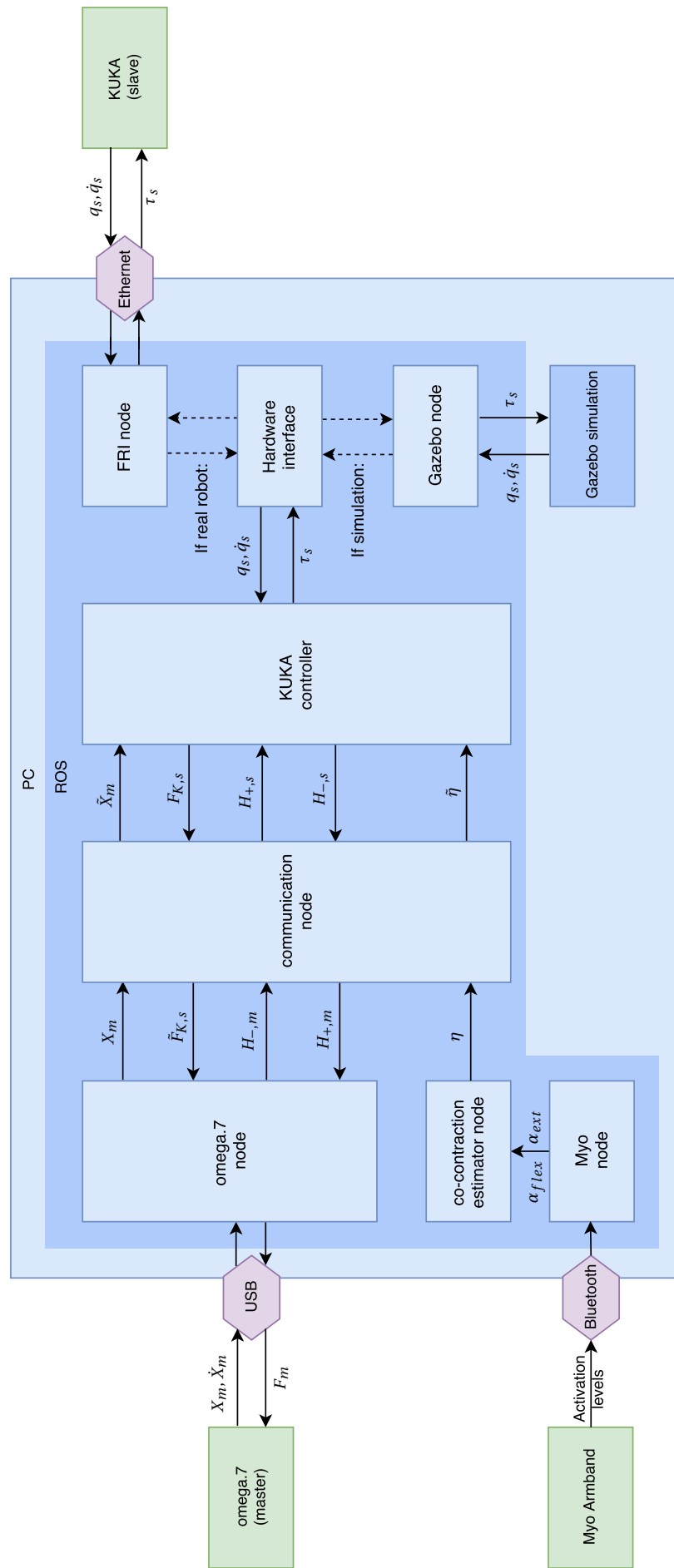


Figure 4.10: Schematic overview of the implementation of the discussed design in the teleoperation system as a whole. The designed software runs on one central PC, indicated by the blocks. Communication with hardware is arranged through three communication ports. Information is exchanged between the blocks of software and hardware as indicated by the arrows.

5 Experiments

A number of experiments were designed which are aimed at validating the functional design of the teleoperation system and validating the hypotheses that were stated in Section 3.6. The validation of the functional design consists of a few very basic experiments all executed in simulation while one of these experiments was repeated on the real KUKA arm to indicate differences with respect to the used model. Next, a short experiment is detailed which was used to get an indication of the static friction levels in the real KUKA hardware, in order to compare it to the used model in simulation. Finally, for the purpose of validating the hypotheses, experiments were conducted using test subjects. A procedure is detailed which was used to calibrate the co-contraction level estimation for every test subject, after which the experiments are described that were conducted by the test subject while they were controlling the simulated KUKA model in Gazebo.

5.1 Validating the functional design

In validating the functional design, first the overall 3-DOF functioning of the teleoperation controller was tested while using the simulated robotic arm and the real KUKA arm. The set-ups of the simulation and hardware experiment are shown in the screenshot and photo of Figure 5.1.

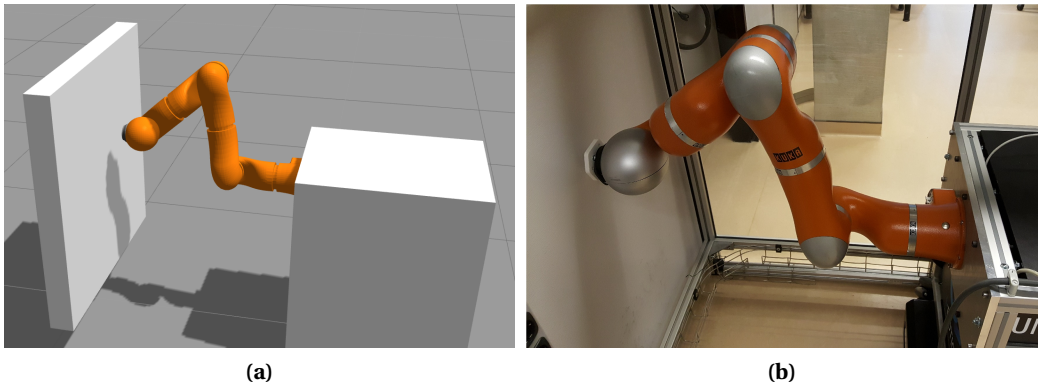


Figure 5.1: Set-up configurations during the functional design validation experiments while using (a) the simulated KUKA in Gazebo and (b) the real KUKA hardware.

5.1.1 Overall 3-DOF functioning

Initial testing was done while controlling the simulated KUKA model in Gazebo. The overall functionality in 3-DOF was tested by one operator moving the master device in x -, y -, and z -direction. Perpendicular to the robot's x -direction, a simulated wall was placed such that force application against a static object could be tested as well. The impedance setting was fixed at the maximum setting indicated in Table 4.2. Tests were conducted with and without an added communication delay of 10 [msec].

Next, the experiment without the added time delay was repeated while using the real KUKA robot. This is expected to indicate differences in the dynamic properties between the Gazebo model and the real KUKA robot.

5.1.2 Energy compensation for impedance modulation

The next experiment that was conducted is expected to indicate if the energy algorithms presented in Sections 4.4.6 and 4.4.7 properly compensate for the effects of impedance modu-

lation and control action saturation on the energy tank levels. It will be checked if the expected behaviour, as illustrated in Figure 4.7, occurs while using the designed algorithms. In this simulation experiment, the simulated wall of Figure 5.1a was used to control a positional difference between the master and slave devices. While at rest, with a certain positional difference, the co-contraction level η was changed from low to high or the other way around, just like suggested in Figure 4.7. Then, the positional difference was brought back to zero, to see what this has done to the level of the energy tanks of both devices.

5.2 Indication of static friction levels in the KUKA hardware

Although identifying proper friction characteristics generally requires complex identification procedures, a short experiment was conducted to get a basic idea of the static friction levels in the KUKA robot. First, a torque was placed on every joint individually by pulling on a force sensor that was attached to the robot's links at a certain radius from the joint centre. For every joint this was done while the designed controller was adapted to command zero torques at all times, while the joint was configured such that it played no role in gravity compensation. Forces were increased until data from the robot indicated that motion of the joint was initiated. These roughly determined force values create an idea of the necessary torque that needs to be applied to every joint to overcome static friction. Furthermore, tests were done to see if any torque was applied by the motors during this procedure or during steady velocity motion to see if any indication could be found on a form of friction compensation by the FRI.

5.3 Experiments using test subjects

Ten test subjects participated in an experiment during which they were instructed to control the simulated KUKA model in Gazebo while holding the omega.7 and while wearing the Myo Armband around their forearm. None of these subjects had any experience in operating a tele-robot. The test subjects were between the ages of 25 and 61 (mean age of 46, standard deviation of 13 years) and were all in good health, not having any problems with sight, hearing and the functioning of their dominant arm and hand. Six females and four males participated, including eight right-handed and two left-handed persons. Figure 5.2 shows a photo of the experiment set-up.



Figure 5.2: Photo of the used experiment set-up in which test subjects controlled the simulated KUKA model in Gazebo while holding the omega.7 haptic device and while wearing the Myo Gesture Control Armband.

The main goal of the experiments in which test subjects were used is to validate the hypotheses that were presented in Section 3.6. With this validation, final conclusions can be formed on whether the goal of this research was reached, regarding the effectiveness and the intuitiveness of the designed teleoperation system.

The three hypotheses focus on human co-contraction behaviour, the effects on time delay in the communication channel and the behaviour of the variable impedance controller. More specifically, the following factors should be tested to fully validate the hypotheses:

- Co-contraction behaviour: test if significant changes in co-contraction behaviour occur when the task objective is switched between careful interaction (low interaction forces) and accurate positioning (high rejection of disturbing forces).
- Communication delay: check if controller efforts increase in impact situations when a communication delay is added to the system. Furthermore, test if there is any controller behaviour that disturbs the user (decrease of transparency).
- Impedance modulation: test if the test subjects are able to modulate the impedance level of the controller in an intuitive way and if this results in the task-dependent desired effects (high positioning accuracy, low controller efforts and a high level of stability).

The design of the experiments was based on this list of requirements. The performance of the designed variable impedance controller was tested and compared to controllers with a constant high and constant low impedance. First, the test subjects were asked to complete a calibration procedure in which the co-contraction behaviour could already be tested and which gave information on the muscles activation levels of the individual subjects. After completing this procedure, they were instructed to complete a number of tasks in which the three impedance settings and the above listed factors were all tested. These procedures are further detailed in this section.

5.3.1 Calibration of the co-contraction level estimation

Every time the Myo Armband was placed or moved around the forearm of every individual test subject, a calibration process took place to determine the maximum and minimum registered activation levels of the flexor and extensor muscles of the test subject. While using the following process, all relevant activation levels were determined with one experiment containing two tasks.

Every test subject was asked to hold on to the omega.7 while the weight of the arm was supported on a table and the Myo Armband was worn around the forearm, configured just below the elbow. A program was started that centred the omega.7 using a simple PD controller. Through a keyboard command, a disturbance of the omega.7's measured horizontal y -position was enabled. This disturbance was designed as a multisine consisting of four waves with quite randomly chosen frequencies between 1 and 10 [Hz], such that no repetition of the disturbance can be recognised by the test subject. The amplitudes were chosen such that the maximum total amplitude would never surpass 2.5 [cm].

A live graph visible only to the experiment leader showed the Myo's activation level estimations of the flexor and extensor muscles of interest. The test subjects were expected to apply two different types of reaction to the disturbing forces:

Follow the motions: the test subjects were instructed to let the omega.7 dictate the motions by trying not to interfere. The measured activation levels of the relevant muscles were used to quantify the minimum activation levels $\alpha_{min,flex}$ and $\alpha_{min,ext}$.

Minimise displacement: next, the test subjects were expected to keep the omega.7 as much in one place as possible. The corresponding muscle activation levels were used to quantify the settings of $\alpha_{max,flex}$ and $\alpha_{max,ext}$.

During the first type of behaviour, low co-contraction behaviour of the test subjects is expected. This low impedance behaviour will result in a compliant arm which will then follow the motions of the omega.7. During the second type of behaviour, high impedance behaviour of the human arm will be needed to keep the omega.7 in place, since the test subject will not be able to anticipate the randomly computed force application by the omega.7. This is expected to result in high levels of co-contraction.

5.3.2 Task execution in simulation

After the calibration procedure was completed, experiments were conducted by the test subjects during which they controlled the KUKA model that is simulated in Gazebo. This section presents details on the experiment conditions and the execution.

Conditions

Two sets of experiments were conducted, in which test subjects were asked to execute specific tasks while controlling the simulated KUKA model in Gazebo. One of the sets was performed without any added communication delays, while the other was performed while a communication delay of 10 [msec] was added. During the execution of a set of experiments, the test subjects were asked to hold on to the omega.7 and wear the Myo Armband as they did during the calibration procedure. The KUKA model was extended with a cylindrical peg as its end effector and the motions of the KUKA were restricted to horizontal y -directional translations. Two types of experiments were conducted within both of the two sets. The first type of experiment was a test of positioning accuracy, in the second type applied control actions were recorded in impact situations. The parameter settings presented earlier in Table 4.2 were used during all experiments. Before the start of the experiments, the test subject watched instructional videos and were given the opportunity to familiarise with the controls to decrease the effects of learning during the recording of the actual experiment.

During every experiment, three impedance settings were tested: low, high and variable impedance. The low and high impedance settings were based on the minimum and maximum impedance levels presented in Table 4.2 respectively. During the variable impedance setting, the impedance modulation laws were activated based on the estimated co-contraction level of the test subject to scale between the low and high impedance settings. The order of application of these settings were randomised for every test subject. The same holds for the order of the tested communication delay settings.

Accuracy experiments

In the simulated environment, two clearly visible cylindrical setpoints were placed on the y -axis of the end effector's motions. These setpoints were static and did not include any collision properties. A static camera angle was used that allows the test subject to clearly see the position of the end effector and the setpoints. A screenshot of this view can be seen in Figure 5.3.

These experiments were conducted on a spoken rhythm: a program was started on the main computer that presented spoken audio commands to the test subject, alternating the commands 'go' and 'stop'. The commands were repeated after each other with constant gaps of 1.5 seconds. Test subjects were asked to move in between the setpoints by following these spoken instruction. Starting at a setpoint, the test subjects were instructed to initiate motion towards the other setpoint at a 'go' command. At the next 'stop' command, the test subjects should have arrived and held the end effector at this setpoint until the next 'go' command. Then, they were allowed to initiate the returning motion towards the first setpoint. At the next 'stop' command, the end effector should have arrived and again be at rest until the next 'go' command. In short, one cycle was equal to four sequential periods of 1.5 seconds: moving - pausing - moving - pausing. The test subjects were asked to repeat ten full cycles for each setting. The test subjects were clearly given the task to pause at the setpoints as accurately as possible in between the 'stop' and 'go' commands. This experiment was repeated once for every impedance level and communication delay setting, resulting in a total of six sets of ten cycles per test subject.

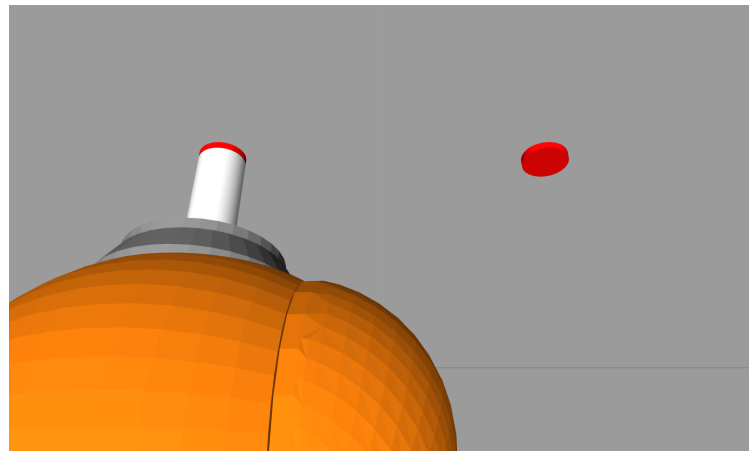


Figure 5.3: Screenshot of the camera angle during the accuracy experiments. The end effector of the KUKA and the setpoints were clearly visible to the test subjects

Impact experiments

During the impact experiments, only one setpoint was used to approximately centre the robot. Accuracy was not of importance during this experiment. After a keyboard command, a simulated invisible block of 5 [kg] travelled towards the simulated end effector at a velocity of 0.2 [m/s]. The direction of this velocity was randomly determined and the motion only started after a random amount of time (between 0 and 3 seconds) had passed since the keyboard command. This random state of the invisible block made the assumption possible that the test subjects could not anticipate the impacts.

Figure 5.4 presents a screenshot of the camera view during this experiment. Note that for illustrative purposes the block is visible in this example.

The test subjects were clearly instructed to try to reduce the interaction forces as much as possible, not fighting any motions of the robot and the omega.7. This experiment was repeated for all three impedance levels and the two communication delay settings as well, while for every of the six sets five impact situations were created and recorded.

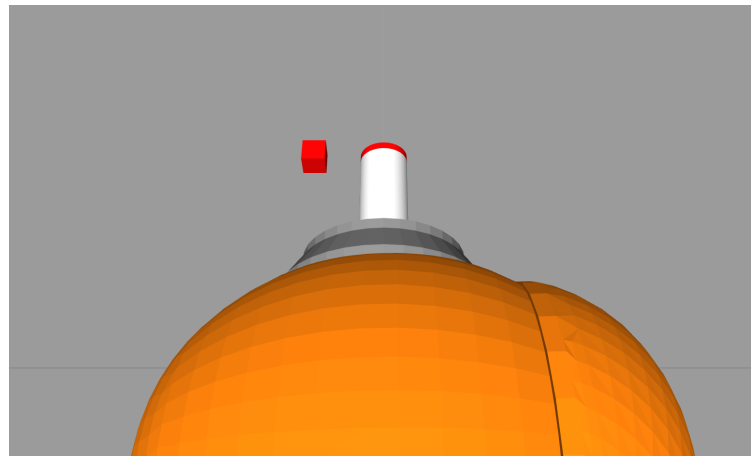


Figure 5.4: Screenshot of the camera angle during the impact experiments. The end effector of the KUKA and the setpoint were clearly visible to the test subjects. The block that caused the impact with the end effector is visible in this screenshot but was invisible to the test subjects during the experiments.

5.4 Data collection and analysis

During the experiments, data was collected to conclude on the performance and behaviour of the test subject and the designed teleoperation control architecture. The collected data and the analysis of it is detailed for every type of experiment below. An overview of all recorded parameters can be seen in Table 5.1.

Parameter	Description	Unit
(x_m, y_m, z_m)	Position of the omega.7 master device along the x , y and z -axes	[m]
(x_s, y_s, z_s)	Position of the simulated KUKA slave device along the x , y and z -axes	[m]
F_{PD}	PD-controller effort during calibration experiments	[N]
$F_{c,m}$	Impedance controller actions applied to the omega.7	[N]
$F_{c,s}$	Impedance controller actions applied to the KUKA arm	[N]
F_{TLC}	Tank Level Controller actions applied to the omega.7	[N]
H_m	Energy tank level of the omega.7 master device	[J]
H_s	Energy tank level of the KUKA slave device	[J]
α_{flex}	Flexor muscle activation level low-pass filtered at 5 [Hz]	[–]
α_{ext}	Extensor muscle activation level low-pass filtered at 5 [Hz]	[–]
η	Estimation of co-contraction level low-pass filtered at 5s [Hz]	[%]
Rhythm	Time stamps of the occurrence of a 'go' or 'stop' audio command	[s]

Table 5.1: Overview of all parameters that were recorded during the experiments, including their description and unit of measure.

Calibration of co-contraction level estimation

During the calibration procedure, the omega.7 was PD-controlled to follow a disturbing motion along the y -axis of the device. In order to visualise the effects of the behaviour of the test subject, both the omega.7's position and applied force (as a result of the PD controller) were recorded. Furthermore, the Myo Armband's measured muscle activation levels were displayed live and recorded as well, after they were low-pass filtered. During the live display, the maximum and minimum values were read directly such that they could be processed in the teleoperation control strategy. The recorded data will be used to study the effects of the disturbance and muscle activation behaviour.

Accuracy experiments

During the accuracy experiments, the setpoint accuracy in between 'stop' and 'go' commands is of interest. For this reason, the positions of the omega.7 and KUKA were recorded together with the moments at which these commands took place (referred to as the 'rhythm' parameter in Table 5.1). Furthermore, the estimated co-contraction levels were recorded to see if task-dependent behaviour can be recognised in any of the impedance strategies that were tested.

During the data analysis, the position and co-contraction level data were categorised in periods of motion between setpoints and periods of pausing at a setpoint. The borders of these periods are clearly indicated by the recorded rhythm of audio commands. Of the ten cycles that were recorded for every setting, the final five cycles are analysed to decrease the effects of learning for every setting. Within these five cycles, ten periods of motion and ten periods of pausing at a setpoint take place. In order to quantify the level of positioning accuracy, the mean absolute setpoint errors during these ten periods of pausing were computed. As for the co-contraction levels, the mean values were computed for the pausing and the moving periods during these last ten sets. This might indicate a difference in co-contraction level behaviour during motion and pausing periods.

Impact experiments

During the impact experiments, the reaction of the impedance controller and the estimated co-contraction levels were recorded. The controller behaviour can then be examined while regarding the co-contraction levels of the test subject and the added time delay in the communication channel. For every experiment, the controller forces were quantified by computing the mean absolute values of the peak controller forces that were applied at each of the five impacts per setting. Furthermore, the average co-contraction level during these impacts was computed such that it can be compared to the behaviour seen in the accuracy experiment.

Statistics

To conclude on the effects of the applied settings, the overall means and standard deviations of the found mean position errors and peak controller forces were computed. Differences between settings were assessed on their significance by using paired t-tests. Resulting p -values were computed for every comparison of two data sets. The lower this p -value, the lower the chance that the difference in mean values was not caused by the change of setting that is analysed. Generally, for p -values below 0.05 it is concluded that the difference between the means are statistically significant.

6 Results

This chapter contains the results of the experiments that were defined in the previous chapter. First, the results of validating the functional design are presented. Then, an indication is created of the static friction levels contained in the real KUKA hardware. Next, the observed behaviour during the calibration of co-contraction levels is discussed and finally, the results of the task execution experiments conducted by test subjects are detailed.

6.1 Validating the functional design

The results of the experiments that are aimed at validating the functional design of the system are presented in this section. First, the general 3-DOF functioning of the transparency and stability layers of the system is demonstrated and behaviour will be compared for the simulated and real KUKA robotic arm. Next, the functioning of the designed energy compensation algorithm is demonstrated which is used to cope with the variable impedance of the controller and the clipping of impedance control actions.

6.1.1 Overall 3-DOF functioning

Figure 6.1 presents graphs of the 3-DOF positions of both the master and slave devices, the Cartesian forces that were commanded by the stability layer and that were applied to the systems. Furthermore, the behaviour of the stability layer is shown, including the energy tank levels of both systems and the forces added by the TLC.

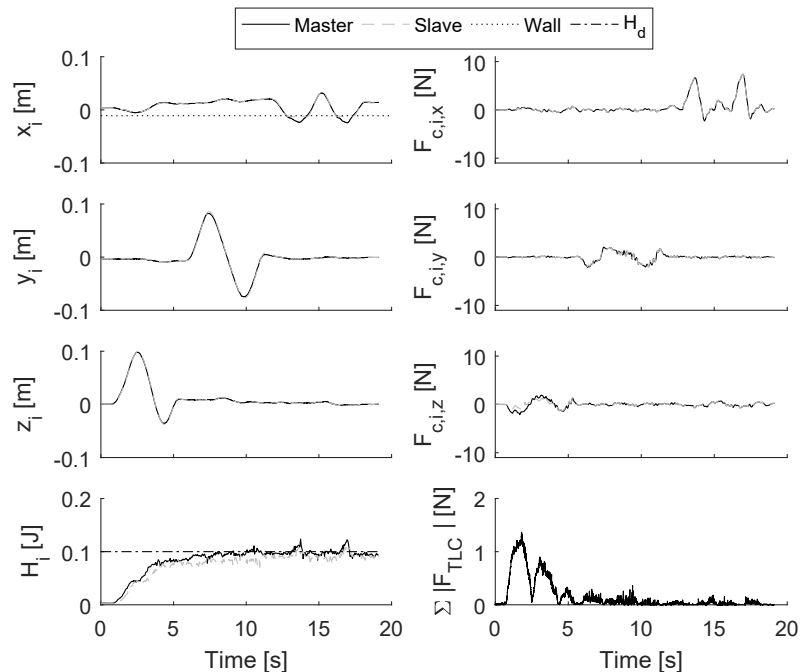


Figure 6.1: Results of the functionality experiment in 3-DOF without any added communication delay while using the simulated KUKA robot. The positions of both devices are plotted next to the applied forces that were computed by the stability layer for every translational coordinate and for both devices ($i = m$ or s). The functioning of the stability layer is indicated by the recorded energy tank levels and the sum of the absolute values of all actions applied by the TLC.

During this experiment, motion was sequentially initiated in z -, y - and x -direction while a wall was located perpendicular to the x -direction. Figure 6.1 shows that the system behaves

as expected, allowing for both motion and force control and keeping the interactions stable. It can be seen that the TLC mainly acts in the beginning, to fill up the tank until it reaches H_d .

Figure 6.2 shows the results of this experiment repeated with an added delay in the communication channel of 10 [msec]. It can be seen that, although the system still functions properly and remains stable, the stability layer has to put more effort in to keep the energy tank levels from decreasing too much. This additional energy leaking was expected as a result of the added communication delay. Some oscillation was perceived by the operator, which is also visible in the force plots of Figure 6.2. However, because of the functioning of the passivity layer, diverging behaviour is limited and any oscillations were always damped out over time.

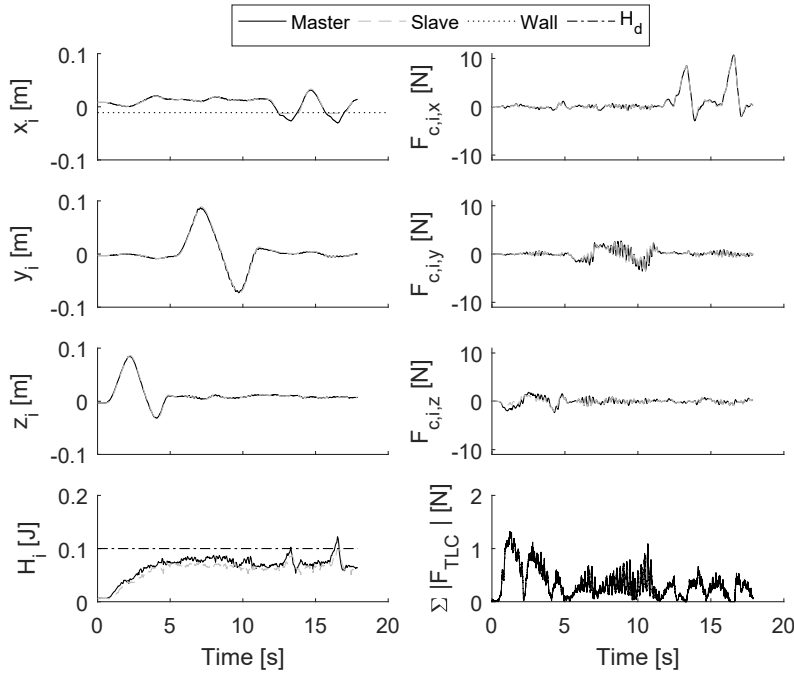


Figure 6.2: Results of the functionality experiment in 3-DOF with an added communication delay of 10 [msec] while using the simulated KUKA robot. The positions of both devices are plotted next to the applied forces that were computed by the stability layer for every translational coordinate and for both devices ($i = m$ or s). The functioning of the stability layer is indicated by the recorded energy tank levels and the sum of the absolute values of all actions applied by the TLC.

The first test, in which no additional communication delay was applied, was repeated on the real KUKA robot. From the start, it was noticeable that the operator had to invest a lot more effort to move the robot around in comparison to the control of the simulated model. This also clearly shows in the force plots of Figure 6.3. Furthermore, although no communication delay was added, the TLC had to act a lot more than during the simulation experiment. Because it was harder to move the robot around, more energy was generally present in the controller which most likely increased energy leaking. The plot of the tank levels also indicates that quite a lot of energy had to be added by the master device to initiate motion while the slave device consumed a lot of energy. This made it hard for the energy transfer protocol to balance the tank levels.

A logical reason for this behaviour would be the presence of unmodelled friction. Especially initiating motions was troublesome, suggesting relatively large quantities of static friction being present in the real KUKA robot. Creating motion in y -direction was particularly difficult, which can be related to the amount of joints that have to rotate when using the configuration that was presented in Figure 5.1. Later in this chapter, in Section 6.2, the results of the identification experiment of static friction parameters are presented and more details are discussed on the effects of this presumed static friction.

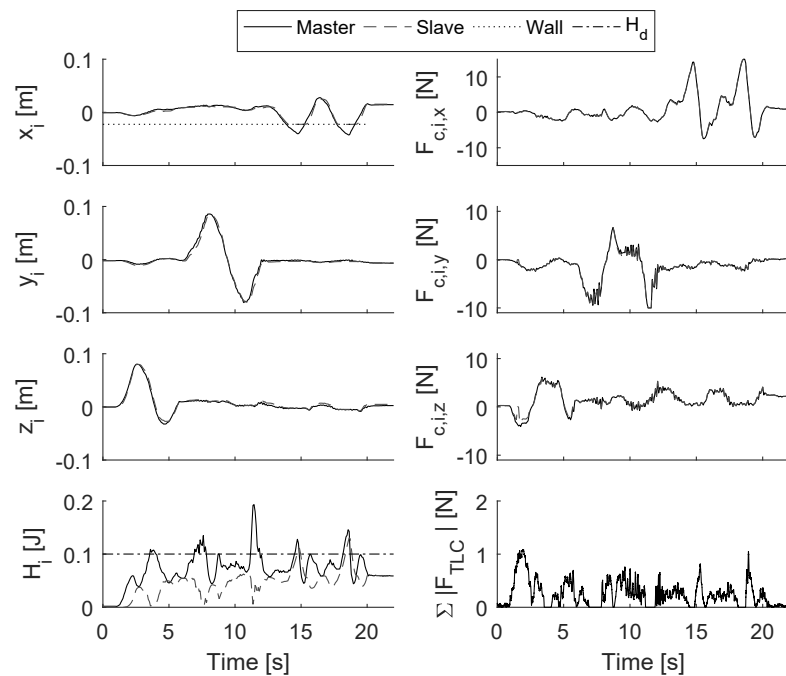


Figure 6.3: Results of the functionality experiment in 3-DOF while using the real KUKA robot. The positions of both devices are plotted next to the applied forces that were computed by the stability layer for every translational coordinate and for both devices ($i = m$ or s). The functioning of the stability layer is indicated by the recorded energy tank levels and the sum of the absolute values of all actions applied by the TLC.

6.1.2 Energy compensation for impedance modulation

Figure 6.4 shows the results of the experiment in which the slave device was pushed against a wall to create a positional difference between the two devices. This compresses the virtual spring of the controller, after which the stiffness level of the controller was switched by letting the operator switch the co-contraction level. Then, the virtual spring was relaxed again. The graphs show that the energy compensation algorithm works within the tested circumstances, adding energy to the tank during the co-contraction increase and removing energy during the decrease as described in Section 4.4.6. Furthermore, it can be seen that impedance control actions were clipped in the high impedance cases. The energy tank levels were corrected for this effect as well as discussed in Section 4.4.7. As a result, the energy level was restored when the virtual spring reaches its relaxed state again. This experiment was repeated multiple times, also while a communication delay of 10 [msec] was added. No significant differences were noted when compared to the example that is presented here.

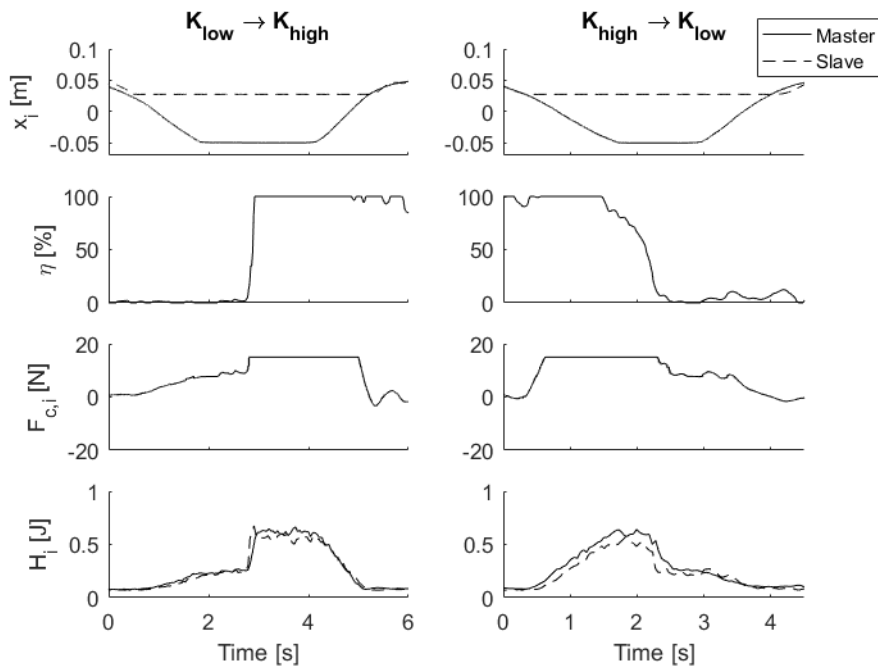


Figure 6.4: Results of the experiment that validates the energy compensation method for impedance modulation. The positional difference of master and slave devices, the co-contraction level of the operator, the (possibly clipped) force application on the devices and the energy tank levels plotted. In the plots on the left, the stiffness level of the controller is increased by increasing the co-contraction level, while in the plots on the right the stiffness level is decreased.

6.2 Indication of static friction levels in the KUKA hardware

In order to get an indication of the static friction levels in the KUKA hardware, joint torques were applied experimentally to see how much torque would be needed to initiate even the slightest motion of the joints. Table 6.1 gives an overview of these torques for clockwise and counter-clockwise rotations of every joint. A full overview of data, including force measurements and the applied radii, can be found in Appendix A.

Joint name	$T_{fr} \curvearrowleft$ [Nm]	$T_{fr} \curvearrowright$ [Nm]
A1	0.390	0.975
A2	0.487	0.683
E1	0.488	0.585
A3	0.488	0.488
A4	0.330	0.330
A5	0.638	0.468
A6	0.450	0.240

Table 6.1: Computed static friction torques T_{fr} in the KUKA joints for clockwise and counter-clockwise rotations

The first thing that can be noticed is the dependency on direction of rotation in some joints. Mainly joint A1, the joint that is closest to the base of the robot, suffers from a great dependency on direction when it comes to static friction forces. It has to be noted that this joint plays a large role in gravity compensation in the used wall-mounted configuration, and although it was calibrated a couple of times to be sure, slight deviations in gravity compensation calculations could be the cause of this effect. No indication of other forms of dynamics compensation became evident from the internal KUKA joint torque data, not during the initiation of motions and not during a constant velocity of the joints. These situations were repeated for every joint as well while the particular joint was configured such that it played no role in gravity compensation. A literature study on any internal compensation of dynamical effects like friction did not give any results either. It is expected that the only compensation used in the FRI is gravity compensation.

The significance of these static friction torques is illustrated by analysing the joint torques that were commanded during the first 3-DOF functionality experiment of Section 6.1.1. During this experiment, the simulated KUKA arm was controlled while no time delay was added to the communication channel. Figure 6.5 gives an overview of these torques for consecutive z -, y - and x -directional motions. Remember that pushing against a wall occurred in the x -direction. The maximum absolute torque values found during each of the directions of motion are presented in Table 6.2.

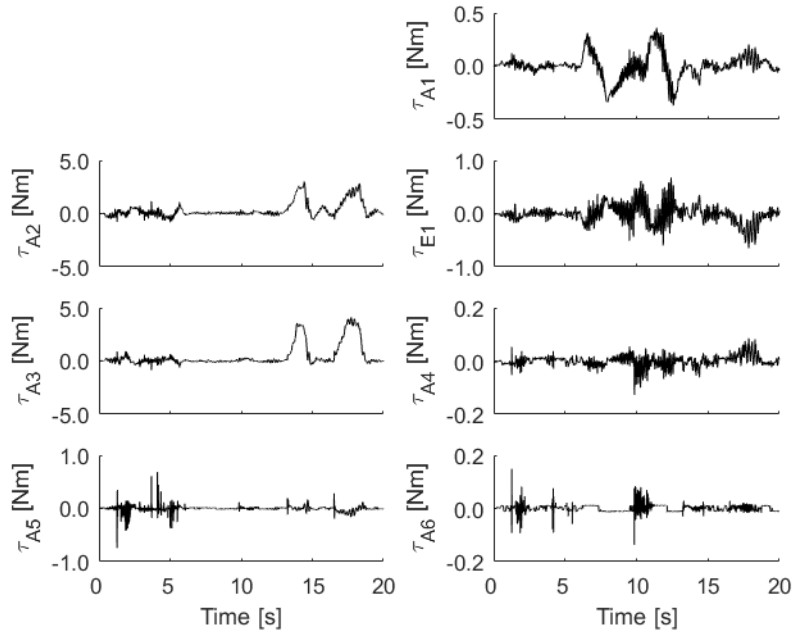


Figure 6.5: Commanded torques in every joint of the KUKA slave robot during the 3-DOF functionality experiment of Section 6.1.1 while controlling the simulated model without added time delay.

Maximum joint torques [Nm]

Joint name	Direction of motion		
	<i>z</i>	<i>y</i>	<i>x</i>
A1	0.12	0.37	0.20
A2	1.16	0.36	3.01
E1	0.19	0.68	0.65
A3	0.91	0.31	4.09
A4	0.05	0.13	0.09
A5	0.74	0.12	0.28
A6	0.15	0.14	0.03

Table 6.2: Maximum values of the absolute joint torques that were commanded during the 3-DOF functionality experiment for every direction of end effector motion while controlling the simulated model without added time delay.

From this data it can be concluded that, during free space motions, the torques generally did not exceed 1 [Nm]. Most maximum torques are even lower than 0.4 [Nm]. This means that the added static friction torques will drastically increase the effort that has to be put in to create similar motions on the real KUKA arm, which agrees with the behaviour seen in the hardware experiment. The only exceptions in maximum torques are seen in joints A2 and A3 during the force application against a solid wall.

6.3 Calibration of the co-contraction level estimation

During the experiments in which test subjects were used, all test subjects first completed the calibration procedure described in Section 5.3.1. During these procedures it was identified that the minimum activation levels were registered roughly the same for every test subject, ranging between 20 and 50. The maximum levels however were very different for every test subject and can all be found in Appendix B. As an example, Figure 6.6 gives an example of behaviour that was seen during these procedures. For all test subjects, the increase in muscle activation levels was quite distinctive when they were trying to hold the omega.7 in one place. The figure also shows the resulting omega.7 position and the resulting force application determined by the installed PD controller. It can be seen that the position amplitudes are clearly decreased during the increased co-contraction behaviour. This did not directly translate into an increase of PD controller actions, because although the position errors entering the PD controller were increased, the velocity of the omega.7 decreased resulting in a smaller damping action. This is the result of the added disturbance only being placed on the position signal and not the velocity signal.

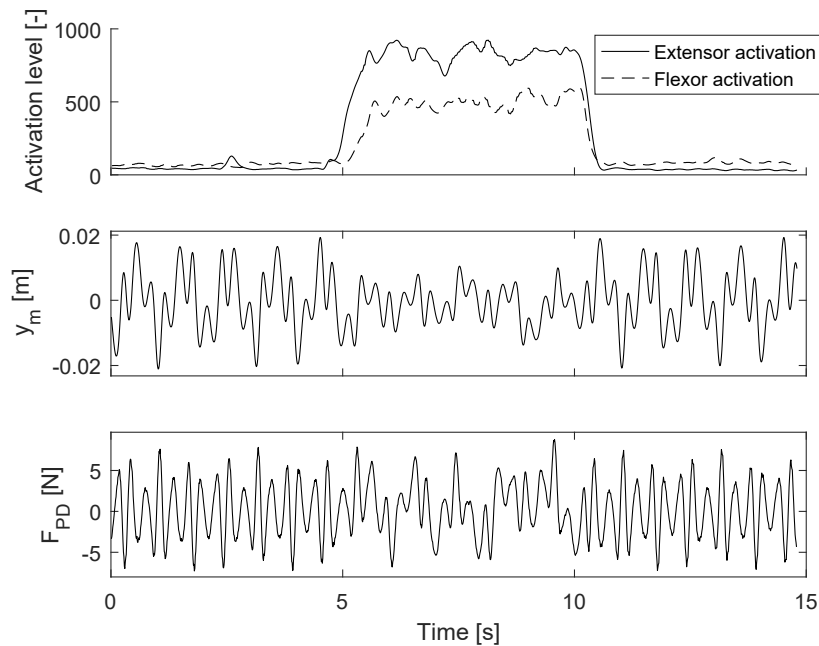


Figure 6.6: Example results of a calibration procedure for estimating the co-contraction levels of the user. Both the extensor and flexor muscle activation levels are shown, together with the motion and force application of the omega.7 master device.

6.4 Task execution in simulation

This section presents the results of the experiments during which test subjects conducted tasks while using the simulated KUKA robot. First, a general overview will be created to show the most significant overall results of the experiments. Next, the results of the accuracy experiment and the impact experiment are discussed in more detail. The consequences of impedance levels and communication delay settings will be discussed by viewing computed mean values of the results and by assessing the significance of the differences between these values. Paired t-tests were executed to conclude on the statistic significance of these differences.

6.4.1 Overall results

The resulting mean absolute positioning errors and mean absolute controller peak forces are plotted for all subjects in Figure 6.7 (without communication delay) and Figure 6.8 (with communication delay). An overview of all results is presented in Appendix C for the accuracy experiments and in Appendix D for the impact experiments.

At first glance, some grouping of data can be recognised when comparing the low, high and variable impedance settings. In general it looks like the variable impedance settings succeeds in creating the desired behaviour, resulting in relatively low values for both the mean positioning errors and the mean peak controller forces. With the added communication delay, the results seem more spread out but still variable impedance seems to result in the most optimal setting of the three. The overall mean values and standard deviations are computed and displayed in Table 6.3 for the accuracy experiments and in Table 6.4 for the impact experiments. The significance of the differences of these means and possible explanations will be discussed over the next sections.

Overall mean absolute positioning errors and standard deviations [mm]

Delay = 0 [msec]				Delay = 10 [msec]			
	Impedance type:				Impedance type:		
	Low	High	Var.		Low	High	Var.
Mean	4.49	1.75	2.70	Mean	4.25	3.34	2.70
Std. Dev.	1.47	0.82	1.49	Std. Dev.	1.99	2.14	0.94

Table 6.3: Overall mean values and standard deviations of the absolute positioning errors recorded during the accuracy experiments with and without the added communication delay of 10 [msec].

Overall mean absolute peak controller forces and standard deviations [N]

Delay = 0 [msec]				Delay = 10 [msec]			
	Impedance type:				Impedance type:		
	Low	High	Var.		Low	High	Var.
Mean	1.59	3.16	1.76	Mean	1.73	3.95	2.06
Std. Dev.	0.14	0.25	0.27	Std. Dev.	0.19	0.20	0.30

Table 6.4: Overall mean values and standard deviations of the absolute peak controller forces recorded during the impact experiments with and without the added communication delay of 10 [msec].

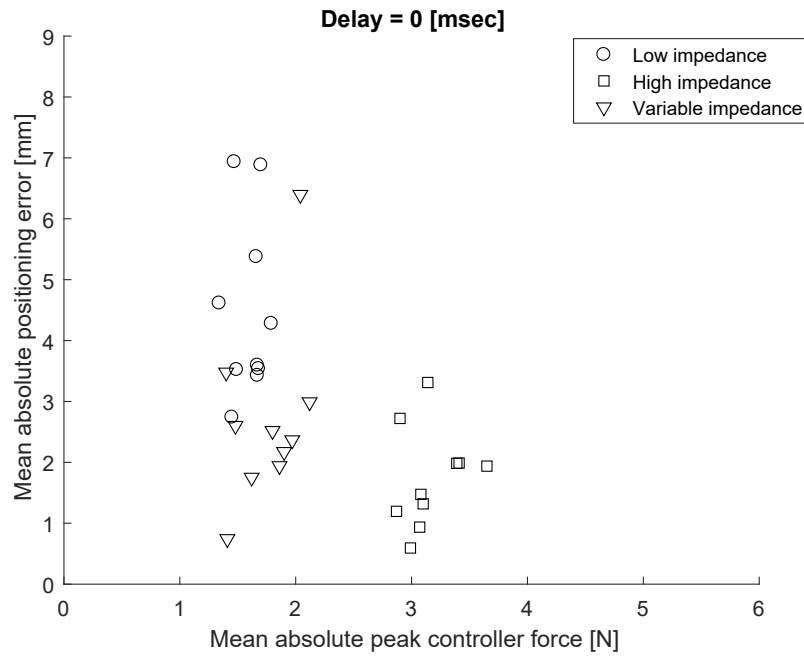


Figure 6.7: Results of the accuracy experiment versus the results of the impact experiment, for all three impedance setting and all test subjects while no communication delay was added to the system.

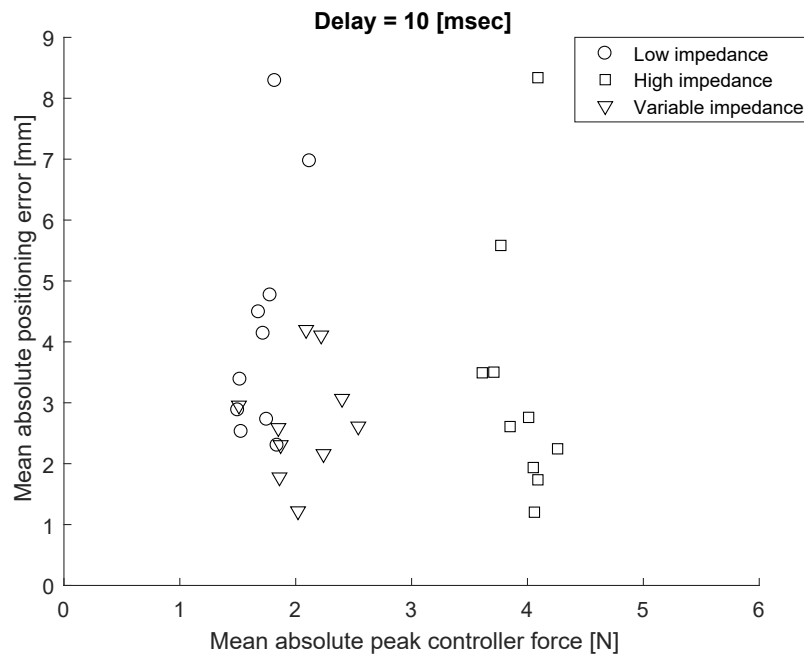


Figure 6.8: Results of the accuracy experiment versus the results of the impact experiment, for all three impedance setting and all test subjects while a communication delay of 10 [msec] was added to the system.

6.4.2 Accuracy experiments

The means that were presented in Table 6.3 are plotted in the bar graph of Figure 6.9. An overview of the collected positioning and co-contraction data can be found in Appendix C. In Appendix E, figures are presented for an example test subject to illustrate typical behaviour seen during these experiments.

Table 6.5 below presents the average co-contraction values computed for the pausing and moving periods and the overall average of these periods combined. In general it is noticed that all test subjects applied co-contraction during the execution of this task. Between the moving and pausing periods and the varying impedance levels, no significant differences were noted.

While an increase in impedance level was expected to result in better positioning accuracy, a similar positive effect is desired for the variable impedance strategy. Table 6.6 presents these changes in percentages and expresses the *p*-value to indicate the significance of this change.

For no added time delay, both the high and variable impedance settings improved the positioning accuracy with respect to the low impedance setting, in which the high impedance setting resulted in the best performance. Both changes can be viewed as statistically significant because of their low *p*-values ($p < 0.05$). The low impedance setting generally showed wobbly behaviour of the slave robot making it hard to position accurately, while the high and variable impedance settings resulted in a stiffer connection. Because co-contraction levels were estimated around 30% on average, the impedance level was generally higher than the low impedances setting but still significantly lower than the high impedance setting. This seemed to translate in the mid-ranged positioning error magnitudes.

In case of the added time delay, the difference in positioning accuracy between the high and low impedance setting became smaller resulting in a difference that cannot be labelled as significant any more. This is due to a combination of smaller mean differences and a larger spread (larger standard deviations, see Table 6.3). The variable impedance setting however performed significantly better than the low impedance setting during the time delayed communication. The mid-ranged impedance level resulting from the medium co-contraction levels seems to be a more optimal setting between a low impedance controlled, wobbly robot and a high impedance controlled, more unstable robot.

The effect of time delay is further indicated by the numbers in Table 6.7. For both the low and variable impedance settings the mean errors changed slightly although these changes cannot be viewed as significant. In the high impedance case however, the errors almost doubled in magnitude. This was clearly the result of undesired motions in both the master and slave device, resulting in decreased transparency. An example of this effect can be found in Figure E.5 of Appendix E.

Mean co-contraction levels [%]						
Delay = 0 [msec]				Delay = 10 [msec]		
	Impedance type:			Impedance type:		
	Low	High	Var.	Low	High	Var.
Pausing	36.07	29.45	30.02	36.94	33.38	31.05
Moving	35.05	29.34	31.11	32.44	31.68	30.90
Total	35.56	29.39	30.57	34.69	32.53	30.97

Table 6.5: Overall mean co-contraction levels during the accuracy experiments for periods of pausing, moving and these periods combined. Computed for all impedance settings with and without the added communication delay of 10 [msec].

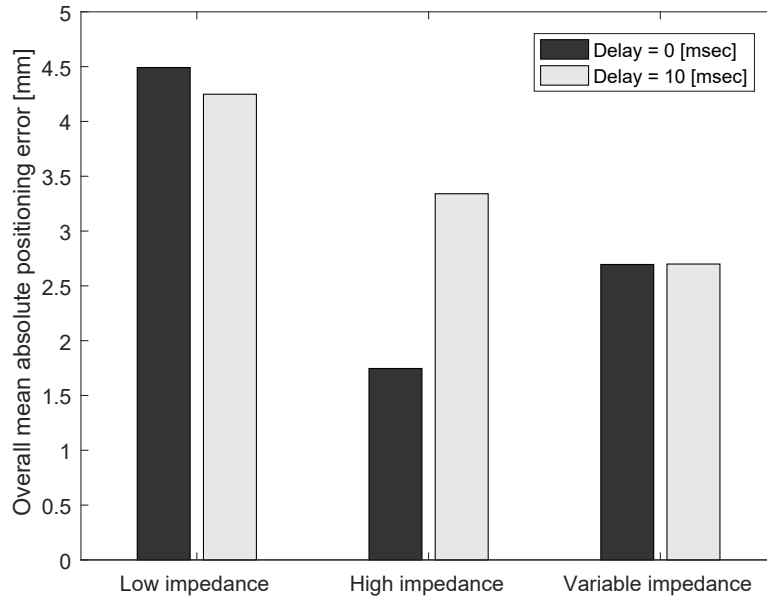


Figure 6.9: Overall mean absolute positioning errors for all tested impedance levels and communication delay settings.

Change of mean absolute positioning error for compared impedance settings

	Delay = 0 [msec]		Delay = 10 [msec]	
	Impedance type: Low → High Low → Var.		Impedance type: Low → High Low → Var.	
Change	↓ 61.12%	↓ 39.99%	↓ 21.37%	↓ 36.47%
p-value	0.00	0.02	0.23	0.03

Table 6.6: Percentage of change in overall mean absolute positioning error and the corresponding *p*-values when comparing the low impedance setting to the high and variable impedance settings with and without the added time delay of 10 [msec].

Change of mean absolute positioning errors for delay = 0 → 10 [msec]

	Impedance type: Low High Var.		
Change	↓ 5.42%	↑ 91.28%	↑ 0.15%
p-value	0.60	0.02	0.99

Table 6.7: Percentage of change in overall mean absolute positioning error and the corresponding *p*-values which resulted from the addition of the communication delay of 10 [msec] for all impedance settings.

6.4.3 Impact experiments

Figure 6.10 presents the overall mean absolute peak controller forces that were computed from the impact experiment data, as previously shown in Table 6.4. Example figures can be found for the impact experiment's results of one test subject in Appendix F.

Table 6.8 shows the mean computed co-contraction estimations recorded during these experiments. Overall it can be concluded that these co-contraction levels are significantly lower than during the accuracy experiment. This created a more compliant connection between the master and slave device during the variable impedance setting, much more comparable to the low impedance setting.

This time, with respect to the high impedance level, a low impedance level was expected to reduce peak controller forces in impact situations. Furthermore, the same behaviour would be desired from the variable impedance strategy. From the data presented in Figure 6.10 it looks like this is indeed the case.

Table 6.9 indicates this decrease of peak controller forces when comparing the high impedance setting to the low and variable impedance settings. The mean values are clearly decreased with clear statistical significance while using either the low or variable impedance setting. This also holds for the situation in which a communication delay was added to the system. As expected, the variable impedance setting seems to resemble the low impedance setting during the execution of this task.

The effect of time delay is also visible in Figure 6.10, showing an increase in peak controller forces for every impedance setting. These increases are listed in Table 6.10, indicating that all these increases are statistically significant. This is clearly a result of the decreased transparency in which the reaction of the impedance controller is dominant at the slave side rather than the operator's reaction to the impact. Although for the variable impedance setting an increase of peak controller forces is seen as well, the peak forces are still significantly lower with respect to the high impedance setting as was indicated in Table 6.9, creating a successful result for the variable impedance controller.

Mean co-contraction levels [%]							
Delay = 0 [msec]			Delay = 10 [msec]				
	Impedance type:			Impedance type:			
	Low	High	Var.	Low	High	Var.	
Mean	4.88	5.19	4.30	Mean	6.76	6.57	8.63

Table 6.8: Overall mean co-contraction levels during the impact experiments. Computed for all impedance settings with and without the added communication delay of 10 [msec].

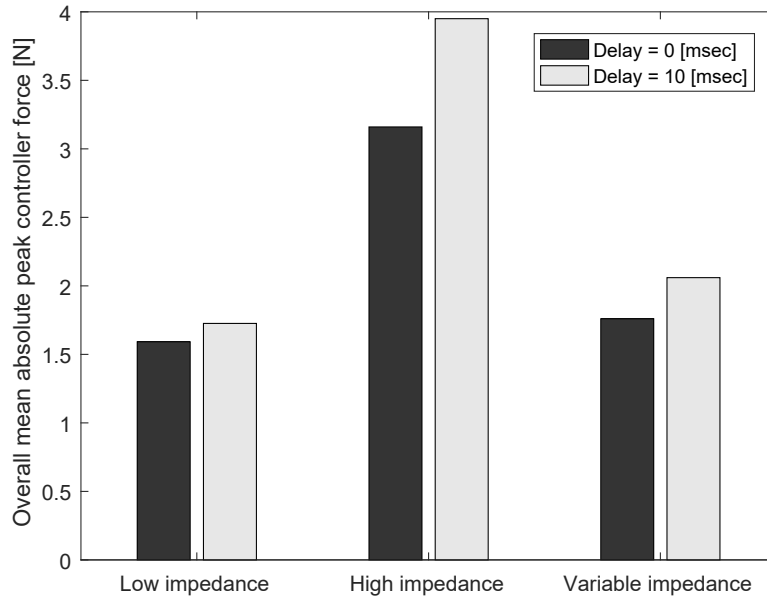


Figure 6.10: Overall mean absolute peak controller forces for all tested impedance levels and communication delay settings.

Change of mean absolute peak controller forces for compared impedance settings

	Delay = 0 [msec]		Delay = 10 [msec]	
	Impedance type: High → Low High → Var.		Impedance type: High → Low High → Var.	
Change	↓ 49.62%	↓ 44.30%	↓ 56.30%	↓ 47.85%
p-value	0.00	0.00	0.00	0.00

Table 6.9: Percentage of change in overall mean absolute peak controller forces and the corresponding p -values when comparing the high impedance setting to the low and variable impedance settings with and without the added time delay of 10 [msec].

Change of mean absolute peak controller forces for delay = 0 → 10 [msec]

	Impedance type: Low High Var.		
Change	↑ 8.42%	↑ 25.00%	↑ 17.05%
p-value	0.02	0.00	0.00

Table 6.10: Percentage of change in overall mean absolute peak controller forces and the corresponding p -values which resulted from the addition of the communication delay of 10 [msec] for all impedance settings.

7 Conclusions

The conclusions of this research are described in this chapter by reviewing the main goal and the stated hypotheses. The main goal of this research was stated in Chapter 1 as the following:

"Create a teleoperation system that presents force feedback to the operator in which EMG data from the operator's muscles is implemented in the control architecture to increase the intuitiveness and effectiveness of the execution of telemanipulation tasks while the system is subjected to time delays in its communication channel."

This goal focusses on the design of a teleoperation system and on its intuitiveness and effectiveness while executing telemanipulation tasks. Looking at the overall design of the system, it is fully functional and the resulting system behaves as expected as was shown in the results of the validation experiments (Section 6.1). A few limitation became evident, mainly as a result of limited transparency properties of the KUKA slave robot. Friction seemed to be a general cause of limited functionality of the controller, which was lowered in simulation such that the functionality of the controller itself could be tested properly. In general, the functionality of impedance controllers in a teleoperation control system suffers from dominant dynamics of the robotic devices. This also became apparent when testing communication delay settings, during which the significant inertia properties of both the KUKA hardware and simulated model caused transparency problems. These dominant inertia properties caused relatively large quantities of energy leaking which is why the added communication delays were limited to 10 [msec]. The proposed variable impedance controller, or any impedance controller for that matter, would be more effective and more robust if used with a more transparent robotic slave device or when a form of friction and/or inertia compensation would have been applied.

In assessing the intuitiveness and effectiveness of the designed teleoperation system, three hypothesis were stated in Chapter 3. These hypotheses were related to the expected co-contraction behaviour of the human operators, the influences of time delayed communication and the desired functioning of the variable impedance controller.

The first hypothesis includes the expected co-contraction characteristics:

"During the execution of a positioning task focussed on accuracy, a person will try to reject disturbing forces by increasing the co-contraction level of the arm. During a task in which the focus is placed on careful interaction, a person will try to minimise contact forces by lowering this co-contraction level."

The calibration process that was used to set the minimum and maximum muscle activation levels of the test subjects actually relied on this hypothesis being true. Indeed, muscle activation levels of both the flexor and extensor muscles were significantly lower when the test subjects tried to minimise the interaction forces between them and the omega.7 haptic device. When the test subjects tried to keep the omega.7 in place, they rejected the disturbing forces to some extent by increasing the activation of the flexor and extensor muscle pair resulting in a higher level of co-contraction. This behaviour was seen for all test subjects and was the first clear proof of this hypothesis being true.

Next, during the task execution experiments, again clear difference were seen in co-contraction behaviour. All test subjects used relatively low co-contraction levels during the impact experiment to reduce the interaction forces between the robot and its environment as much as possible. During the accuracy experiments, they all used significantly higher co-contraction levels with the goal of precision in mind.

Overall it is concluded that this hypothesis indeed holds, which presents the opportunity to use this intuitive muscular behaviour in the control architecture of the teleoperation system.

The second hypothesis, regarding the effects of time delayed communication, was stated as the following:

"If a time delay is added to the communication channel of the teleoperation system, controller efforts will increase during impact situations. Furthermore, this delay will cause additional unstable behaviour and will require the stability layer to intervene more aggressively, both resulting in decreased transparency."

It first claims that controller efforts will increase during impact situations if a time delay is added to the communication channel of the teleoperation system. This part of the hypothesis was proven by the data resulting from the impact experiment as shown in Section 6.4.3. Figure 6.10 in this section shows an increase of measured control efforts for all impedance levels while paired t-tests showed this increase was significant for all impedance settings. This confirms the expectations, presenting a problem that is created during time delayed communication and which can especially harm safety when a controller with a high impedance setting is used.

The second part of this hypothesis claims that the added communication delay will cause additional unstable behaviour. This was expected to decrease the transparency level of the system resulting in decreased effectiveness. Furthermore, the stability layer was expected to intervene more to keep interactions safe, which also would come at the cost of the transparency level.

This hypothesis definitely holds for the tested high impedance setting. Not only did the mean peak controller efforts rise, the mean positioning errors increased as well. The added time delay resulted in mean positioning errors that almost doubled in magnitude. A shaking behaviour of both the master and slave robots was clearly visible for both the master and slave devices as represented in the example graph of Figure E.5 in Appendix E. The fact that the stability layer has to intervene more was already shown in de 3-DOF functionality experiments. This added damping keeps the devices from destabilising completely, however it does add an additional feeling of sluggishness to the robot. For the low and variable impedance settings this hypothesis is not proven because of the limited amount of active behaviour that occurred. The influence on both the positioning accuracy and the controller efforts was far less significant for these settings.

The final hypothesis then describes the desired behaviour of the designed variable impedance control approach:

"Modulating the impedance characteristic of a haptic controlled teleoperated robot through EMG allows an operator to intuitively adapt the behaviour of the robot such that the operator can make use of the advantages of both relatively high and low impedance behaviour."

Combined with the overview of advantages which is referred to (see Table 3.2) it can be stated that the variable impedance approach was expected to result in a controller that is transparent when desired (e.g. during accurate positioning) but which is also relatively save (low controller efforts) and relatively stable (low energy leakage). Furthermore, the proposed method that uses EMG data to modulate the impedance level of the controller was expected to result in an intuitive control approach.

Data shows that during the accuracy experiment, the impedance level of the controller was automatically increased as a result of the increased co-contraction level of the test subjects. When no communication delay was added, the high impedance setting clearly performed best as a result of the highest level of transparency. Although the positioning errors for the variable impedance setting were a bit larger, most likely due to an overall lower level of impedance, it clearly outperformed the low impedance setting. The latter was also true when the time delay of the communication channel was increased. Because of the large amount of active behaviour

seen during the high impedance setting, the accuracy of this setting decreased drastically resulting in the best accuracy for the variable impedance controller. This seems to be the result of a more optimal level of impedance creating a better balance between transparency and stability. It is expected that the lower amount of active behaviour seen in the variable impedance controller was mainly a result of the settings that created this medium impedance level. Lower values of maximum muscle activation levels for instance would have created higher impedance levels which might have resulted in the same stability problems for the variable impedance setting. No significant difference in impedance levels was spotted for periods of moving and pausing, which could have suggested another form of active behaviour limitation. Overall, it can be concluded that the variable impedance setting outperformed the low impedance setting when it comes to accuracy and that indeed, the test subjects were able to make advantage of the higher impedance behaviour that resulted from the variable impedance setting.

During the impact experiment, the variable impedance setting was desired to show more resemblance with the low impedance setting to decrease controller efforts in impact situations. This corresponds with the behaviour seen, in which the controller efforts of the low and variable impedance settings were very comparable and were indeed much lower than for the high impedance setting. This means the behaviour of the robot was properly adapted resulting in a more compliant connection between the master and slave device during this experiment that was focussed on careful interaction rather than accuracy.

It is important to remember that the test subjects were not aware of the fact that they were able to change the controller's behaviour by altering their muscle activation. This means that the behaviour of the variable impedance controller was set unintentionally, while it matched the desired task-dependent characteristics. Since it resulted in an increase of positioning accuracy when compared to the low impedance setting and a decrease in controller efforts when compared to the high impedance setting it can be concluded that indeed, this setting made use of the advantages of the desired impedance levels and that the control of the variable impedance level was intuitive.

Based on this validation of the hypotheses it can be concluded that the second part of the research goal was also reached, adding effectiveness of the teleoperation system in an intuitive way for the tested circumstances.

8 Recommendations

The described research presented the design of a new teleoperation architecture, including initial testing of very basic functionalities and tasks. For future work, it is recommended to further test the design to validate the chosen approaches and to reduce the limitations that were indicated.

The experiments that were conducted showed that the controller is fully functional when used on a simulated, more transparent and more ideal model of the KUKA LWR4+ robot. Limitations of the impedance control approach showed as a result of the relatively high inertia and friction properties, especially when compared to the used omega.7 master device. Since the controller was designed in a generalised way, it allows for implementation on other robotic devices. Degrees of freedom can easily be restricted which means that more simplistic robotic devices can be used for testing as well. If implementation on the current KUKA robot is desired, methods of dynamics compensation can be researched which superpose torques that compensate for disturbing dynamics like friction. It will however be a challenge to guarantee the passivity of such approaches, which will be necessary to guarantee the stability of the teleoperation system as a whole.

Besides possible future work on hardware implementation, other experiments can be carried out to expand the knowledge on the functionality of the designed control approach. During the presented research, experiments of a very basic nature were conducted to validate the hypotheses. Now that the basic functionality seems promising, next steps can be taken to for instance test a larger variety or combination of other tasks and operators.

Future testing could include:

- Testing a larger variety of tasks, for instance including insertion tasks, vibration isolation and force application.
- Combining tasks to for instance test the possibilities of quickly switching between the tested accurate positioning and careful interaction. This will give more information on the ability to dexterously modulate the impedance level intuitively.
- Subjective measures can be included in future research to get an idea of how the operators experience the interaction with the devices and the impedance modulation. There is still quite some uncertainty when it comes to the level of intuitiveness in other, not yet tested situations like during environment contact or force application tasks.
- Conducting tests with more experienced operators might yield different results than the tests with inexperienced operators. Part of the measured co-contraction behaviour could be a result of a more tense, uncomfortable attitude of the participating test subjects.
- During the experiment, the test subjects were never aware of the fact that they were able to modulate the impedance level of the controller through their muscle activation. Including this awareness in future testing might show different behaviour and could show if operators can use this awareness properly and what the effect is on the intuitiveness of task execution.

These additional test will give more information on the effectiveness and intuitiveness of the impedance modulation approach that uses the EMG-based co-contraction estimation. When added to the results that were already presented, future work will hopefully contribute to the conclusions on possible helpful implementations of the designed method.

Appendices

A Indication of static friction in KUKA joints

Joint name	r [cm]	$F_{fr} \curvearrowleft$ [N]	$F_{fr} \curvearrowright$ [N]	$T_{fr} \curvearrowleft$ [Nm]	$T_{fr} \curvearrowright$ [Nm]
A1	19.5	2	5	0.390	0.975
A2	19.5	2.5	3.5	0.487	0.683
E1	19.5	2.5	3	0.488	0.585
A3	19.5	2.5	2.5	0.488	0.488
A4	5.5	6	6	0.330	0.330
A5	8.5	7.5	5.5	0.638	0.468
A6	3.0	15	8	0.450	0.240

Table A.1: Computed static friction torques T_{fr} in the KUKA joints for clockwise and counter-clockwise rotations from measured forces F_{fr} at a radius r from the centre of the joints.

B Results of the calibration procedures using test subjects

Subject	$\alpha_{ext,max}$	$\alpha_{flex,max}$
1	500	150
2	200	100
3	200	100
4	350	300
5	800	200
6	650	300
7	300	150
8	400	300
9	250	400
10	1050	900

Table B.1: Maximum extensor and flexor muscle activation levels ($\alpha_{ext,max}$ and $\alpha_{flex,max}$ respectively) established during the calibration procedures for every individual test subject.

C Results of the accuracy experiments using test subjects

C.1 Without added communication delay

Mean absolute positioning errors [mm]				Mean co-contraction level during pausing (and moving) [%]			
Subject no.	Impedance type:			Subject no.	Impedance type:		
	Low	High	Var.		Low	High	Var.
1	3.54	3.31	6.40	1	22.64 (21.56)	25.07 (25.52)	19.96 (18.41)
2	6.88	1.20	2.99	2	69.08 (62.88)	53.96 (47.72)	61.22 (56.13)
3	3.59	0.94	2.52	3	30.78 (32.59)	40.98 (45.23)	31.07 (32.13)
4	5.38	1.99	2.37	4	53.53 (56.04)	30.14 (30.93)	34.58 (37.18)
5	4.28	1.47	1.94	5	15.27 (12.39)	12.14 (14.08)	11.85 (11.15)
6	6.94	1.98	2.60	6	18.09 (18.75)	22.22 (21.17)	28.40 (29.55)
7	4.62	1.32	3.48	7	9.57 (13.16)	2.67 (4.81)	3.93 (8.23)
8	3.52	2.72	2.17	8	48.74 (51.16)	55.75 (51.34)	36.11 (36.30)
9	2.74	0.59	0.74	9	47.82 (44.23)	26.45 (26.63)	42.28 (51.87)
10	3.43	1.94	1.75	10	45.17 (37.76)	25.08 (25.94)	30.84 (30.16)

Table C.1: Overview of the results of the accuracy experiments without the added communication delay. Mean absolute positioning errors and mean co-contraction levels during pausing (and moving) are shown.

C.2 With added communication delay of 10 [msec]

Mean absolute positioning errors [mm]				Mean co-contraction level during pausing (and moving) [%]			
Subject no.	Impedance type:			Subject no.	Impedance type:		
	Low	High	Var.		Low	High	Var.
1	4.14	8.34	4.11	1	16.84 (18.24)	23.85 (25.28)	16.81 (17.52)
2	4.49	3.49	2.61	2	73.83 (62.32)	62.13 (56.63)	39.55 (36.06)
3	4.77	2.61	4.20	3	40.05 (34.86)	49.65 (48.20)	57.31 (54.22)
4	6.97	5.58	3.07	4	40.52 (37.61)	23.57 (23.06)	24.52 (24.38)
5	2.30	1.94	2.16	5	9.31 (8.31)	11.87 (11.77)	10.62 (13.12)
6	8.29	3.50	2.31	6	22.36 (20.39)	23.28 (23.66)	28.99 (31.11)
7	3.39	2.24	2.96	7	1.36 (4.56)	11.01 (12.51)	3.94 (7.25)
8	2.88	1.73	2.59	8	69.35 (53.92)	59.63 (52.14)	53.18 (47.77)
9	2.53	1.20	1.22	9	69.73 (60.09)	37.37 (34.55)	50.31 (52.38)
10	2.73	2.76	1.78	10	26.01 (24.10)	31.40 (29.01)	25.27 (25.19)

Table C.2: Overview of the results of the accuracy experiments with the added communication delay of 10 [msec]. Mean absolute positioning errors and mean co-contraction levels during pausing (and moving) are shown.

D Results of the impact experiments using test subjects

D.1 Without added communication delay

Mean absolute peak control forces [N]				Mean co-contraction level [%]			
Subject no.	Impedance type:			Subject no.	Impedance type:		
	Low	High	Var.		Low	High	Var.
1	1.68	3.14	2.04	1	10.29	10.77	10.34
2	1.70	2.87	2.12	2	22.46	26.09	10.89
3	1.67	3.07	1.80	3	1.56	3.09	0.71
4	1.66	3.41	1.97	4	4.56	4.65	7.29
5	1.79	3.08	1.86	5	1.53	2.15	1.77
6	1.47	3.39	1.48	6	0.27	0.79	0.08
7	1.34	3.10	1.40	7	0.18	0.37	0.05
8	1.49	2.90	1.90	8	7.49	3.89	11.75
9	1.45	2.99	1.41	9	0.01	0.01	0.00
10	1.67	3.65	1.62	10	0.41	0.09	0.08

Table D.1: Overview of the results of the impact experiments without the added communication delay. Mean absolute peak control forces and mean co-contraction levels are shown.

D.2 With added communication delay of 10 [msec]

Mean absolute peak control forces [N]				Mean co-contraction level [%]			
Subject no.	Impedance type:			Subject no.	Impedance type:		
	Low	High	Var.		Low	High	Var.
1	1.72	4.09	2.22	1	8.07	5.67	7.23
2	1.68	3.61	2.54	2	25.28	19.38	38.96
3	1.78	3.85	2.09	3	5.55	10.01	4.43
4	2.12	3.77	2.40	4	5.70	10.73	8.95
5	1.84	4.05	2.24	5	6.15	1.04	5.24
6	1.82	3.71	1.87	6	0.00	0.31	0.05
7	1.52	4.26	1.51	7	3.46	1.30	3.08
8	1.50	4.09	1.85	8	9.52	10.61	11.18
9	1.53	4.06	2.02	9	3.83	6.56	7.13
10	1.75	4.01	1.86	10	0.04	0.12	0.09

Table D.2: Overview of the results of the impact experiments with the added communication delay of 10 [msec]. Mean absolute peak control forces and mean co-contraction levels are shown.

E Plots of example results of the accuracy experiments

E.1 Without added communication delay

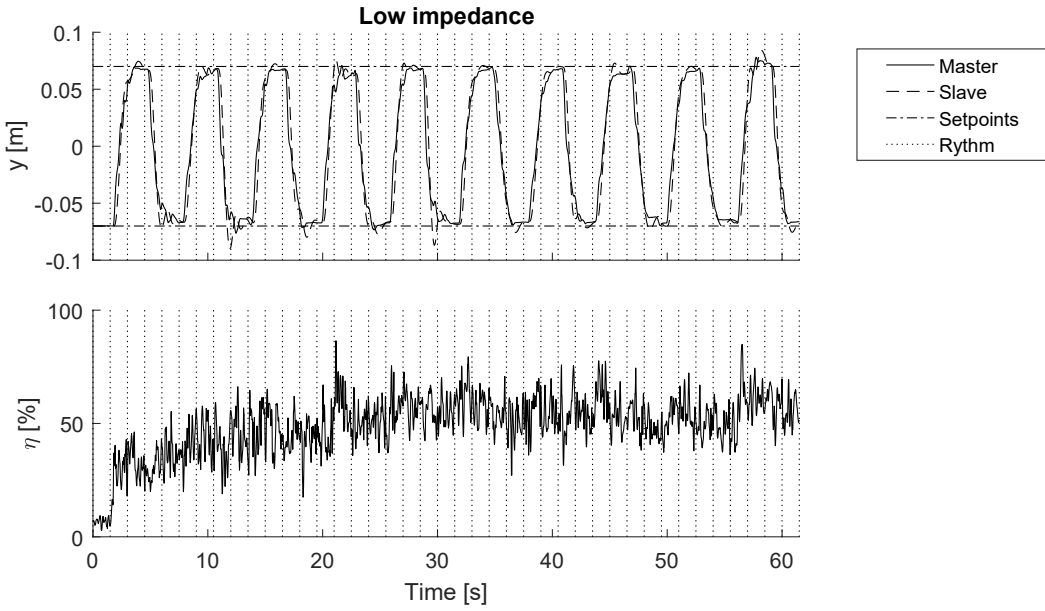


Figure E.1: Example result of the accuracy experiment for the low impedance setting without added communication delay. The master and slave positions are indicated with respect to the set-points. Furthermore, the estimated co-contraction level of the test subject is shown. The rhythm of the audio commands is indicated by the dotted vertical lines.

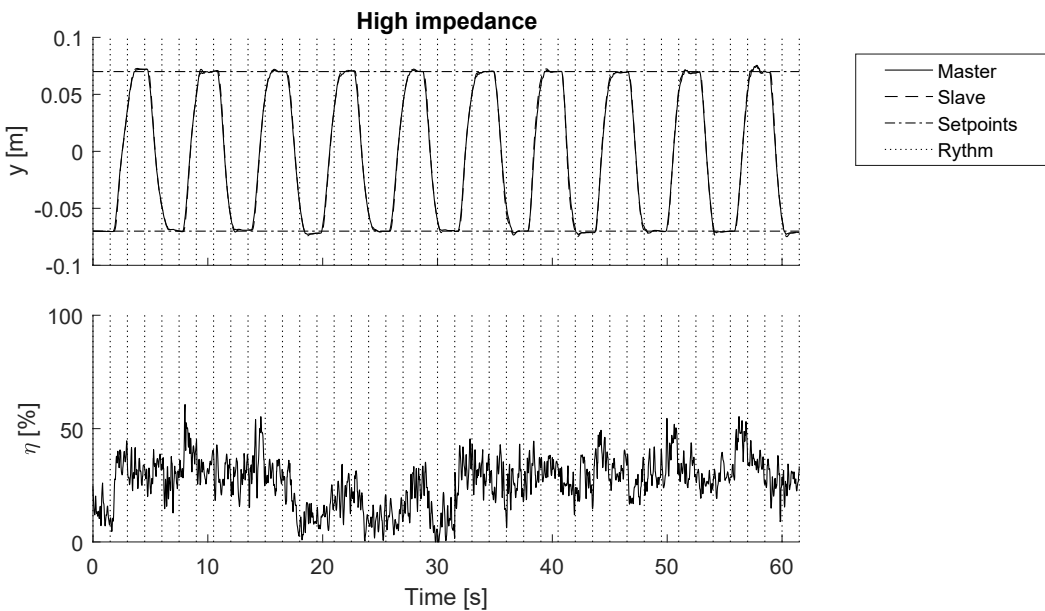


Figure E.2: Example result of the accuracy experiment for the high impedance setting without added communication delay. The master and slave positions are indicated with respect to the set-points. Furthermore, the estimated co-contraction level of the test subject is shown. The rhythm of the audio commands is indicated by the dotted vertical lines.

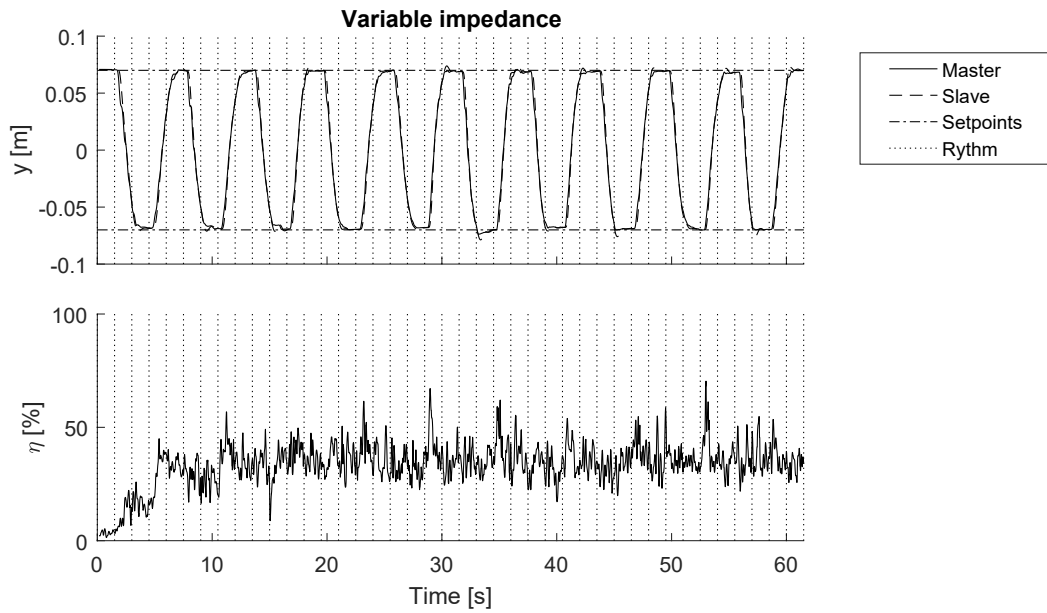


Figure E.3: Example result of the accuracy experiment for the variable impedance setting without added communication delay. The master and slave positions are indicated with respect to the set-points. Furthermore, the estimated co-contraction level of the test subject is shown. The rhythm of the audio commands is indicated by the dotted vertical lines.

E.2 With added communication delay of 10 [msec]

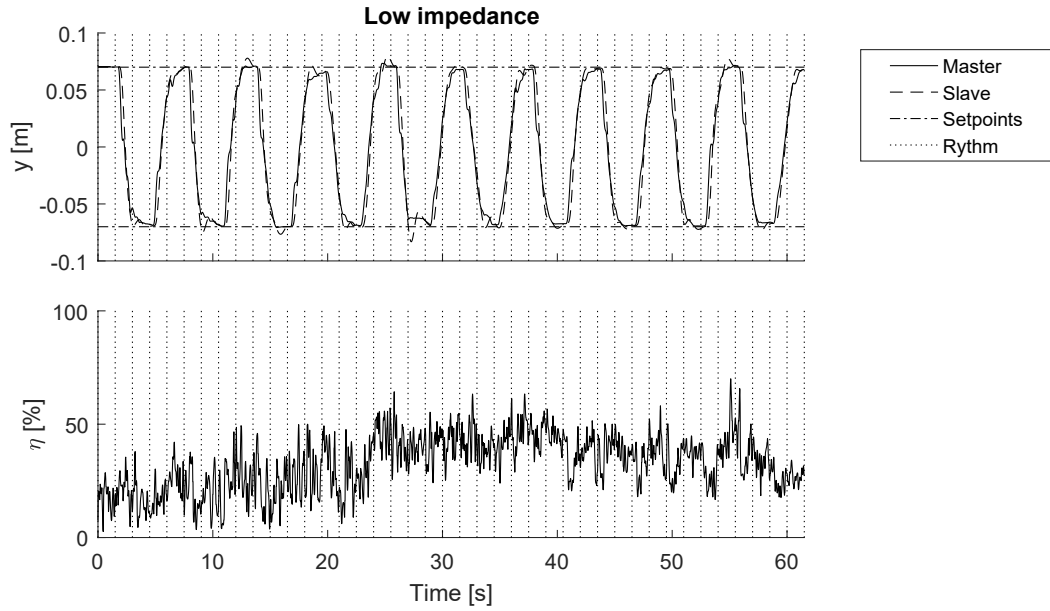


Figure E.4: Example result of the accuracy experiment for the low impedance setting with the added communication delay of 10 [msec]. The master and slave positions are indicated with respect to the setpoints. Furthermore, the estimated co-contraction level of the test subject is shown. The rhythm of the audio commands is indicated by the dotted vertical lines.

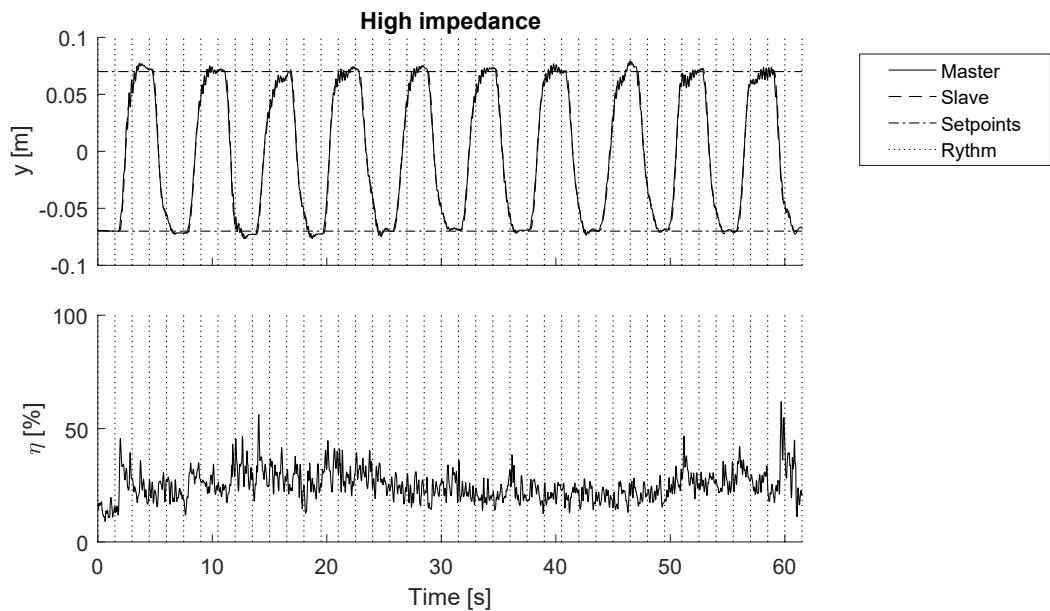


Figure E.5: Example result of the accuracy experiment for the high impedance setting with the added communication delay of 10 [msec]. The master and slave positions are indicated with respect to the setpoints. Furthermore, the estimated co-contraction level of the test subject is shown. The rhythm of the audio commands is indicated by the dotted vertical lines.

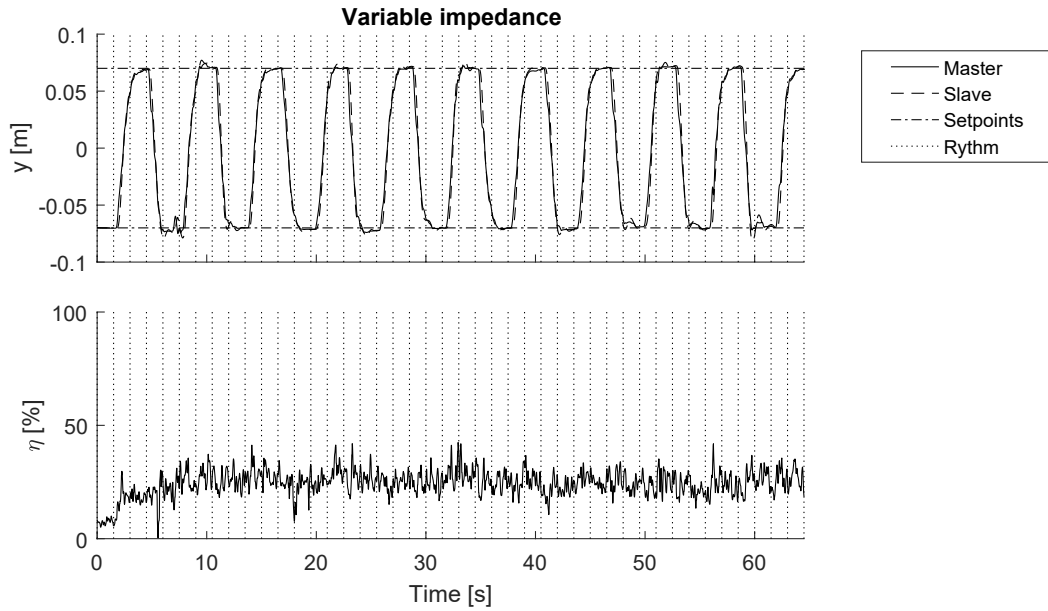


Figure E.6: Example result of the accuracy experiment for the variable impedance setting with the added communication delay of 10 [msec]. The master and slave positions are indicated with respect to the setpoints. Furthermore, the estimated co-contraction level of the test subject is shown. The rhythm of the audio commands is indicated by the dotted vertical lines.

F Plots of example results of the impact experiments

E.1 Without added communication delay

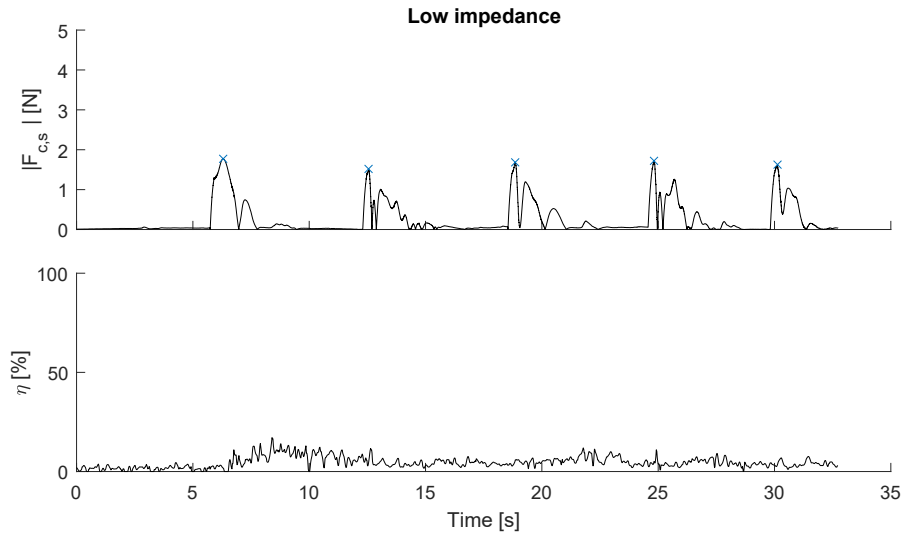


Figure E.1: Example results of the impact experiment for the low impedance setting without the added communication delay. The slave's impedance control force is shown, the peak values are indicated by the cross symbols. Furthermore, the estimated co-contraction level of the test subject is shown.

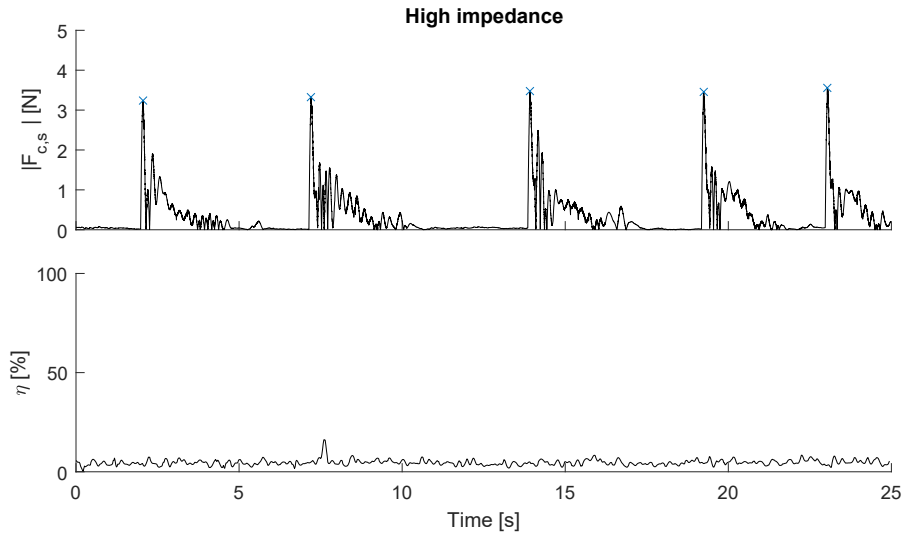


Figure E.2: Example results of the impact experiment for the high impedance setting without the added communication delay. The slave's impedance control force is shown, the peak values are indicated by the cross symbols. Furthermore, the estimated co-contraction level of the test subject is shown.

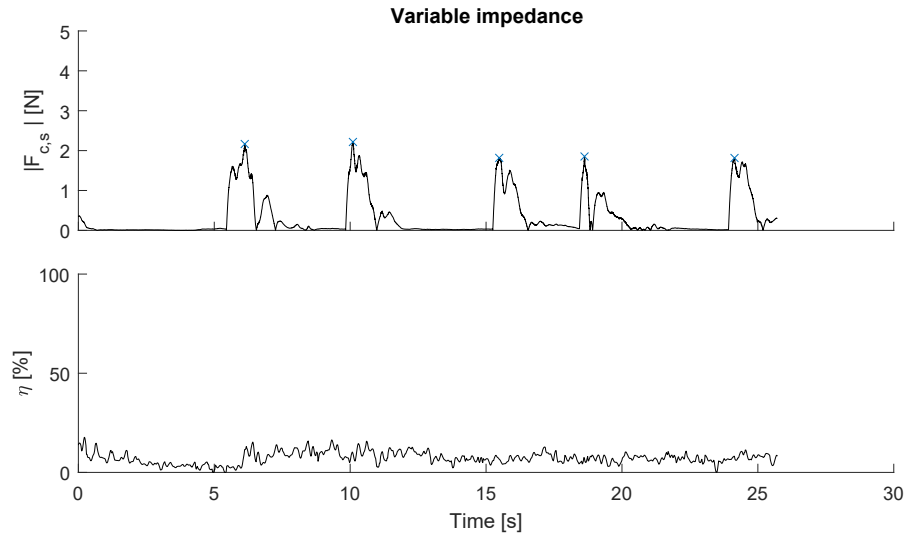


Figure E.3: Example results of the impact experiment for the variable impedance setting without the added communication delay. The slave's impedance control force is shown, the peak values are indicated by the cross symbols. Furthermore, the estimated co-contraction level of the test subject is shown.

F.2 With added communication delay of 10 [msec]

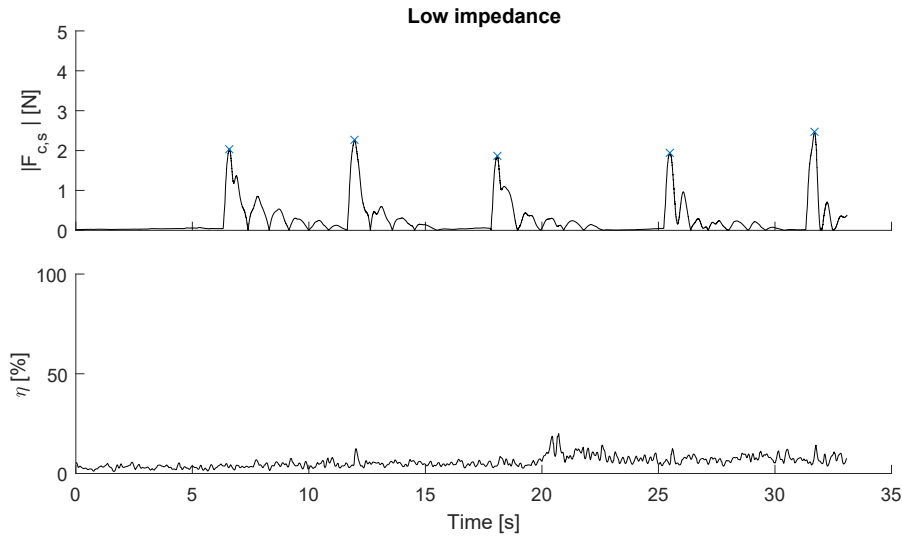


Figure F.4: Example results of the impact experiment for the low impedance setting with the added communication delay of 10 [msec]. The slave's impedance control force is shown, the peak values are indicated by the cross symbols. Furthermore, the estimated co-contraction level of the test subject is shown.

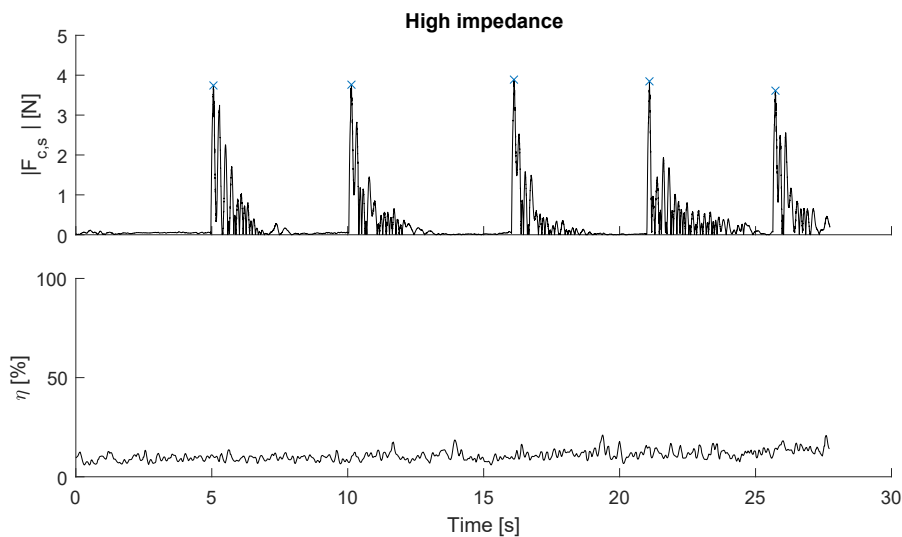


Figure F.5: Example results of the impact experiment for the high impedance setting with the added communication delay of 10 [msec]. The slave's impedance control force is shown, the peak values are indicated by the cross symbols. Furthermore, the estimated co-contraction level of the test subject is shown.

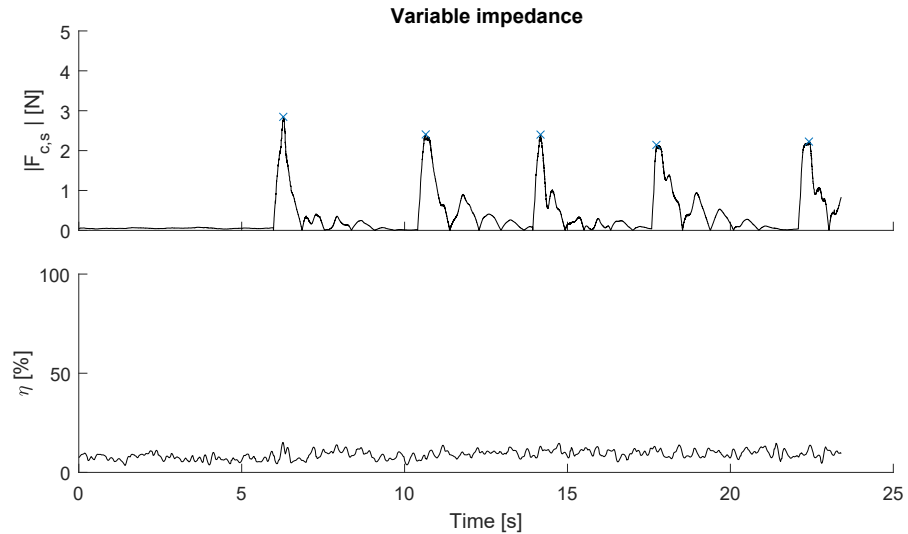


Figure F.6: Example results of the impact experiment for the variable impedance setting with the added communication delay of 10 [msec]. The slave's impedance control force is shown, the peak values are indicated by the cross symbols. Furthermore, the estimated co-contraction level of the test subject is shown.

G Implementation and use of software packages

G.1 Overview

In this final appendix, an overview of the used software packages is given and details on the implementation and use are discussed. All software packages can be accessed by members of the i-Botics group on the git repositories of TNO and the University of Twente. For a general overview of the interconnection of nodes in the fully functional teleoperation system, see Figure 4.10.

G.2 Software packages

The software packages created during this research are the following:

- *omega_x* (passive branch): takes care of control and communication regarding the omega.7 haptic device. It can also be used for the omega.6 (which does not contain the gripper action).
- *kuka-lwr* (i-Botics branch): contains the KUKA controllers, Gazebo models and hardware interfacing necessary to control the KUKA hardware through the FRI or the simulated model.
- *myo_arband*: with this package, muscle activation and gesture control data can be read from the Myo Armband. It also includes software to estimate the co-contraction levels and low-pass filter the computed signals.
- *myo_omega_kuka_connection*: this package can be used to connect the three devices to each other. It contains the overall communication structure and scripts that can be used to calibration the co-contraction level estimation.

These packages are tested for Gazebo 7 and ROS Indigo and Kinetic, running on Ubuntu 14 and 16. Other freely available packages on which the software depends are *ros_keyboard* (to add the functionality of keyboard commands) and *ros_control* (to create the interfacing between the KUKA robot or simulated model and the KUKA controllers).

G.3 ROS nodes

The ROS nodes that are used, as indicated with their more general names in the overview of Figure 4.10, are the following:

- *omega_passive_node*: this is the omega node that takes care of communication with the omega haptic device. It also includes the transparency and stability layers of the master controller and sends information to the communication channel.
- *myo-rawNode*: this node captures the muscle activation data from the Myo Armband through the Bluetooth connection.
- *cocon_level*: from the muscle activation data, this node determines the co-contraction level estimation and applies low-pass filtering.
- *communication_node*: this node takes care of the communication between the master and slave sides of the system. It is able to hold on to messages for a specified amount of time before passing them to the other side to create a communication delay.

As for controlling the KUKA hardware and model, the nodes are part of the hardware interface. The *lwr_hw_fri_node* is able to load a controller and connect it to the KUKA hardware (through the FRI) while Gazebo is able to launch a node that loads a controller to control

the simulated model. The controller which is loaded by one of these nodes, referenced to as the KUKA controller if Figure 4.10, is a script that is called the *movit_controller* (short for the *myo_omega_variable_impedance_teleoperation_controller*). This controller contains the transparency and stability layers for the slave device. It is written in a general form such that the same controller can be loaded by either the FRI node or the Gazebo node.

G.4 Settings

The settings used in the teleoperation system can be adapted in the YAML files located in the config folder of the *myo_omega_kuka_connection* package. These settings include all parameters seen in Table 4.2, toggling degrees of freedom, force feedback and energy monitoring functionalities and specifying the minimum and maximum muscle activation levels of the operator. These settings should only be adjusted with care. A safe approach is to always test settings in simulation while force feedback is disabled.

G.5 Launch files

Launch files are created to quickly start the teleoperation system. A distinction is made between a demo launch and the launch of the experiment set-up. These launch files are all located in the *myo_omega_kuka_connection* package.

Demo

The demo launch file launches the control of the simulated KUKA model. Through keyboard commands, the impedance setting can be changed. By opening the ros_keyboard application and pressing ‘1’, the low impedance setting is activated, pressing ‘2’ activates the high impedance setting and pressing ‘3’ activates the variable impedance setting. Furthermore, recording of data into a rosbag file can be started by pressing ‘r’ and stopped by pressing ‘s’.

If the master device is pulled back (toward the operator) as far as possible, the following launch files will spawn objects to create a tangible remote environment:

- *spawn_table.launch*: spawns a fixed table with a fixed block attached.
- *spawn_objects.launch*: spawn additional non-fixed objects on the table.
- *spawn_wall.launch*: spawns a fixed wall in front of the robot.
- *spawn_test_block.launch*: spawns fixed block with some textures and a hole.

If control of the KUKA hardware is desired, the demo launch file can be launched with the following additional commands: *use_sim:=false lwrPowered:=true*.

Experiments

In order to recreate the experiments which were conducted using test subjects, the experiment launch file can be used. Before starting the experiment, the *calibrate_myo* launch file can be started to start the calibration procedure of the muscle activation levels. By opening the ros_keyboard application and pressing the spacebar, the motion of the haptic device can be toggled on and off.

After launching the experiment, the simulated slave robot can be controlled while the user only sees its end effector. Again, the impedance settings can be altered through the keyboard commands 1-3 and recording can be started and stopped. Furthermore, pressing ‘p’ will start the accuracy experiment and pressing ‘f’ will start the impact experiment. During the impact experiment, pressing ‘f’ again will initiate the motion of the small block that will hit the robot’s end effector.

Bibliography

- Ajoudani, A., N. Tsagarakis and A. Bicchi (2012), Tele-impedance: Teleoperation with impedance regulation using a body-machine interface, *International Journal of Robotics Research*, vol. 31(13), pp. 1642–1655.
- Brygo, A., I. Sarakoglou, N. Tsagarakis and D. Caldwell (2015), Tele-manipulation with a humanoid robot under autonomous joint impedance regulation and vibrotactile balancing feedback, in *IEEE-RAS International Conference on Humanoid Robots*, volume 2015–February, pp. 862–867.
- Chen, J., M. Glover, C. Li and C. Yang (2016), Development of a user experience enhanced tele-operation approach, in *ICARM 2016 - 2016 International Conference on Advanced Robotics and Mechatronics*, pp. 171–177.
- Colgate, J. and G. Schenkel (1997), Passivity of a class of sampled-data systems: Application to haptic interfaces, *Journal of Robotic Systems*, vol. 14(1), pp. 37–47.
- Force Dimension website (retrieved June 14th 2017), omega.7 product overview.
<http://www.forcedimension.com/products/omega-7/overview>
- Franken, M., S. Misra and S. Stramigioli (2012), Stability of position-based bilateral telemanipulation systems by damping injection, in *Proceedings - IEEE International Conference on Robotics and Automation*, pp. 4300–4306.
- Franken, M., S. Stramigioli, S. Misra, C. Secchi and A. MacChelli (2011), Bilateral telemanipulation with time delays: A two-layer approach combining passivity and transparency, *IEEE Transactions on Robotics*, vol. 27(4), pp. 741–756.
- Gazebo website (retrieved July 14th 2017).
<http://www.gazebosim.org>
- Gilroy, A., B. MacPherson, L. Ross, M. Scuenke, E. Schulte and U. Schumacher (2011), *Atlas of Anatomy*, New York; Stuttgart: Thieme, latin nomenclature edition, ISBN 9781604061000.
- Hamilton, N., W. Weimar and K. Luttgens (2011), *Kinesiology: Scientific Basis of Human Motion*, McGraw-Hill Education - Europe, 12th edition, ISBN 9780078022548.
- Hannaford, B. and J.-H. Ryu (2002), Time-domain passivity control of haptic interfaces, *IEEE Transactions on Robotics and Automation*, vol. 18(1), pp. 1–10.
- Hashtroodi-Zaad, K. and S. Salcudean (2001), Analysis of control architectures for teleoperation systems with impedance/admittance master and slave manipulators, *International Journal of Robotics Research*, vol. 20(6), pp. 419–445.
- Hill, M. and G. Niemeyer (2009), Real-time estimation of human impedance for haptic interfaces, in *Proceedings - 3rd Joint EuroHaptics Conference and Symposium on Haptic Interfaces for Virtual Environment and Teleoperator Systems, World Haptics 2009*, pp. 440–445.
- Hogan, N. (1989), Controlling impedance at the man/machine interface, in *Proceedings, 1989 International Conference on Robotics and Automation*, pp. 1626–1631.
- Hokayem, P. and M. Spong (2006), Bilateral teleoperation: An historical survey, *Automatica*, vol. 42(12), pp. 2035–2057.
- Jubien, A., M. Gautier and A. Janot (2014), Dynamic identification of the Kuka LightWeight robot: Comparison between actual and confidential Kuka's parameters, in *IEEE/ASME International Conference on Advanced Intelligent Mechatronics, AIM*, pp. 483–488.
- Kim, J., P. Chang and H.-S. Park (2005), Transparent teleoperation using two-channel control architectures, in *2005 IEEE/RSJ International Conference on Intelligent Robots and Systems, IROS*, pp. 2824–2831.

- Kim, J.-P. and J. Ryu (2010), Robustly stable haptic interaction control using an energy-bounding algorithm, *International Journal of Robotics Research*, vol. 29(6), pp. 666–679.
- KUKA Roboter GmbH (2012), *Lightweight Robot 4+ Specification*, Version: Spez LBR+ V6 en (PDF), Issued 17.12.2012.
- Lawrence, D. (1993), Stability and Transparency in Bilateral Teleoperation, *IEEE Transactions on Robotics and Automation*, vol. 9(5), pp. 624–637.
- Med-Info (retrieved June 28th 2017), Illustratieve anatomie, Schouder & armen.
http://www.med-info.nl/anatomie_arm.html
- Myo website (retrieved June 21th 2017), Myo Tech Specs page.
<https://www.myo.com/techspecs>
- Niemeyer, G. and J.-J. Slotine (1991), Stable Adaptive Teleoperation, *IEEE Journal of Oceanic Engineering*, vol. 16, pp. 152–162.
- Osu, R., D. Franklin, H. Kato, H. Gomi, K. Domen, T. Yoshioka and M. Kawato (2002), Short- and long-term changes in joint co-contraction associated with motor learning as revealed from surface EMG, *Journal of Neurophysiology*, vol. 88(2), pp. 991–1004.
- Osu, R. and H. Gomi (1999), Multijoint muscle regulation mechanisms examined by measured human arm stiffness and EMG signals, *Journal of Neurophysiology*, vol. 81(4), pp. 1458–1468.
- Ott, C., R. Mukherjee and Y. Nakamura (2010), Unified Impedance and Admittance Control, in *2010 IEEE International Conference on Robotics and Automation*, pp. 554–561, ISSN 1050-4729.
- ROS website (retrieved July 10th 2017).
<http://www.ROS.org>
- Schreiber, G., A. Stemmer and R. Bischoff (2010), The Fast Research Interface for the KUKA Lightweight Robot, in *IEEE Workshop on Innovative Robot Control Architectures for Demanding (Research) Applications How to Modify and Enhance Commercial Controllers (ICRA 2010)*, pp. 15–21.
- Shin, E.-C., J.-H. Ryu and G.-H. Yang (2015), Estimation of human arm impedance in accordance with the master device types and gripping posture, in *IEEE/ASME International Conference on Advanced Intelligent Mechatronics, AIM*, volume 2015-August, pp. 1744–1748.
- Walker, D., R. Wilson and G. Niemeyer (2010), User-controlled variable impedance teleoperation, in *Proceedings - IEEE International Conference on Robotics and Automation*, pp. 5352–5357.
- Weir, D. and J. Colgate (2008), *Haptic Rendering: Foundations, Algorithms and Applications*, A K Peters/CRC Press, chapter 7. Stability of Haptic Displays, pp. 123–156, ISBN 978-1-4398-6514-9.